THE DEVELOPMENT AND IMPLEMENTATION OF NOVEL PEPTIDE FRAGMENTATION METHODS FOR PROTEOMICS

by

Aaron R. Ledvina

A dissertation submitted in partial fulfillment of

The requirements for the degree of

Doctor of Philosophy

(Chemistry)

at the

UNIVERSITY OF WISCONSIN-MADISON

2012

Date of final oral examination: 3/29/2012

The dissertation is approved by the following members of the Final Oral Committee

Joshua J. Coon, Professor, Chemistry

Michael R. Sussman, Professor, Biochemistry

Lloyd M. Smith, Professor, Chemistry

David J. Pagliarini, Assistant Professor, Biochemistry

Frank N. Keutsch, Assistant Professor, Chemistry

THE DEVELOPMENT AND IMPLEMENTATION OF NOVEL PEPTIDE FRAGMENTATION METHODS FOR PROTEOMICS

Aaron R. Ledvina

Under the supervision of Assistant Professor Joshua J. Coon

At the University of Wisconsin-Madison

The work described herein can be broadly classified as 1) The development of techniques to improve the efficacy of electron transfer dissociation (ETD) in proteomics applications, 2) The extension of infrared multiphoton dissociation (IRMPD) to a variety of mass spectrometry instrumentation, with evaluation of the potential utility, and 3) The development of an MS/MS multiplexing technique.

Chapters two through four outline the progression of activated-ion ETD. During this technique, precursor peptides are bombarded with IR photons during electron transfer dissociation; in so doing the gas phase secondary structure is continuously disrupted, leading to considerable improvement in the dissociation efficiency. This proof of concept for this idea was performed on stand-alone ion trap instrumentation, but as the utility became apparent, the technique was extended to a hybrid mass spectrometer comprising both ion trap and orbitrap mass analyzers.

In chapters five and six, I describe the first implementation of IRMPD on an orbitrap-containing mass spectrometer. I similarly describe the implementation of IRMPD on a dual-cell ion trap mass spectrometer, undertaking a large study and

concluding that IRMPD represents an excellent option for the interrogation of isobaric-tagged peptides.

Finally, I present a novel spectral multiplexing scheme. This technique involves the fragmentation of peptide precursors using resonant-excitation collisional activation (CAD). The fragments of several CAD events from different peptide precursors are stored in an external RF device, and analyzed in a single orbitrap m/z analysis step, resulting in considerable duty cycle improvement.

Acknowledgements

I would be remiss if I didn't extend a sincere and well-earned thank you to Professor Joshua J. Coon. It is difficult to put into words all of the amazing opportunities and experiences I have had since joining his research group. His ability to obtain resources, gather talent, and scientific intuition are, in my opinion, of the highest caliber. Moreover, despite my messy, destructive and generally inept early days in the lab, he was patient with me and allowed me to learn and become the scientist I am today.

I also thank current and former lab members of Joshua J. Coon's research group. I would like to specifically mention Graeme C. McAlister, who undertook the substantial task of teaching me mass spectrometry basics. I also would like to thank former lab members Danielle L. Swaney, David M. Good, Doug Phanstiel, Paul Grimsrud, Qiangwei Xia, Violet M. Lee and Craig D. Wegner for being wonderful people from whom I learned much. Jason Russell, who has been with me since the start of our time in Madison has been an invaluable colleague and in addition to solving innumerable LC problems found time to teach me beer-brewing fundamentals. I would like to thank current Coon group members Justin Brumbaugh, Derek Bailey, Dominic Colosi, Alex Hebert, Anna Larson, Molly McDevitt, Amelia Peterson, Greg Potts, Alicia Richards, Chris Rose, Arne Ulbrich, Catie Vincent, and Chenxi Yang for being the best group of co-workers I can imagine.

I am also grateful opportunity to work with an amazing group of diverse collaborators, who have helped me mature as a scientist. Specifically I would like to thank John Syka, Jae Schwartz, George Stafford, Jens Griep-Raming, Jennifer Brodblet, Frank Turecek, Mike Rosenblatt, Jack Simons, Julian Saba, Rosa Viner, and Lisa Vasicek. I would not be where I am and who I am without their invaluable support.

I thank my family and friends for supporting me throughout my time in graduate school. It is no doubt due to the wonderful upbringing that my parents, Mark and Connie, gave me that I have reached this point. Also, thanks to me sister, Adrianne, who has been a friend to me throughout my life. Finally, I cannot express the gratitude I have for my wonderful wife and best friend, Anelle, who has been steadfast and loving in her support of me throughout my time at UW Madison.

Table of Contents

| Chapter 1: Introduction | 1 | |
|---|-------|--|
| Chapter 2: Infrared Photoactivation Reduces Peptide Folding and Hydrogren | -Atom | |
| Migration Following ETD Tandem Mass Spectrometry | | |
| Summary | 21 | |
| Introduction | 21 | |
| Results | 24 | |
| Discussion | 33 | |
| Methods | 33 | |
| References | 35 | |
| Chapter 3: Activated-Ion Electron Transfer Dissociation Improves the Ability of Electron Transfer Dissociation to Identify Peptides in a Complex Mixture | | |
| Summary | 37 | |
| Introduction | 37 | |
| Results | 40 | |
| Discussion | 59 | |
| Methods | 60 | |
| References | 62 | |
| Chapter 4: A Segmented Cell for Expedient Activated Ion Electron Transfer Dissociation | | |
| Summary | 66 | |

| ١/ | |
|----|--|
| v | |
| | |

| Introduction | 67 |
|---|-----|
| Results | 72 |
| Discussion | 93 |
| Methods | 95 |
| References | 103 |
| | |
| hapter 5: Implementing Photodissociation in an Orbitrap Mass Spectrometer | |
| Summary | 107 |
| Introduction | 107 |
| Results | 108 |
| Discussion | 119 |
| Methods | 121 |
| References | 123 |
| | |
| hapter 6: Infrared Multiphoton Dissociation for Quantitative Shotgun Proteomics | |
| Summary | 125 |
| Introduction | 125 |
| Results | 128 |
| Discussion | 150 |
| Methods | 151 |
| References | 154 |
| | |

Chapter 7: Increased Throughput of Proteomics Analysis by Mutiplexing High-

Resolution Tandem Mass Spectra

| | vii |
|--------------|-----|
| Summary | 159 |
| Introduction | 159 |
| Results | 164 |
| Discussion | 176 |
| Methods | 176 |
| References | 177 |

List of Figures

| Figure | Name | Page |
|--------|--|------|
| 1.1 | MS/MS Dissociation Techniques | 3 |
| 1.2 | Electron Transfer Dissociation Mechanism | 8 |
| 1.3 | Activated-Ion ETD Scheme | 12 |
| 2.1 | ETD vs. AI-ETD for Two Peptides | 25 |
| 2.2 | Compilation of ETD vs. AI-ETD Sequence Coverage | 27 |
| 2.3 | Product Ion Isotope Distributions for Various Techniques | 29 |
| 2.4 | Laser Power vs. Isotopic Distributions | 30 |
| 2.5 | AI-ETD of Various Ubiquitin Precursor Charge States | 32 |
| 3.1 | Instrument Scheme of Modified QLT | 42 |
| 3.2 | Peptide Spectral Matches vs. Laser Power | 45 |
| 3.3 | Probability of Observation of Product Ions | 46 |
| 3.4 | AI-ETD vs. ETcaD | 56 |
| 3.5 | CAD vs. ETD vs. AI-ETD of a Phosphopeptide | 58 |
| 3.6 | Probability of Observation of Product Ions | 46 |
| 4.1 | Determination of LMCO in Segmented Cell | 74 |
| 4.2 | QLT vs. Segmented Cell ETD Reaction Rate | 76 |
| 4.3 | QLT vs. Segmented Cell for ETD Reagent Accumulation | 78 |
| 4.4 | Multiple Precursor Fills Schematic | 80 |
| 4.5 | Product Ion S/N vs. Number of Fills | 82 |
| 4.6 | 60S Ribosomal Protein ETD in OLT vs. Segmented Cell | 83 |

List of Figures continued...

| 4.7 | Peptide IDs in QLT vs. Segmented Cell | 87 |
|------|---|-----|
| 4.8 | AI-ETD in the Segmented Cell vs. ETD in QLT | 89 |
| 4.9 | Phosphopeptide IDs in QLT vs. Segmented Cell | 91 |
| 4.10 | AI-ETD in the Segmented Cell of a Phosphopeptide | 92 |
| 4.11 | Schematic of Segmented Cell | 98 |
| 4.12 | Schematic of a Modified Hybrid Mass Spectrometer | 100 |
| 5.1 | Schematic of a Hybrid Mass Spectrometer modified for IRMPD | 111 |
| 5.2 | Effect of Pressure on Photodissociation Efficiency | 111 |
| 5.3 | C-trap RF Amplitude vs. Product Ion S/N | 113 |
| 5.4 | IRMPD of PPITC-derivatized peptide | 115 |
| 5.5 | IRMPD vs. HCD for Fibrinopeptide A | 117 |
| 5.6 | IRMPD of Ubiquitin with Orbitrap m/z Analysis | 118 |
| 5.7 | Summed b- and y- abundances for IRMPD and HCD | 120 |
| 5.8 | Diagram of IR Photon Introduction to Hybrid Mass Spectrometer | 122 |
| 6.1 | Peptide Spectral Matches for IRMPD vs. CAD | 130 |
| 6.2 | Peptide Spectral Matches overlap of IRMPD and CAD | 131 |
| 6.3 | IRMPD for TMT-tagged WAAAKAAAK | 133 |
| 6.4 | b- and y- type ions and TMT Reporter Tag Ion Formation | 134 |
| 6.5 | MS ³ of y- type Product Ions Form Reporter Tag | 136 |
| 6.6 | Peptide PSMs for Fixed RF Amplitude, Fixed IR Activation Time | 137 |
| 6.7 | TMT Accuracy for Fixed RF Amplitude, Fixed IR Activation Time | 139 |

List of Figures continued...

| 6.8 | TMT Signal for Fixed RF Amplitude, Fixed IR Activation Time | 140 |
|------|---|-----|
| 6.9 | PSMs and Accuracy for IRMPD using Adjustable Activation Time | 142 |
| 6.10 | TMT Signal for Fixed RF Amplitude, Dynamic IR Activation Time | 144 |
| 6.11 | HCD Energy vs. PSMs and TMT tag Intensity | 146 |
| 6.12 | IRMPD Activation Coefficient vs. PSMs and TMT tag Intensity | 148 |
| 6.13 | IRMPD vs. beam-type Activation for MAAAKAAAK | 149 |
| 6.14 | Dual-Cell QLT Modified to Perform IRMPD | 152 |
| 7.1 | Multiplexing Workflow | 166 |
| 7.2 | In Silico Multiplexing | 168 |
| 7.3 | Mowse Score Distributions | 169 |
| 7.4 | Mowse Scores Before and After Deconvolution | 172 |
| 7.5 | Complementary Pairs Detected vs. Mass Window | 173 |

List of Tables

| Table | Name | Page |
|-------|--|------|
| 3.1 | PSM Numbers for AI-ETD at Various Laser Powers | 44 |
| 3.2 | PSM Numbers for AI-ETD, ETD, and CAD | 49 |
| 3.3 | PSM Numbers for AI-ETD, ETD, and CAD by Precursor Charge State | 50 |
| 3.4 | Analysis of SCX Fractions with AI-ETD, ETD, and CAD | 52 |
| 3.5 | AI-ETD vs. ETcaD Peptide Spectral Matches | 54 |
| 6.1 | PSMs and Quantitative Error vs. IRMPD Coefficient | 145 |
| 7.1 | Multiplexing vs. Control Peptide Spectral Matches | 175 |

Abbreviations and Acronyms

%B Percent solvent B in HPLC applications

2D Two-dimensional

3D Three-dimensional

ACN Acetonitrile

ACTH Adrenocorticotropic hormone

μm Micrometer / micron

AGC Automatic gain control

AI-ECD Activated-ion electron capture dissociation

AI-ETD Activated-ion electron transfer dissociation

AP Atmospheric pressure

APCI Atmospheric pressure chemical ionization

btCAD Beam-type collisional dissociation

CAD Resonant-excitation collision activated dissociation

CI Chemical ionization

CSIT Charge-sign independent trapping

cm Centimeter

Da Dalton

DIA Data-independent-acquisition

ECD Electron capture dissociation

ESI Electrospray ionization

ETcaD Supplemental activation of ETD

Abbreviations and Acronyms continued...

ETD Electron transfer dissociation

ETnoD Non-dissociative electron transfer dissociation

eV Electron-volts

FDR False discovery rate

FT Fourier transform

FT-ICR Fourier transform ion cyclotron resonance

HASTE High-amplitude short time excitation

HCD High energy beam type collision activated dissociation

HEK Human embryonic kidney

HPC High pressure cell

hES human embryonic stem cells

HPLC High performance liquid chromatography

HT Hadamard transform

iHCD Inlet beam-type collisional dissociation

IMAC Immobilized metal affinity chromatography

IR Infrared

IRMPD Infrared multiphoton dissociation

iTRAQ Isobaric tag for relative and absolute quantitation

kDa Kilo Dalton

LC Liquid chromatography

LMCO Low mass cutoff

Abbreviations and Acronyms continued...

LPC Low pressure cell

LTQ Commercial name for linear ion trap

Lys-C Lysine-c

ml Milliliter

mm Millimeter

mM Millimolar

ms Millisecond

MS The field of mass spectrometry

MS1 Precursor ion mass analysis

MS/MS Tandem mass spectrometry

MS² Tandem mass spectrometry

m/z mass to charge

MHz Mega hertz

NCE Normalized collision energy

nHPLC nanoscale high performance liquid chromatography

OD Optical Density

OMSSA Open Mass Spectrometry Search Algorithm

PD Photon-based peptide dissociation

PSM Peptide spectral match

PTM Post-translational modification

PTR Proton transfer reaction

Abbreviations and Acronyms continued...

QIT quadrupole ion trap

QLT linear quadrupole ion trap

q-value Reduced Mathieu parameter

R Resolving power

RF Radio frequency

r_o Inscribed radius

S/N Signal to noise

SCX Strong cation exhange

SPE Solid phase extraction

TMT Tandem mass tag

UVPD Ultraviolet photodissociation

TFA Trifluoroacetic acid

 V_{Pk-Pk} Volts peak to peak

W Watts

z charge

Chapter 1

Introduction

Large-scale, mass-spectrometry (MS)-based analysis, catalyzed by the development of soft ionization techniques, has become a staple of modern proteomics. The aims of these analyses vary depending upon the specific experiment, but the overall goal is typically to identify and quantify protein expression levels on a global scale. Most modern proteomics experiments begin with the proteolytic digestion of proteins extract because peptides are easier to separate and analyze using current technology. The resulting mixture of peptides can comprise tens of thousands of different peptides, necessitating one or more phases of liquid chromatography separation with the eluent analyzed using a mass spectrometer.

The scope of the biological insights which can be gained using high-throughput proteomics has provided a powerful incentive to improve mass spectrometer instrument design. Novel instrument configurations (e.g., dual cell ion traps), and the combination of sensitive quadrupole ion trap mass analyzers with high mass accuracy and resolution Fourier transform mass analyzers (*i.e.*, orbitrap and ion cyclotron resonance, FT-ICR) have greatly enhanced the overall data quality which proteomics experiments can provide.¹⁻³

Ideally, the mass spectrometer provides the mass and charge state of each peptide present within the mixture. However, to identify and potentially quantitate each peptide present,

or gain information about any post-translation modifications (PTMs) which may be present, an additional measurement is required, namely, the tandem mass spectrum (MS/MS) of each peptide.

During an MS/MS experiment, selected peptides are isolated in the gas phase from co-ionizing peptides and through various means ($vide\ infra$) are fragmented. Most MS/MS techniques result in the fragmentation of inter-residue bonds, providing information about the primary structure of the peptide. Ideally, a single fragmentation technique would provide a homogenous series of product ions allowing for the unambiguous determination of the primary sequence of the precursor peptide with indifference to precursor m/z, charge state, the present of PTMs, or peptide size. Moreover, the ideal fragmentation technique would be fast; the high throughput nature of modern proteomics dictates that to target as many peptides as possible, MS/MS events must consume as little time as possible. The search for such a method has resulted in the description of an impressive array of diverse peptide dissociation techniques. Shown in **Figure 1** are a few of the more common peptide dissociation techniques.

Collisional Activation Techniques

Collisional activation techniques are by far the most pervasive peptide fragmentation techniques. This is largely due to the relative ease of implementation of such techniques on virtually every type of mass spectrometer commercially available. For ion trap mass spectrometers, this often takes the form of resonant-excitation collisional activation (ion

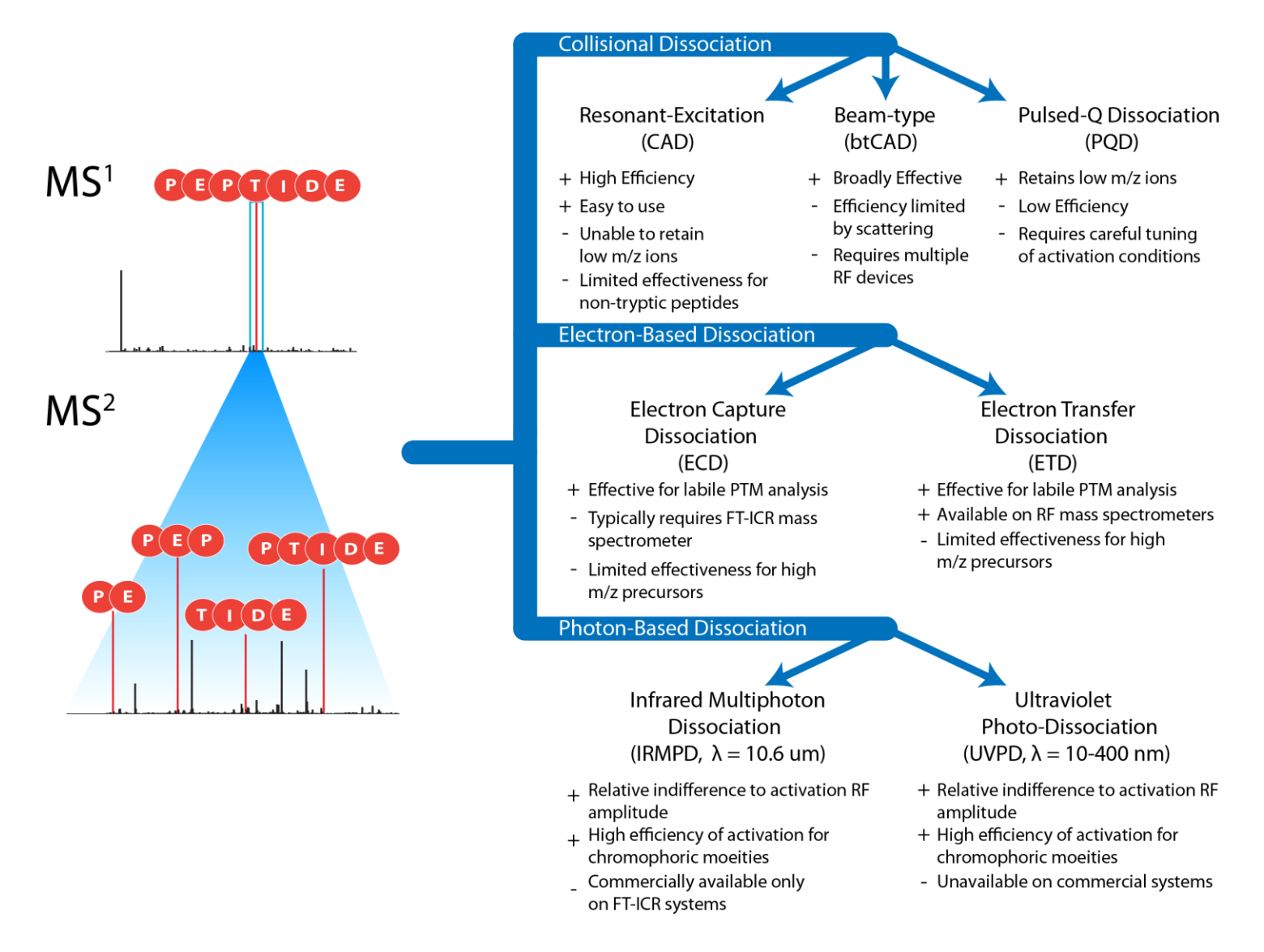


Figure 1. Broadly, collisional dissociation, electron-based dissociation, and photon-based dissociation comprise the majority of common tandem mass spectrometry methods utilized for proteomics.

trap CAD, CAD). During CAD, a supplementary AC voltage is applied at the resonant frequency of the precursor peptide of interest. This induces energetic collisions with the bath gas and a competitive process, resonant ejection of the ions from the trap; the relative partitioning is dictated by the reduced Mathieu parameter (q-value). collision with a neutral bath gas molecule imparts a small amount of energy to the peptide precursor, which is re-distributed throughout the covalent bonds of the peptide. The peptide internal energy continues to increase until the energy of activation corresponding to the weakest covalent (or non-covalent) bond is reached. This is most commonly the peptide bond, the cleavage of which generates b- and y- type fragment ions. CAD has the highest efficiency of precursor to product ion conversion, in large part because product ions formed via CAD are not susceptible to secondary fragmentation. CAD also requires the least amount of user expertise. CAD has limited effectiveness, however, for peptides modified with a labile moiety, namely phospho-peptides. The loss of the phosphoryl group represents a low-energy fragmentation pathway; consequently CAD spectra are typically dominated by the fragment corresponding to the neutral loss, offering limited information about the site of phosphorylation or the peptide primary sequence.⁴ Additionally, the presence of internal basic amino acid residues (e.g., lysine or arginine) can prevent the random distribution of protonated amide linkages, a virtual prerequisite for successful CAD MS/MS. This in turn largely limits CAD to the analysis of proteins digested with trypsin.^{3,5,6} An additional drawback of CAD is incompatibility with isobaric tag-based peptide quantitation techniques iTRAQ and TMT (low mass cutoff is typically too high to retain reporter ions).⁷⁻⁹

In addition to resonant-excitation collisional activation, so-called 'beam-type' activation (btCAD) is commonly employed for proteomics experiments. During this process, ions are shuttled from one region of a mass spectrometer to another, typically by using differential DC offsets placed on RF devices throughout the mass spectrometer. Provided that precursor ions possess sufficient translational kinetic energy, collisions with neutral gas species deposit energy to the peptide. btCAD is utilized on quadrupole-time-of-flight, triple quadrupole, and more recently, ion trapping mass spectrometers. 10 While this process is superficially similar to CAD, the resulting spectra are quite different because each singular collision between the precursor peptide and neutral gas molecule is of a much higher energy than the CAD process. These higher energy collisions results in much larger discreet jumps in internal energy; this means the activation energy of several covalent bonds are exceeded simultaneously. This leads to vastly improved performance for the interrogation of peptides modified with labile PTMs. Another advantage btCAD affords is high efficiency of activation at relatively low RF amplitudes, making btCAD compatible with the analysis of isobaric tagged-peptides. Drawbacks associated with btCAD is the requirement for an external RF device to serve as the collision cell, although recent work has demonstrated that the ESI ion injection optics of stand-alone ion traps can serve this function effectively.¹¹

Photon-based Activation Techniques

In addition to collision-based peptide dissociation, there is keen interest in photon-based (PD) peptide fragmentation techniques. During this process, peptides are bombarded

with photons, accumulate internal energy, and subsequently dissociate. A general advantage of photodissociation techniques is that the photon flux, total irradiation period, and photon wavelength can be varied, enabling a high degree of tunability. Additionally, photo-dissociation potentially allows for selective activation of molecules depending upon the presence or absence of chromophoric moieties (*e.g.* phosphopeptides or disulfide bonds). Finally, photon-based activation methods are performed with relative indifference to the RF amplitude of the device where ions are confined, allowing for the retention of low m/z fragment ions. The photon wavelengths most commonly used for proteomics applications are $\lambda = 10.6$ um (infrared multiphoton dissociation, IRMPD) and $\lambda = 10-400$ nm (ultraviolet photodissociation, UVPD). 15-18

A general disadvantage of photodissociation is that the only commercial mass spectrometer allowing for IRMPD are expensive FT-ICR instrumentation. In **chapter 5**, we describe the first ever extension of IRMPD to a hybrid mass spectrometer comprising both orbitrap and ion trap m/z analyzers. A primary reason why IRMPD has not been widely adopted as a dissociation technique on more ubiquitous ion trapping instrumentation is because the activation efficiency of peptide cations, at typical ion trap operating pressures (~1 mTorr), is relatively low due to the competitive process of collisional cooling. ¹⁹ Efforts made to improve the efficiency include dynamic adjustment of ion trap pressure, ^{20,21} increased photon flux, ²² pre-activation prior to or during IRMPD *via* either resonant excitation of peptides through the attachment of chromogenic moieties. ^{13,14,25,26} Though each of these approaches enables efficient IRMPD, an

attractive and straightforward solution is to perform IRMPD in the low pressure region of a dual-cell quadrupole linear ion trap (dual-cell QLT).^{2,27} In **chapter 6**, we demonstrate that this technique is slightly superior to CAD for the analysis of complex peptide mixtures derived using trypsin. We also report activation conditions which simultaneously provide effective peptide sequencing and good quantitative accuracy. Moreover, we show a preliminary comparison of IRMPD to beam-type collisional activation suggesting that IRMPD may be superior for the generation of isobaric reporter tag.

Electron-based fragmentation techniques

In 1998, Roman Zubarev, working in Fred McLafferty's lab, described a novel peptide fragmentation technique termed "Electron Capture Dissociation" (ECD).²⁸ Typically, during ECD peptides are ionized via ESI, and transferred to the penning trap of an FT-ICR and exposed to free electrons at near-thermal energy. Upon the exothermic (~6 eV) capture of a free electron, the peptide is converted into an unstable radical, which subsequently fragments the N-C_a bond of the peptide, producing so-called c- and z[•]-type ions (**Fig. 2**). While the exact mechanism has undergone numerous refinements, ²⁹⁻³² experimentally ECD very clearly possesses unique and attractive fragmentation attributes. Of particular interest is ECD's unique propensity to preserve labile post-translation modifications (PTMs) and relative indifference to peptide amino acid composition.³³ However, for efficient fragmentation, peptides must be immersed within a dense population of free electrons, a prerequisite not easily met within more common, less

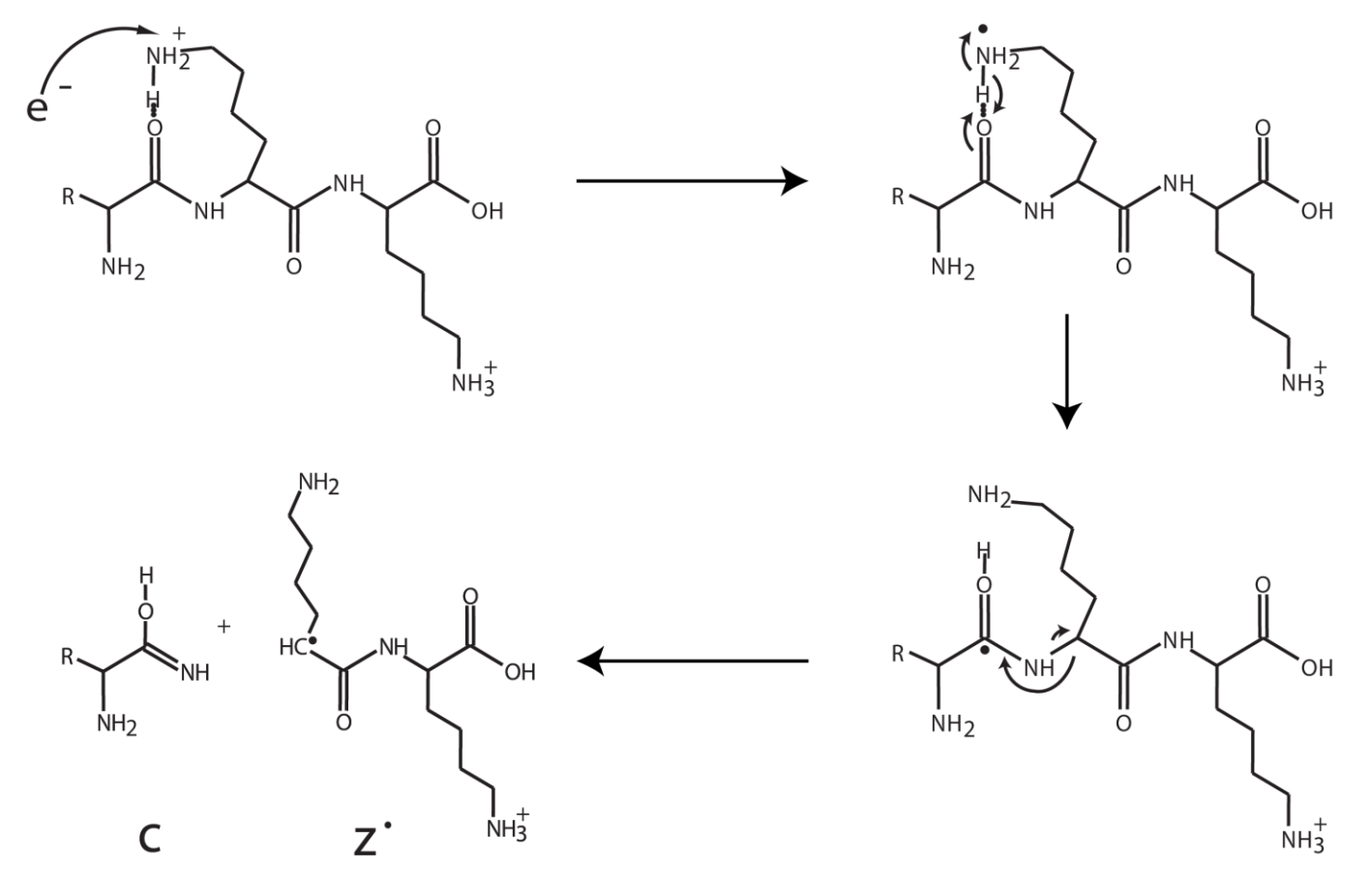


Figure 2. Transfer of an electron to peptide cations results in the formation of a radical cation. Subsequent electron re-arrangement ultimately results in the fragmentation of the N-C_{α} bond and production of c- and z[•]-type fragment ions.

expensive RF ion traps. While several groups have made progress on ways to implement ECD in RF devices with encouraging results, such implementations remain non-trivial, largely limiting ECD to FT-ICR mass spectrometers.³⁴⁻³⁷

A major breakthrough occurred in 2004, when John Syka and Josh Coon, under the supervision of Donald Hunt, discovered a way to effect ECD-like fragmentation within the confines of an RF device, a process they termed "Electron Transfer Dissociation" (ETD).³⁸ During ETD, peptide cations are reacted with reagent radical anions; the radical ions transfer an electron to the cationic peptides, ultimately resulting in dissociation of the peptide into c- and z - type ions. Previous ion-ion experiments had demonstrated that gas phase anions can alternatively abstract a proton from a precursor peptide, so-called Indeed, electron transfer and proton transfer are proton transfer reaction (PTR). competitive processes for ion-ion reactions between cationic peptides and reagent anions. Only when the appropriate anionic reagent is selected (moderate electron affinity and high Franck-Condon overlap)³⁹ can the electron transfer channel can be maximized.⁴⁰ There are a number of potential ways that ETD can be schematically implemented within a mass spectrometer. The original description of ETD utilized so-called charge-sign independent trapping (CSIT), in which cation peptides and reagent anions are confined within the same spatial region of a mass spectrometer at the same time.³⁸ Alternatively, Liang et al. described the storage of cations within O2 of a modified triple quadrupole mass spectrometer while passing reagent ions through Q2, which they termed "transmission mode". 41,42 Since the original implementation using a linear ion trap, 38 ETD has been implemented on numerous types of MS instrumentation, including 3-D RF traps, ⁴³ modified quadrupole/time-of-flight, ⁴⁴ hybrid mass spectrometers comprising both RF ion traps and orbitraps, ^{1,45} and FT-ICR instrumentation. ^{46,47}

ETD has allowed researchers to routinely investigate areas of proteomes that were previously difficult or impossible to characterize, including whole protein analysis, 48,49 combinatorial PTM patterns of histones, 50-52 localization and characterization of sites of glycosylation, 53-57 and global phosphorylation analysis, 58-60 to name a few. Nonetheless, opportunities to improve ETD persist. As noted by ourselves and others, ETD suffers from poor fragmentation efficiency for high m/z peptides. 61-65 Ideally, each ETD event results in the transfer of an electron to the precursor, followed by a radical rearrangement that ultimately the production of c- and z- ions. Sometimes, however, precursor peptides capture an electron but fail to separate into c- and z-type ions. The probability of precursor peptides undergoing non-dissociative electron transfer (ETnoD) is elevated for high precursor m/z peptides. 65 Shortly after the inception of ECD, McLafferty observed similar effects for ECD, positing that non-covalent interactions bind the dissociated cand z- ion pairs together. 66 Practitioners of ECD devised a number of techniques to mitigate the detrimental effects of non-dissociative electron transfer. Termed "activatedion ECD" (AI-ECD), these techniques shared the common strategy of disruption of noncovalent cation peptide interactions. 67-72 This disruption leads to more efficient generation of c- and z- type ions, and consequently higher fragmentation efficiency and bond heterogeneity.

Efforts to similarly improve the fragmentation efficiency for ETD have proceeded down a number of paths. McLuckey and co-workers report that ETD performed at elevated

bath gas temperatures results in improved ETD efficiency. 73 Alternatively, ETnoD products can be coaxed into their component c- and z- type product ions using either resonant excitation or beam-type collisional activation, termed ETcaD. 61,65 effective for increasing peptide sequence coverage, ETcaD techniques produce primarily odd electron c-type ions (c[•]-) and even electron z-type ions. These product ions, both of which are shifted ~1 Da from their theoretical value, are believed to result from the abstraction of a hydrogen atom from the c-type ion by the z- type ion while the two ions are bound together by non-covalent interactions.⁷⁴ ETcaD spectra thus contain product ion isotopic envelopes comprising both odd and even electron species, complicating both manual and automated spectral interpretation. In chapters 2-4, the bombardment of participating ions with IR photons concomitant to ETD reactions is described, a technique we term "Activated-Ion ETD", AI-ETD. By increasing the internal energy of peptides using IR photons, the average gas phase conformation of said peptides is manipulated into a more ETD-friendly state; this results in a decreased probability of non-dissociative electron transfer events, particularly for high m/z precursors (Fig 3.). Moreover, AI-ETD possesses a key advantage over ETcaD in that the supplemental activation takes place concomitant to ETD. Hydrogen abstraction between newly formed c- and z'-type ions happens on a very rapid timescale, perhaps within microseconds; hence, any activation of the ETnoD products subsequent to ion-ion reaction will almost certainly produce even electron z- and odd electron c^{\bullet} - type product ions. 63,75

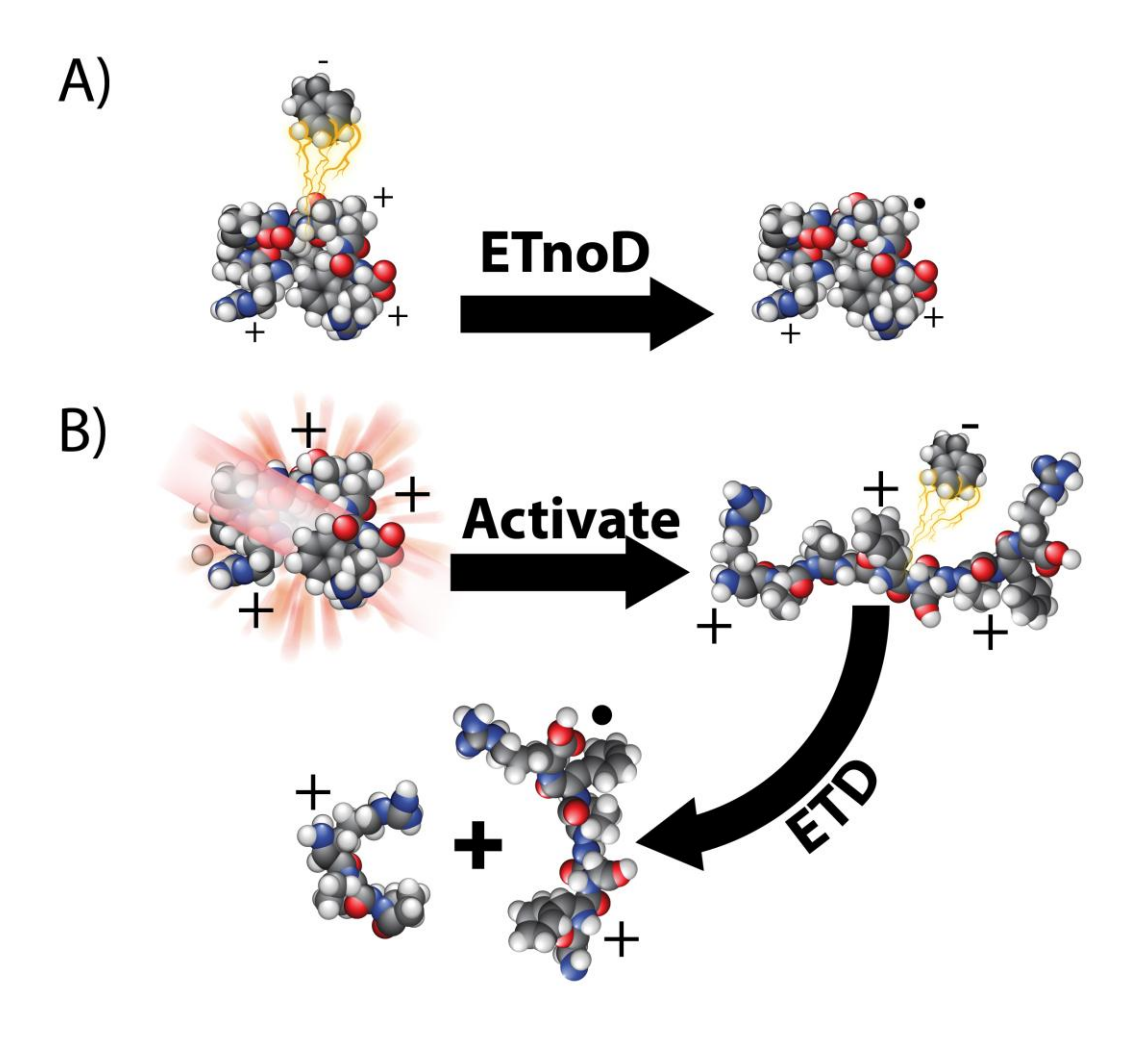


Figure 3. (A) ETD of low charge density frequently results in non-dissociative electron transfer products (ETnoD) because of non-covalent interactions binding the c- and z- ion pair together. (B) By continuously disrupting the peptide secondary structure using IR photons, however, the probability of the c- and z- ions dissociating from one another is increased.

bombarding peptides concomitant to ion-ion reactions, gas phase non-covalent interactions are continuously disrupted, subsequently leading to a more ETD-friendly gas phase conformations and efficient separation of newly formed c- and z^c- type product ions, and limiting the opportunities for hydrogen abstraction to take place.

Other Factors Influencing Experimental Success

While sequence-informative peptide dissociation can represent an experimental lynchpin, it is nonetheless one component among many for bottom-up proteomics workflows. There are a number of other factors (e.g., sample preparation, separation conditions, m/z analyzer, informatics, duty cycle) which strongly influence overall success of a given experiment. In **chapter 7**, I describe an alternative route to improve MS/MS duty cycle through the use of a multiplexing scheme implemented on a hybrid mass spectrometer comprising both ion trap and orbitrap m/z analyzers. During multiplexing, multiple peptide precursors are sequentially isolated and fragmentated using CAD. The product ions from each CAD activation event are co-mingled in an external RF device (i.e., c-trap) and simultaneously analyzed in a single orbitrap m/z analysis, resulting in considerable duty cycle savings.

Summary of work presented here

The chapters herein describe the development of novel peptide fragmentation methods and their application to proteomics research. Chapters 2 through 4 outline the

progression of AI-ETD from promising idea to successful implementation on a state of the art hybrid mass spectrometer comprising both ion trap and orbitrap mass analyzers and outfitted with a dedicated ion-ion reaction vessel. Chapter 5 describes the first implementation of IRMPD on a mass spectrometer comprising the orbitrap mass analyzer. Chapter 6 similarly describes the application of IRMPD performed in the low pressure region of a dual-cell ion trap mass spectrometer to large-scale, isobaric tag-based quantitation studies. Finally, in chapter 7 I present a novel spectral multiplexing scheme, in which multiple peptide precursor are sequentially isolated and fragmented using CAD. The product ions from each CAD activation event are co-mingled in an external RF device and simultaneous analyzed in a single orbitrap m/z analysis event, resulting in considerable duty cycle savings.

References

- McAlister, G. C. *et al.* A proteomics grade electron transfer dissociation-enabled hybrid linear ion trap-orbitrap mass spectrometer. *J. Proteome Res.* **7**, 3127-3136, doi:10.1021/pr800264t (2008).
- Second, T. P. *et al.* Dual-Pressure Linear Ion Trap Mass Spectrometer Improving the Analysis of Complex Protein Mixtures. *Analytical Chemistry* **81**, 7757-7765, doi:10.1021/ac901278y (2009).
- Michalski, A. *et al.* Ultra High Resolution Linear Ion Trap Orbitrap Mass Spectrometer (Orbitrap Elite) Facilitates Top Down LC MS/MS and Versatile Peptide Fragmentation Modes. *Molecular & cellular proteomics : MCP* 11, O111.013698 (2012).
- Schroeder, M. J., Shabanowitz, J., Schwartz, J. C., Hunt, D. F. & Coon, J. J. A neutral loss activation method for improved phosphopeptide sequence analysis by quadrupole ion trap mass spectrometry. *Anal. Chem.* **76**, 3590-3598, doi:10.1021/ac0497104 (2004).
- Wysocki, V. H., Tsaprailis, G., Smith, L. L. & Breci, L. A. Special feature: Commentary Mobile and localized protons: a framework for understanding peptide dissociation. *J. Mass Spectrom.* **35**, 1399-1406, doi:10.1002/1096-9888(200012)35:12<1399::aid-jms86>3.0.co;2-r (2000).

- Dongre, A. R., Jones, J. L., Somogyi, A. & Wysocki, V. H. Influence of peptide composition, gas-phase basicity, and chemical modification on fragmentation efficiency: Evidence for the mobile proton model. *J. Am. Chem. Soc.* **118**, 8365-8374, doi:10.1021/ja9542193 (1996).
- Ross, P. L. *et al.* Multiplexed protein quantitation in Saccharomyces cerevisiae using amine-reactive isobaric tagging reagents. *Mol. Cell. Proteomics* **3**, 1154-1169, doi:10.1074/mcp.M400129-MCP200 (2004).
- 8 Thompson, A. *et al.* Tandem mass tags: A novel quantification strategy for comparative analysis of complex protein mixtures by MS/MS. *Anal. Chem.* **75**, 1895-1904. doi:10.1021/ac0262560 (2003).
- 9 Want, E. J., Cravatt, B. F. & Siuzdak, G. The expanding role of mass spectrometry in metabolite profiling and characterization. *Chembiochem* **6**, 1941-1951, doi:10.1002/cbic.200500151 (2005).
- Olsen, J. V. *et al.* Higher-energy C-trap dissociation for peptide modification analysis. *Nat. Methods* **4**, 709-712, doi:10.1038/nmeth1060 (2007).
- McAlister, G. C., Phanstiel, D. H., Brumbaugh, J., Westphall, M. S. & Coon, J. J. Higher-energy Collision-activated Dissociation Without a Dedicated Collision Cell. *Mol. Cell. Proteomics* **10**, doi:10.1074/mcp.O111.009456 (2011).
- Agarwal, A., Diedrich, J. K. & Julian, R. R. Direct Elucidation of Disulfide Bond Partners Using Ultraviolet Photodissociation Mass Spectrometry. *Anal. Chem.* **83**, 6455-6458, doi:10.1021/ac201650v (2011).
- Gardner, M. W., Vasicek, L. A., Shabbir, S., Anslyn, E. V. & Brodbelt, J. S. Chromogenic cross-linker for the characterization of protein structure by infrared multiphoton dissociation mass spectrometry. *Anal. Chem.* **80**, 4807-4819, doi:10.1021/ac800625x (2008).
- Pikulski, M., Wilson, J. J., Aguilar, A. & Brodbelt, J. S. Amplification of infrared multiphoton dissociation efficiency in a quadruple ion trap using IR-active ligands. *Anal. Chem.* **78**, 8512-8517, doi:10.1021/ac061472k (2006).
- Brodbelt, J. S. & Wilson, J. J. INFRARED MULTIPHOTON DISSOCIATION IN QUADRUPOLE ION TRAPS. *Mass Spectrom. Rev.* **28**, 390-424, doi:10.1002/mas.20216 (2009).
- Thompson, M. S., Cui, W. D. & Reilly, J. P. Fragmentation of singly charged peptide ions by photodissociation at lambda=157 nm. *Angew. Chem.-Int. Edit.* **43**, 4791-4794 (2004).
- 17 Reilly, J. P. ULTRAVIOLET PHOTOFRAGMENTATION OF BIOMOLECULAR IONS. *Mass Spectrom. Rev.* **28**, 425-447, doi:10.1002/mas.20214 (2009).
- Little, D. P., Speir, J. P., Senko, M. W., Oconnor, P. B. & McLafferty, F. W. INFRARED MULTIPHOTON DISSOCIATION OF LARGE MULTIPLY-CHARGED IONS FOR BIOMOLECULE SEQUENCING. *Anal. Chem.* **66**, 2809-2815, doi:10.1021/ac00090a004 (1994).

- Black, D. M., Payne, A. H. & Glish, G. L. Determination of cooling rates in a quadrupole ion trap. *J. Am. Soc. Mass Spectrom.* **17**, 932-938, doi:10.1016/j.jasms.2006.01.001 (2006).
- Boue, S. M., Stephenson, J. L. & Yost, R. A. Pulsed helium introduction into a quadrupole ion trap for reduced collisional quenching during infrared multiphoton dissociation of electrosprayed ions. *Rapid Commun. Mass Spectrom.* **14**, 1391-1397, doi:10.1002/1097-0231(20000815)14:15<1391::aid-rcm36>3.0.co;2-o (2000).
- Hashimoto, Y., Hasegawa, H. & Waki, L. High sensitivity and broad dynamic range infrared multiphoton dissociation for a quadrupole ion trap. *Rapid Commun. Mass Spectrom.* **18**, 2255-2259, doi:10.1002/rcm.1619 (2004).
- 22 Newsome, G. A. & Glish, G. L. Improving IRMPD in a Quadrupole Ion Trap. *J. Am. Soc. Mass Spectrom.* **20**, 1127-1131, doi:10.1016/j.jasms.2009.02.003 (2009).
- Hashimoto, Y., Hasegawa, H., Yoshinari, K. & Waki, I. Collision-activated infrared multiphoton dissociation in a quadrupole ion trap mass spectrometer. *Anal. Chem.* **75**, 420-425, doi:10.1021/ac025866x (2003).
- Payne, A. H. & Glish, G. L. Thermally assisted infrared multiphoton photodissociation in a quadrupole ion trap. *Anal. Chem.* **73**, 3542-3548, doi:10.1021/ac010245+ (2001).
- Kjeldsen, F., Giessing, A. M. B., Ingrell, C. R. & Jensen, O. N. Peptide sequencing and characterization of post-translational modifications by enhanced ion-charging and liquid chromatography electron-transfer dissociation tandem mass spectrometry. *Anal. Chem.* **79**, 9243-9252, doi:10.1021/ac701700g (2007).
- Madsen, J. A. & Brodbelt, J. S. Comparison of Infrared Multiphoton Dissociation and Collision-Induced Dissociation of Supercharged Peptides in Ion Traps. *J. Am. Soc. Mass Spectrom.* **20**, 349-358, doi:10.1016/j.jasms.2008.10.018 (2009).
- Gardner, M. W. *et al.* Infrared Multiphoton Dissociation of Peptide Cations in a Dual Pressure Linear Ion Trap Mass Spectrometer. *Anal. Chem.* **81**, 8109-8118, doi:10.1021/ac901313m (2009).
- Zubarev, R. A., Kelleher, N. L. & McLafferty, F. W. Electron capture dissociation of multiply charged protein cations. A nonergodic process. *J. Am. Chem. Soc.* **120**, 3265-3266, doi:10.1021/ja973478k (1998).
- Syrstad, E. A. & Turecek, F. Toward a general mechanism of electron capture dissociation. *J. Am. Soc. Mass Spectrom.* **16**, 208-224, doi:10.1016/j.jasms.2004.11.001 (2005).
- Turecek, F. N-C(alpha) bond dissociation energies and kinetics in amide and peptide radicals. Is the dissociation a non-ergodic process? *J. Am. Chem. Soc.* **125**, 5954-5963, doi:10.1021/ja021323t (2003).
- Zubarev, R. A. Electron-capture dissociation tandem mass spectrometry. *Curr. Opin. Biotechnol.* **15**, 12-16, doi:10.1016/j.copbio.2003.12.002 (2004).
- Leymarie, N., Costello, C. E. & O'Connor, P. B. Electron capture dissociation initiates a free radical reaction cascade. *J. Am. Chem. Soc.* **125**, 8949-8958, doi:10.1021/ja028831n (2003).

- Zubarev, R. A., Zubarev, A. R. & Savitski, M. M. Electron capture/transfer versus collisionally activated/induced dissociations: Solo or duet? *J. Am. Soc. Mass Spectrom.* **19**, 753-761, doi:10.1016/j.jasms.2008.03.007 (2008).
- Baba, T., Hashimoto, Y., Hasegawa, H., Hirabayashi, A. & Waki, I. Electron capture dissociation in a radio frequency ion trap. *Anal. Chem.* **76**, 4263-4266, doi:10.1021/ac049309h (2004).
- Silivra, O. A., Kjeldsen, F., Ivonin, I. A. & Zubarev, R. A. Electron capture dissociation of polypeptides in a three-dimensional quadrupole ion trap: Implementation and first results. *J. Am. Soc. Mass Spectrom.* **16**, 22-27, doi:10.1016/j.jasms.2004.09.015 (2005).
- Bushey, J. M., Baba, T. & Glish, G. L. Simultaneous Collision Induced Dissociation of the Charge Reduced Parent Ion during Electron Capture Dissociation. *Anal. Chem.* **81**, 6156-6164, doi:10.1021/ac900627n (2009).
- Ding, L. & Brancia, F. L. Electron capture dissociation in a digital ion trap mass spectrometer. *Anal. Chem.* **78**, 1995-2000, doi:10.1021/ac0519007 (2006).
- Syka, J. E. P., Coon, J. J., Schroeder, M. J., Shabanowitz, J. & Hunt, D. F. Peptide and protein sequence analysis by electron transfer dissociation mass spectrometry. *Proc. Natl. Acad. Sci. U. S. A.* **101**, 9528-9533, doi:10.1073/pnas.0402700101 (2004).
- Gunawardena, H. P. *et al.* Electron transfer versus proton transfer in gas-phase ion/ion reactions of polyprotonated peptides. *J. Am. Chem. Soc.* **127**, 12627-12639, doi:10.1021/ja0526057 (2005).
- Coon, J. J., Syka, J. E. P., Schwartz, J. C., Shabanowitz, J. & Hunt, D. F. Anion dependence in the partitioning between proton and electron transfer in ion/ion reactions. *Int. J. Mass Spectrom.* **236**, 33-42, doi:10.1016/j.ijms.2004.05.005 (2004).
- Hager, J. W. A new linear ion trap mass spectrometer. *Rapid Commun. Mass Spectrom.* **16**, 512-526, doi:10.1002/rcm.607.abs (2002).
- Liang, X. R., Hager, J. W. & McLuckey, S. A. Transmission mode Ion/Ion electron-transfer dissociation in a linear ion trap. *Anal. Chem.* **79**, 3363-3370, doi:10.1021/ac062295q (2007).
- Hartmer, R. & Lubeck, M. New approach for characterization of post translational modified peptides using ion trap MS with combined ETD/CID fragmentation. *LC GC Eur.*, 11-13 (2005).
- 44 Xia, Y. *et al.* Implementation of ion/ion reactions in a quadrupole/time-of-flight tandem mass spectrometer. *Anal. Chem.* **78**, 4146-4154, doi:10.1021/ac0606296 (2006).
- McAlister, G. C., Phanstiel, D., Good, D. M., Berggren, W. T. & Coon, J. J. Implementation of electron-transfer dissociation on a hybrid linear ion traporbitrap mass spectrometer. *Anal. Chem.* **79**, 3525-3534, doi:10.1021/ac070020k (2007).
- Kaplan, D. A. *et al.* Electron transfer dissociation in the hexapole collision cell of a hybrid quadrupole-hexapole Fourier transform ion cyclotron resonance mass

- spectrometer. *Rapid Commun. Mass Spectrom.* **22**, 271-278, doi:10.1002/rcm.3356 (2008).
- Wang, Z. H. *et al.* Extensive Crosstalk Between O-GlcNAcylation and Phosphorylation Regulates Cytokinesis. *Sci. Signal.* **3**, doi:ra2
- 10.1126/scisignal.2000526 (2010).
- 48 Kelleher, N. L. Top-down proteomics. *Anal. Chem.* **76**, 196A-203A, doi:10.1021/ac0415657 (2004).
- Chi, A., Bai, D. L., Geer, L. Y., Shabanowitz, J. & Hunt, D. F. Analysis of intact proteins on a chromatographic time scale by electron transfer dissociation tandem mass spectrometry. *Int. J. Mass Spectrom.* **259**, 197-203, doi:10.1016/j.ijms.2006.09.030 (2007).
- Coon, J. J. *et al.* Protein identification using sequential ion/ion reactions and tandem mass spectrometry. *Proc. Natl. Acad. Sci. U. S. A.* **102**, 9463-9468, doi:10.1073/pnas.0503189102 (2005).
- Phanstiel, D. *et al.* Mass spectrometry identifies and quantifies 74 unique histone H4 isoforms in differentiating human embryonic stem cells. *Proc. Natl. Acad. Sci. U. S. A.* **105**, 4093-4098, doi:10.1073/pnas.0710515105 (2008).
- Young, N. L. *et al.* High Throughput Characterization of Combinatorial Histone Codes. *Mol. Cell. Proteomics* **8**, 2266-2284, doi:10.1074/mcp.M900238-MCP200 (2009).
- Chalkley, R. J., Thalhammer, A., Schoepfer, R. & Burlingame, A. L. Identification of protein O-GlcNAcylation sites using electron transfer dissociation mass spectrometry on native peptides. *Proc. Natl. Acad. Sci. U. S. A.* **106**, 8894-8899, doi:10.1073/pnas.0900288106 (2009).
- Khidekel, N. *et al.* Probing the dynamics of O-GlcNAc glycosylation in the brain using quantitative proteomics. *Nat. Chem. Biol.* **3**, 339-348, doi:10.1038/nchembio881 (2007).
- Hogan, J. M., Pitteri, S. J., Chrisman, P. A. & McLuckey, S. A. Complementary structural information from a tryptic N-linked glycopeptide via electron transfer ion/ion reactions and collision-induced dissociation. *J. Proteome Res.* **4**, 628-632, doi:10.1021/pr049770q (2005).
- Darula, Z., Chalkley, R. J., Baker, P., Burlingame, A. L. & Medzihradszky, K. F. Mass spectrometric analysis, automated identification and complete annotation of O-linked glycopeptides. *Eur. J. Mass Spectrom.* **16**, 421-428, doi:10.1255/ejms.1028 (2010).
- Scott, N. E. *et al.* Simultaneous Glycan-Peptide Characterization Using Hydrophilic Interaction Chromatography and Parallel Fragmentation by CID, Higher Energy Collisional Dissociation, and Electron Transfer Dissociation MS Applied to the N-Linked Glycoproteome of Campylobacter jejuni. *Mol. Cell. Proteomics* **10**, doi:M000031
- 10.1074/mcp.M000031-MCP201 (2011).
- Swaney, D. L., Wenger, C. D., Thomson, J. A. & Coon, J. J. Human embryonic stem cell phosphoproteome revealed by electron transfer dissociation tandem

- mass spectrometry. *Proc. Natl. Acad. Sci. U. S. A.* **106**, 995-1000, doi:10.1073/pnas.0811964106 (2009).
- Chi, A. *et al.* Analysis of phosphorylation sites on proteins from Saccharomyces cerevisiae by electron transfer dissociation (ETD) mass spectrometry. *Proc. Natl. Acad. Sci. U. S. A.* **104**, 2193-2198, doi:10.1073/pnas.0607084104 (2007).
- Molina, H., Horn, D. M., Tang, N., Mathivanan, S. & Pandey, A. Global proteomic profiling of phosphopeptides using electron transfer dissociation tandem mass spectrometry. *Proc. Natl. Acad. Sci. U. S. A.* **104**, 2199-2204, doi:10.1073/pnas.0611217104 (2007).
- Swaney, D. L. *et al.* Supplemental activation method for high-efficiency electron-transfer dissociation of doubly protonated peptide precursors. *Anal. Chem.* **79**, 477-485, doi:10.1021/ac061457f (2007).
- Ledvina, A. R. *et al.* Infrared Photoactivation Reduces Peptide Folding and Hydrogen-Atom Migration following ETD Tandem Mass Spectrometry. *Angew. Chem.-Int. Edit.* **48**, 8526-8528, doi:10.1002/anie.200903557 (2009).
- Ben Hamidane, H. *et al.* Electron Capture and Transfer Dissociation: Peptide Structure Analysis at Different Ion Internal Energy Levels. *J. Am. Soc. Mass Spectrom.* **20**, 567-575, doi:10.1016/j.jasms.2008.11.016 (2009).
- Good, D. M., Wirtala, M., McAlister, G. C. & Coon, J. J. Performance characteristics of electron transfer dissociation mass spectrometry. *Mol. Cell. Proteomics* **6**, 1942-1951, doi:10.1074/mcp.M700073-MCP200 (2007).
- Han, H. L., Xia, Y. & McLuckey, S. A. Beam-type collisional activation of polypeptide cations that survive ion/ion electron transfer. *Rapid Commun. Mass Spectrom.* **21**, 1567-1573, doi:10.1002/rcm.2994 (2007).
- Horn, D. M., Ge, Y. & McLafferty, F. W. Activated ion electron capture dissociation for mass spectral sequencing of larger (42 kDa) proteins. *Anal. Chem.* **72**, 4778-4784, doi:10.1021/ac000494i (2000).
- Cooper, H. J., Hakansson, K. & Marshall, A. G. The role of electron capture dissociation in biomolecular analysis. *Mass Spectrom. Rev.* **24**, 201-222, doi:10.1002/mas.20014 (2005).
- Oh, H. *et al.* Secondary and tertiary structures of gaseous protein ions characterized by electron capture dissociation mass spectrometry and photofragment spectroscopy. *Proc. Natl. Acad. Sci. U. S. A.* **99**, 15863-15868, doi:10.1073/pnas.212643599 (2002).
- Oh, H. B. & McLafferty, F. W. A variety of activation methods employed in "activated-ion" electron capture dissociation mass spectrometry: A test against bovine ubiquitin 7+ions. *Bull. Korean Chem. Soc.* **27**, 389-394 (2006).
- Senko, M. W., Speir, J. P. & McLafferty, F. W. COLLISIONAL ACTIVATION OF LARGE MULTIPLY-CHARGED IONS USING FOURIER-TRANSFORM MASS-SPECTROMETRY. *Anal. Chem.* **66**, 2801-2808, doi:10.1021/ac00090a003 (1994).

- Breuker, K., Oh, H. B., Horn, D. M., Cerda, B. A. & McLafferty, F. W. Detailed unfolding and folding of gaseous ubiquitin ions characterized by electron capture dissociation. *J. Am. Chem. Soc.* **124**, 6407-6420, doi:10.1021/ja012267j (2002).
- Horn, D. M., Breuker, K., Frank, A. J. & McLafferty, F. W. Kinetic intermediates in the folding of gaseous protein ions characterized by electron capture dissociation mass spectrometry. *J. Am. Chem. Soc.* **123**, 9792-9799, doi:10.1021/ja003143u (2001).
- Pitteri, S. J., Chrisman, P. A. & McLuckey, S. A. Electron-transfer ion/ion reactions of doubly protonated peptides: Effect of elevated bath gas temperature. *Anal. Chem.* **77**, 5662-5669, doi:10.1021/ac050666h (2005).
- O'Connor, P. B. *et al.* Long-lived electron capture dissociation product ions experience radical migration via hydrogen abstraction. *J. Am. Soc. Mass Spectrom.* **17**, 576-585, doi:10.1016/j.jasms.2005.12.015 (2006).
- Lin, C., O'Connor, P. B. & Cournoyer, J. J. Use of a double resonance electron capture dissociation experiment to probe fragment intermediate lifetimes. *J. Am. Soc. Mass Spectrom.* **17**, 1605-1615, doi:10.1016/j.jasms.2006.07.007 (2006).

Chapter 2

Infrared Photoactivation Reduces Peptide Folding and Hydrogen-Atom Migration Following ETD Tandem Mass Spectrometry

Summary

Electron transfer dissociation (ETD) continues to show great promise for large scale protein sequencing; however certain peptide precursor cations are not effectively dissociated (*e.g.*, those having low charge and high m/z ratios). Several years ago, practicioners of electron capture dissociation found that photon bombardment of precursor cations during the dissociation event (activated-ion ECD, AI-ECD) improves the degree of dissociative vs. non-dissociative electron capture. Here, we describe the use of infrared photons for the constant heating of precursor cations during an electron transfer reaction in a dual cell linear ion trap mass spectrometer, a process we term activated-ion ETD, AI-ETD. Using standard peptide and intact protein cations, we show that AI-ETD improves the utility of ETD, particularly for low charge density peptide precursors (*i.e.*, precursor m/z > 800). By manipulating the gas-phase secondary structure of precursor cations, AI-ETD inhibits extensive hydrogen-atom migration, simplifying product ion isotopic envelopes. Finally, the use of AI-ETD requires no additional time beyond that needed for ion-ion reactions.

Introduction

Electron capture dissociation (ECD)¹ – an experiment generally performed within the high magnetic field of a Fourier transform ion cyclotron resonance mass spectrometer – results from the mutual storage of thermal electrons with multiply protonated peptide cations. The technique is particularly useful as it generates random backbone cleavage with little regard to the presence of post-translational modifications (PTMs), amino acid composition, or peptide length. Electron transfer dissociation (ETD),² the ion-ion analogue of ECD, is conducted in radio frequency (RF) quadrupole ion trap devices in which radical anions serve as electron donors. Since it can be implemented on virtually any mass spectrometer with an RF ion transfer or storage device, ETD has become an increasingly widespread dissociation method.

The capture of an electron by peptide cations can trigger a free radical-driven rearrangement resulting in N-C_a backbone cleavage and c- and z•-type fragment ions. Sometimes, however, the precursor cation captures the electron and forms a long-lived, charge-reduced species that does not separate (an ECnoD or ETnoD product).³ This phenomenon becomes more probable with increasing precursor mass-to-charge (m/z) ratio. As the charge density decreases, the magnitude of intramolecular non-covalent interactions increases, so that the newly formed c- and z•-type fragment ions often remain bound following electron capture and cleavage – an obstacle of higher consequence for ETD, which is conducted under conditions of elevated pressure.⁴ McLafferty and coworkers reported that photon bombardment of the precursor cation prior to ECD

(activated ion-ECD, AI-ECD) decreased non-dissociative electron capture,⁵ presumably by destroying the peptide cation's secondary structure prior to electron capture.

ETD is conducted at pressures that are approximately 10⁶ times higher than in ECD (which is carried out at approximately 0.13 Pa). Therefore, precursor cations undergoing ETD are considerably cooler, and pre-activation either with photons or collisions is expected to produce only short-lived (< 1 ms) unfolding. Recently, we examined the use of collisions to coerce the ETnoD products to dissociate *via* a technique coined ETcaD (ETD in conjuction with collisional activation).³ The method increased the number and intensity of N-C_a backbone cleavages; however, the majority of the newly formed fragment ions displayed evidence of hydrogen-atom rearrangement to produce even electron z-type fragments and odd electron c-type products. practitioners propose that such rearrangements result from the c- and z*-type fragment ions being held in close proximity so that an H atom can be abstracted from the c-type and directed to the z*-type product (this hydrogen-atom transfer occurs prior to the separation of the two fragment ions).^{6,7} For large-scale sequencing applications these rearrangements are highly problematic as the mass window needed to define a possible fragment becomes too large.

We considered subjecting the precursor cations to collisional activation through resonant excitation during the entire ion-ion reaction period to inhibit collisional cooling and refolding prior to electron transfer. A side effect of resonant excitation, however, is that the precursor cations would undergo an increase in velocity. Ion-ion reaction rates

are governed by the velocity of the participants and such increases inhibit the ion-ion reaction. McLuckey and co-workers reported the use of elevated bath gas temperature increased the degree of ETD fragmentation, but did not discuss the impact of the method on hydrogen-atom abstraction. We reasoned that infrared photons (10.6 µm) could be used, in conjunction with ion-ion reactions to continuously increase precursor-ion internal energy, destroy non-covalent interaction, and limit hydrogen-atom migration. To test this hypothesis we modified a dual cell linear ion trap system such that an IR beam irradiated the entire axial length of both linear ion traps. Peptide cations and reagent anions (azobenzene) were generated at atmospheric pressure (AP) and introduced through a single AP inlet.

Results

Panels A and B of **Figure 1** present single scan tandem mass spectra acquired following a 100 ms reaction of doubly protonated Substance P cations (RPKPQQFFGLMamide, m/z =674) with radical anions of azobenzene either without (ETD, panel A) or with concomitant photon bombardment (AI-ETD, panel B). ETD

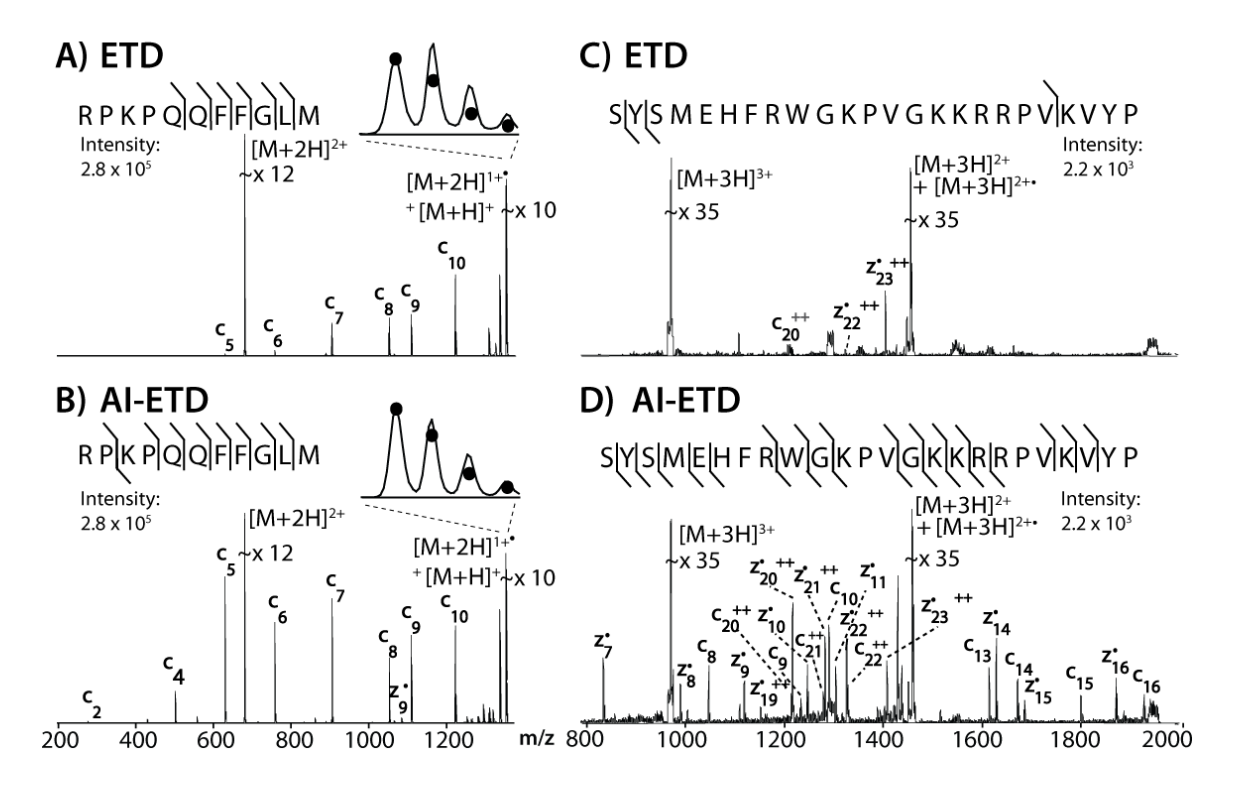


Figure 1. ETD and AI-ETD spectra of A,B) RPKPQQFFGLM and C,D) ACTH for a 100 ms reaction with azobenzene radical anions. For AI-ETD, the laser power was set at 99% laser power.

resulted in the production of six *c-type* product ions. Irradiation of the reactants during the ETD process resulted in the formation of nine *c*- and *z*-type* fragments, virtually all of which showed significant increases in intensity. The inset of panel A displays the isotopic envelope of the charge-reduced precursor, which comprises products of both ETnoD and proton abstraction. Proton abstraction is a side-reaction that competes with electron transfer. The product composition is largely dependent upon the reagent anion: 10 – azobenzene engages in more proton abstraction than our preferred reagent fluoranthene, but is conveniently produced under AP conditions. The inset also shows the theoretical isotopic envelopes of the proton transfer charge-reduction product [M+H]⁺ as filled circles. The heightened distribution of the ¹³C isotopic cluster provides an estimate of the ETnoD population. From the spectrum in Figure 1B we concluded that AI-ETD significantly lessens the degree of ETnoD, presumably by disrupting gas-phase secondary structure and increasing the probability of direct dissociation.

Figure 1 C,D shows the ETD and AI-ETD mass spectra resulting from ETD activation of the triply protonated precursor of the peptide adrenocorticotropic hormone (ACTH, m/z = 978). Similar results were obtained, except in this case ETD produced only three fragment ions whereas AI-ETD resulted in 23 c- or z-type products. Figure 2 displays an expanded dataset with the results listed in order of ascending precursor m/z value. As precursor charge density decreases, the benefits of AI-ETD in terms of both overall product signal and peptide sequence coverage (displayed graphically in the

| peptide | charge state | precursor m/z | fold-increase in product TIC | ETD sequence coverage | Al-ETD sequence coverage | % sequence coverage increase |
|-------------------------------|-----------------|------------------|---------------------------------|-----------------------------|--------------------------------|------------------------------------|
| КАААКАААК | 2 | 415 | 1.3 | 100% | 100% | 0% |
| DRVYIHPFL | 3 | 433 | 1.1 | 89% | 89% | 0% |
| RPKPQQFFGLM | 3 | 450 | 1.6 | 80% | 80% | 0% |
| FSWGAEGQR | 2 | 519 | 2.1 | 75% | 100% | 25% |
| AGCKNFFWKTFTSC | 3 | 546 | 1.9 | 54% | 92% | 38% |
| SYSMEHFRWGKPV- GKKRRPVKVYP | 5 | 587 | 1.3 | 70% | 87% | 17% |
| DRVYIHPFL | 2 | 648 | 1.3 | 44% | 56% | 12% |
| RPKPQQFFGLM | 2 | 675 | 2.7 | 50% | 80% | 30% |
| SYSMEHFRWGKPV- GKKRRPVKVYP | 4 | 734 | 1.9 | 52% | 83% | 31% |
| AGCKNFFWKTFTSC | 2 | 820 | 2.6 | 15% | 85% | 70% |
| SYSMEHFRWGKPV- GKKRRPVKVYP | 3 | 978 | 2.2 | 13% | 70% | 57% |
| AVERAGE | | | 1.8 | 58% | 84% | 26% |

Figure 2. Summary of peptide sequence coverage for ETD and AI-ETD. Italicized, red numbers indicate the maximum possible ETD sequence coverage when disregarding cleavage n-terminal to proline residues. Total Ion Current (TIC) was calculated for ETD and AI-ETD by subtracting unreacted precursor and charge-reduced regions from the overall TIC associated with a given spectrum.

rightmost column) become more distinct. It is well documented that ETD is generally less effective for precursor peptides with a high degree of non-covalent interactions, 11 thus the effect of increasing precursor ion internal energy using IR radiation is exaggerated for high m/z peptides.

We next explored the degree of hydrogen-atom abstraction, as this process was a significant limitation of our previous ETcaD approach. **Figure 3** displays the product ion distributions of the z_6 and c_8 product ions formed following the dissociation of doubly-protonated peptide cations with the sequence FSWGAEGQR by several methods: ETD with A) no other activation, B) concurrent photoactivation (AI-ETD), c) post-activation by photons (ETirD), and D) post-activation through collisions (ETcaD). The intensity scale is identical for all parts of **Figure 2**; filled circles denote the theoretical isotopic distribution of the z^{\bullet} -type ion. Two principle conclusions can be drawn from this data: 1) AI-ETD results in a marked improvement in intensity and a diminished proclivity for hydrogren-atom abstraction as compared to ETD, and 2) remarkably, both post-activation methods (through photons and collisions) produce identical results. However, the increased product formation observed with the post-activation methods is accompanied by a large amount of hydrogen-atom abstraction. These results are consistent across all peptides examined.

We also considered the effect of laser power on the magnitude of hydrogen abstraction. We performed AI-ETD on ACTH at various laser powers from 50 to 99% (maximum: 50W), and monitored the intensity of the signal due to the z_7 and z_7 (Fig. 4).

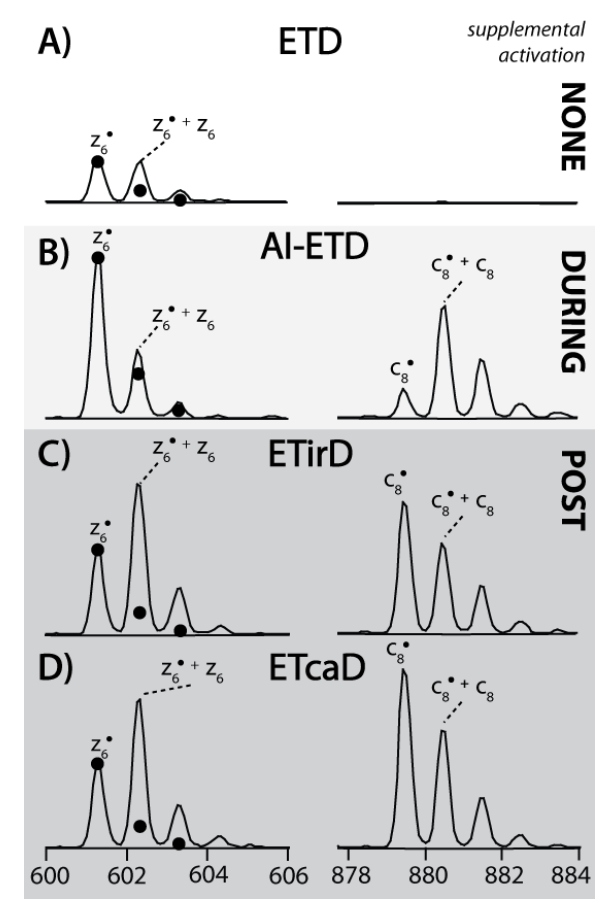


Figure 3. Isotopic distributions of the z^{\bullet}_{6} and c_{8} product ions generated from FSWGAEGQR by A) ETD, B) AI-ETD, C) ETirD, and D) ETcaD in a 100 ms reaction with azobenzene radical anions. For AI-ETD and ETirD, the laser power was set at 99%. Filled circles denote the theoretical distribution of typical ETD product ions.

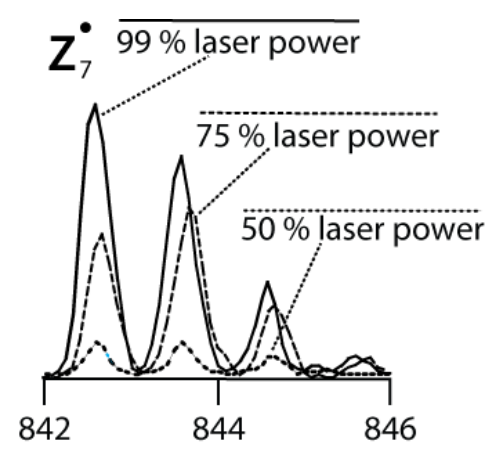


Figure 4. The distribution and intensity of the z_6 product ion generated from a 100 ms ETD reaction of ACTH at various laser powers.

As laser power was increased, the z_7 - type product ion also increased. A simultaneous decrease in the amount of the hydrogen-atom transfer product (*i.e.* z-type product) was observed, which is consistent with previous AI-ECD studies. As a result of the relatively high pressure of the system (ca. 0.63 Pa), IR activation did not induce detectable b-, w-, or y-type fragment formation, even at the highest power settings.

To further confirm our guiding supposition – that concurrent photoactivation during the ion-ion reactions of precursor peptide/protein cations can induce gas-phase unfolding that is maintained in the high-pressure environment of the ion trap – we examined ubiquitin cations with charges ranging from +7 to +10. Studies by Clemmer and co-workers of ubiquitin conformations under similar pressures revealed the +7 charge state to be in a compact conformation (cross-section ca. 1000 Å²) during the time scale of our experiments (10 ms). 12 As the charge state increases, so does the crosssection; thus the +10 precursor was described as elongated (ca. 1500 Å²). Direct ETD of the +7 precursor produced no detectable fragmentation, low-level dissociation was detected for the +8 precursor, and the +9 and +1- precursors underwent significant fragmentation. Figure 5 shows selected fragments derived from the ETD of precursors with charge states between +7 and +10 and those produced by AI-ETD of the +7 precursor. Numerous fragments observed in the AI-ETD spectrum were found only in the ETD spectra of the +9 and +10 precursors. These data provide further evidence that concomitant photoactivation disrupts the secondary structure of the precursor cation during ETD reactions to yield increased fragmentation and diminished hydrogen-atom rearrangement.

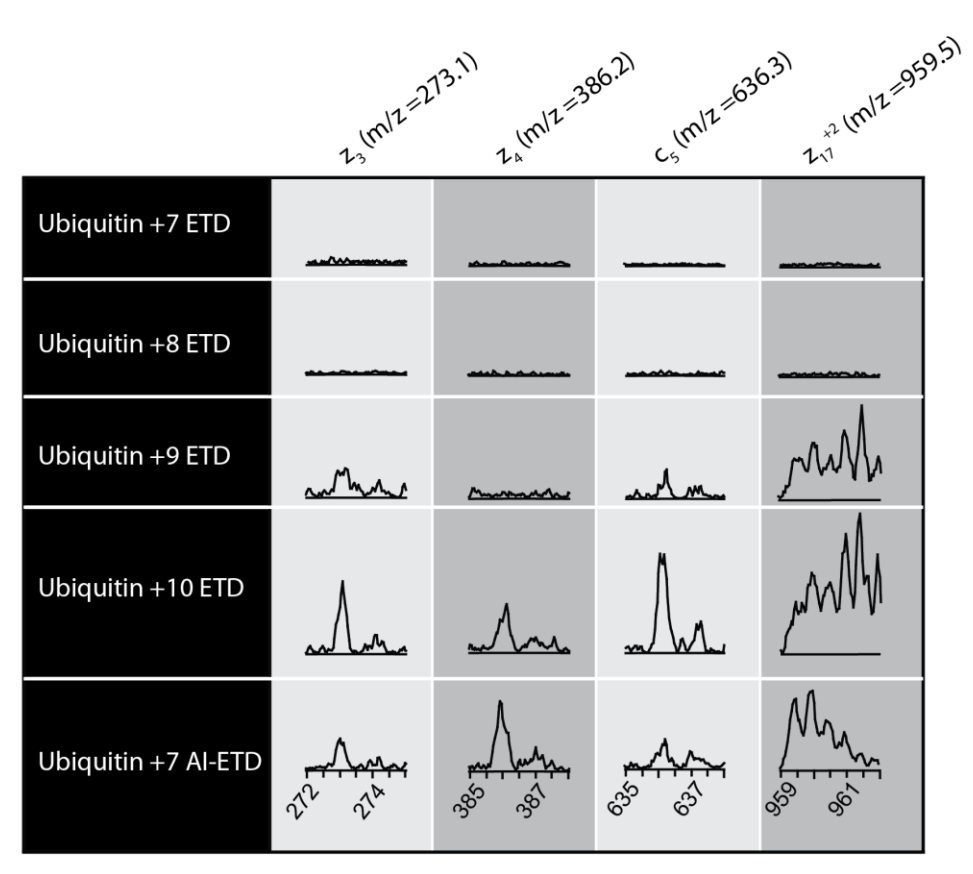


Figure 5. Selected product ion following either ETD or AI-ETD of various precursor charge states of ubiquitin. Product ions z_3 , z_4 , c_5 , and ${z_{17}}^{+2}$ for ETD of +7 through +10 charge states and AI-ETD of the +7 precursor. Results shown represent the average of approximately 150 spectra. Note that AI-ETD leads to the formation of product ions that are only observed upon ETD of higher charge states. Note y-axis scale is ion intensity (arbitrary units) and is fixed for all spectra.

Discussion

Herein we have described AI-ETD and demonstrated that it can substantially improve the utility of ETD for peptide-sequence analysis. The method shows particular promise to enable the use of ETD for low-charge-density peptide precursors (e.g., precursors m/z>800) where gas-phase secondary structure prevents direct formation of c- and z^{\bullet} -type fragment ions, thereby permitting extensive hydrogen-atom migration. By limiting intramolecular interactions, AI-ETD generates isotopic cluster peaks of lower complexity that more closely resemble theoretically predicted c- and z^{\bullet} -type product distributions than those derived from either ETD or post-activation strategies (ETcaD or ETirD). Another advantage of AI-ETD over post-activation is that no additional time (above that needed for ion-ion reaction) is required.

Methods

Materials: Peptides FSWGAEGQR and AGCKNFFWKTFTSC were purchased from BACHEM (Torrance, CA). All other chemicals unless otherwise indicated were purchase from from Sigma Aldrich (St. Louis, MO). Peptide solutions of ACTH (SYSHEMFRWGKPVGKKRRPVKVYP), Substance P (RPKPQQFFGLM), and Angiotensin (DRVYIHPFHL) were prepared by dissolving stock solutions to ~ 10pmol/μL in 70:29.9:0.1 acetonitrile/water/acetic acid by volume. Peptides solutions of FSWGAEGQR and AGCKNFFWKTFTSC were prepared by diluting stock solutions to a

final concentration of ~ 10 pmol/ μL in 49:49:1 methanol/water/acetic acid by volume. Azobenzene was dissolved in toluene to a final concentration of ~ 1 mg/mL.

Instrumentation: All experiments were performed on a dual cell linear ion trap mass spectrometer consisting of a high pressure cell (HPC) and a low pressure cell (LPC) operated at 4.7 mTorr and 0.3 mTorr, respectively. 10.6 um irradiation from a model 48-5 Synrad 50 W CO2 continuous wave laser (Mukilteo, WA) was introduced through a ZnSe window mounted to the back flange of the instrument on-axis with the dual cell trap as previously specified. Instrument firmware was modified to externally trigger the laser concomitant with ion-ion reactions using pin 14 of the J1 connector on the digital printed circuit board. AI-ETD experiments were performed at full laser power unless otherwise specified.

Precursor cations and reagent anions were generated and infused into the mass spectrometer using a pulsed ESI-APCI scheme similar to that described by McLuckey *et al.* ¹⁴ Briefly, the two sources were placed directly in front of the atmospheric inlet of the mass spectrometer. The ESI emitter tip position was optimized at a distance of \sim 35 mm from the inlet. Cations were introduced via direct infusion using a gastight syringe (Hamilton, Las Vegas, NV) at a rate of 1 μ L/min. The ESI emitter tips used were 260 μ m OD, 25 μ m ID, with a 30 μ m length (New Objective). The azobenzene solution was infused into the APCI probe (ThermoFisher Scientific, Bremen, Germany) at a rate of 1.5 μ L/min. To prevent excessive adduction of oxygen with the radical azobenzene formed via APCI, the source region was aspirated with low purity nitrogen. For each scan, the ESI voltage was pulsed from 0 to 2.2 kV and the spray was allowed to stabilize for \sim 300

ms. Following accumulation of cations at an AGC target of 10,000 precursor charges in the HPC, the electrospray voltage was switched back to zero and the corona pin voltage for the APCI source was pulsed from 0 to -5.5 kV and allowed to stabilize for ~400 ms. Anion injection and accumulation for ~10 ms immediately preceded ion-ion reactions. Following ion activation, the product ions were transferred to the LPC for m/z analysis. Note that bombardment of isolated radical anions of azobenzene with IR photons revealed neither dissociation nor electron detachment.

References

- Zubarev, R. A., Kelleher, N. L. & McLafferty, F. W. Electron capture dissociation of multiply charged protein cations. A nonergodic process. *J. Am. Chem. Soc.* **120**, 3265-3266, doi:10.1021/ja973478k (1998).
- Syka, J. E. P., Coon, J. J., Schroeder, M. J., Shabanowitz, J. & Hunt, D. F. Peptide and protein sequence analysis by electron transfer dissociation mass spectrometry. *Proc. Natl. Acad. Sci. U. S. A.* **101**, 9528-9533, doi:10.1073/pnas.0402700101 (2004).
- Swaney, D. L. *et al.* Supplemental activation method for high-efficiency electron-transfer dissociation of doubly protonated peptide precursors. *Anal. Chem.* **79**, 477-485, doi:10.1021/ac061457f (2007).
- Ben Hamidane, H. *et al.* Electron Capture and Transfer Dissociation: Peptide Structure Analysis at Different Ion Internal Energy Levels. *J. Am. Soc. Mass Spectrom.* **20**, 567-575, doi:10.1016/j.jasms.2008.11.016 (2009).
- Horn, D. M., Breuker, K., Frank, A. J. & McLafferty, F. W. Kinetic intermediates in the folding of gaseous protein ions characterized by electron capture dissociation mass spectrometry. *J. Am. Chem. Soc.* **123**, 9792-9799, doi:10.1021/ja003143u (2001).
- Savitski, M. M., Kjeldsen, F., Nielsen, M. L. & Zubarev, R. A. Hydrogen rearrangement to and from radical z fragments in electron capture dissociation of peptides. *J. Am. Soc. Mass Spectrom.* **18**, 113-120, doi:10.1016/j.jasms.2006.09.008 (2007).
- Lin, C., Cournoyer, J. J. & O'Connor, P. B. Probing the gas-phase folding kinetics of peptide ions by IR activated DR-ECD. *J. Am. Soc. Mass Spectrom.* **19**, 780-789, doi:10.1016/j.jasms.2008.01.001 (2008).

- 8 Reid, G. E., Shang, H., Hogan, J. M., Lee, G. U. & McLuckey, S. A. Gas-phase concentration, purification, and identification of whole proteins from complex mixtures. *J. Am. Chem. Soc.* **124**, 7353-7362, doi:10.1021/ja025966k (2002).
- 9 Pitteri, S. J., Chrisman, P. A. & McLuckey, S. A. Electron-transfer ion/ion reactions of doubly protonated peptides: Effect of elevated bath gas temperature. *Anal. Chem.* **77**, 5662-5669, doi:10.1021/ac050666h (2005).
- Gunawardena, H. P. *et al.* Electron transfer versus proton transfer in gas-phase ion/ion reactions of polyprotonated peptides. *J. Am. Chem. Soc.* **127**, 12627-12639, doi:10.1021/ja0526057 (2005).
- Good, D. M., Wirtala, M., McAlister, G. C. & Coon, J. J. Performance characteristics of electron transfer dissociation mass spectrometry. *Mol. Cell. Proteomics* **6**, 1942-1951, doi:10.1074/mcp.M700073-MCP200 (2007).
- Myung, S., Badman, E. R., Lee, Y. J. & Clemmer, D. E. Structural transitions of electrosprayed ubiquitin ions stored in an ion trap over similar to 10 ms to 30 s. *J. Phys. Chem. A* **106**, 9976-9982, doi:10.1021/jp0206368 (2002).
- Gardner, M. W., Vasicek, L. A., Shabbir, S., Anslyn, E. V. & Brodbelt, J. S. Chromogenic cross-linker for the characterization of protein structure by infrared multiphoton dissociation mass spectrometry. *Anal. Chem.* **80**, 4807-4819, doi:10.1021/ac800625x (2008).
- Liang, X., Xia, Y. & McLuckey, S. A. Alternately pulsed nanoelectrospray ionization/atmospheric pressure chemical ionization for ion/ion reactions in an electrodynamic ion trap. *Anal Chem* **78**, 3208-3212 (2006).

Chapter 3

Activated-Ion Electron Transfer Dissociation Improves the Ability of Electron Transfer Dissociation to Identify Peptides in a Complex Mixture

Summary

Using a modified electron transfer dissociation (ETD)-enabled quadrupole linear ion trap (QLT) mass spectrometer, we demonstrate the utility of IR activation concomitant with ETD ion-ion reactions (activated-ion ETD, AI-ETD). Analyzing 12 strong cation exchanged (SCX) fractions of a LysC digest of human cell protein extract using LID, collision-activated dissociation (CAD), and AI-ETD, we find that AI-ETD generates 13 405 peptide spectral matches (PSMs) at a 1% false-discovery rate (1% FDR), surpassing both ETD (7,968) and CAD (10,904). We also analyze 12 SCX fractions of a tryptic digest of human cell protein extract and find that E) produces 6,234 PSMs, AI-ETD 9 130 PSMs, and CAD 15 209 PSMs. Compared to ELD with supplemental collisional activation (ETcaD), AI-ETD generates similar to 80% more PSMs for the whole cell lysate digested with trypsin and similar to 50% more PSMs for the whole cell lysate digested with LysC.

Introduction

Effective peptide fragmentation is a central component of shotgun proteomics, and the success of an experiment often depends upon the choice of fragmentation technique. 1-6 The ideal fragmentation method routinely produces a homologous series of product ions, allowing for confident identification of the interrogated peptide. The most common fragmentation techniques are based on activating a peptide via collisions with inert gas; such techniques comprise both "beam-type" and resonant-excitation collision-activated dissociation (CAD).⁷⁻¹⁰ Discovery-driven proteomics commonly utilizes CAD due to the high efficiency of fragmentation. During CAD, the selected precursor gains internal energy through collisions with neutral gas molecules until the energetic threshold of dissociation is reached. Though effective for peptide cations having a random series of protonated amide linkages, CAD's success depends heavily on peptide charge and amino acid composition. 11,12 Moreover, the presence of labile chemical moieties (e.g., phosphoryl groups) leads to non-random fragmentation, as cleavage of the moiety often represents the lowest energy pathway. Consequent neutral loss of the labile group is thus the dominant CAD fragmentation pathway. 13,14 While this issue has been somewhat mitigated via the use of an additional stage of fragmentation, limitations persist. ¹⁵ In addition to the duty cycle concerns associated with MS3 neutral loss scanning for shotgun proteomics experiments, there have been at least two independent publications reporting that compared to CAD, MS3 neutral loss scanning did not increase coverage of identified phosphopeptides and only slightly improved site localization. 16,17 limitations have sparked interest in the development of alternative peptide fragmentation methods.

Electron-based fragmentation strategies, *i.e.*, electron transfer dissociation (ETD) and electron capture dissociation (ECD), are attractive alternatives. 18-20 While generally less efficient than CAD (precursor-to-product conversion), these techniques demonstrate markedly lower dependence on peptide amino acid composition. ^{21,22} A limitation, however, is an increasing proclivity for non-dissociative electron transfer (ECnoD/ETnoD) with increasing precursor m/z. ^{22,23} Practitioners of ECD utilize either pre- or concomitant peptide activation strategies (activated-ion ECD, AI-ECD) to mitigate the degree of ECnoD.²⁴⁻²⁹ These strategies deposit internal vibrational energy through various means (e.g., IR photons and collisions with gas), disrupting gas phase secondary structures and leading to more efficient ECD. ETD is conducted at pressures several orders of magnitude higher than those used in ECD; thus, peptide cations undergoing ETD are cooler, and pre-activation using either collisions or photons produces only transient (~1 ms) unfolding. A supplemental collisional activation step following the ETD ion-ion reaction, so-called ETcaD, is widely employed to circumvent ETnoD.^{23,30} With careful control of the activation conditions (i.e., resonant activation qvalue and amplitude), ETnoD species are converted almost exclusively into c- and z-type product ions. Though efficient for increasing peptide sequence coverage, ETcaD results primarily in the formation of odd electron c- and even electron z-type ions, shifted ~ 1 Da from their theoretically predicted values. Consequently, ETcaD produces isotopic envelopes comprising a mixture of odd and even electron product ions, complicating spectral interpretation.

Recently, we described the concomitant activation of peptide cations during ETD using IR photons, a process we term activated-ion ETD (AI-ETD). AI-ETD successfully increases the sequence coverage of peptides beyond that attained using unassisted ETD, particularly for high m/z peptides. Moreover, AI-ETD results almost exclusively in production of odd electron z-type and even electron c-type product ions, which match their theoretically predicted m/z values. As a proof of concept, our previous study considered only a handful of peptides and was not suitable for LC separations, an essential component of large-scale experiments. Here we present the modification of a quadrupole linear ion trap (QLT) mass spectrometer that allows AI-ETD to be conducted in an LC-compatible manner. Further, we use this platform to demonstrate the viability of AI-ETD as a peptide fragmentation method for large-scale protein sequence analysis.

Results

Modification of QLT. In our initial description of AI-ETD, we modified a linear ion trap system to implement dual front-end ionization sources (APCI and ESI), which were pulsed for sequential generation of analyte cations and reagent anions.³¹ This configuration provided a line of sight for delivery of photon concentric with the trapping volume at the far end of the traps. While effective for a preliminary evaluation, that arrangement was not suitable for large-scale LC-MS/MS analyses due to the lengthy duty cycle and ESI spray instabilities associated with pulsed spray voltages. We developed a new configuration in pursuance of our key goal for the present study: to evaluate AI-ETD

for LC-MS/MS. The standard ETD-enabled linear ion trap utilizes a chemical ionization source for rapid, robust anion generation. This source opposes the AP inlet as shown in **Figure 1**. Here we modified an instrument in this configuration by inserting a ZnSe window on the rear of the ETD module to transmit IR photons through a stainless steel aperture (diameter = 0.065'') concentric with the trapping volume of the QLT. To allow passage of IR photons to the trapping volume, the ion volume of the NCI source was modified by the addition of a hole (diameter = 0.070'') in the section of the ion volume farthest from the ion trap and the enlargement of the hole in the section closest to the ion trap, both concentric with the QLT trapping volume. We experimented with various diameters for the stainless steel disk, ranging from 0.020" - 0.100". For very small diameters, IR activation was inadequate for AI-ETD; conversely, for larger diameters, the NCI source temperature increased substantially, leading to decreased flux of reagent anions. The selection of 0.065" represents a compromise, with effective IR activation and only minimal NCI source heating. With the use of this diameter disk and 60 W AI-ETD laser power over a 90 min LC-MS/MS analysis, source temperature increased only marginally (~ 2 °C).

Parametric Evaluation of AI-ETD. Our initial studies indicated that laser power influences a number of factors, including the degree of hydrogen abstraction and intensity of product ions. To characterize the effect of laser power on PSM generation for AI-ETD, we designed a series of experiments using AI-ETD at a range of laser powers (12, 24, 36, 48, and 60W) and utilizing a whole cell lysate previously digested with either trypsin or LysC. LC-MS/MS analyses were performed using consecutive

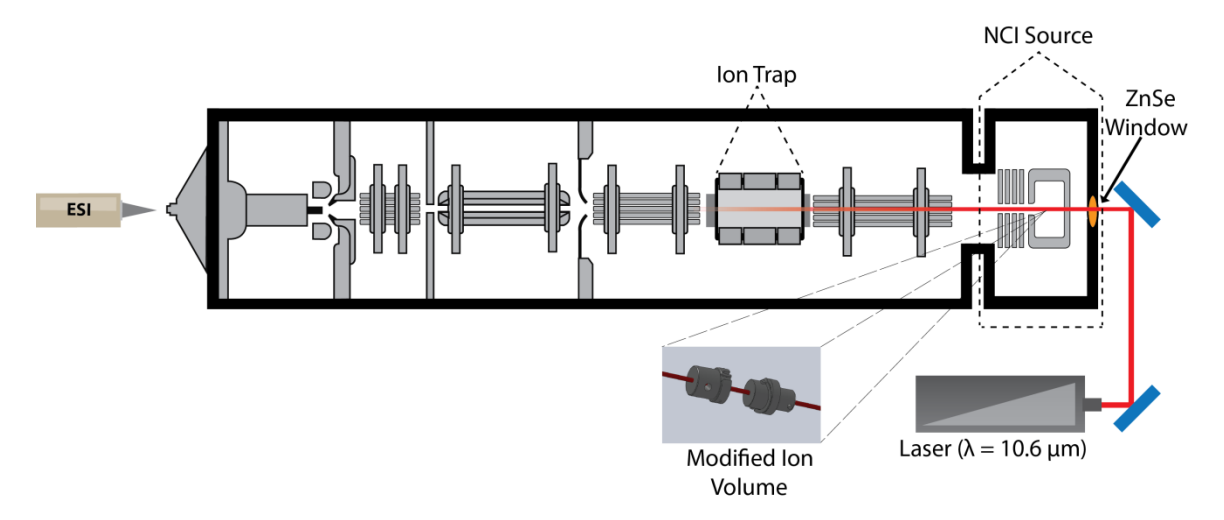


Figure 1. Modified QLT allowing for IR activation concomitant to ETD ion-ion reactions.

ETD, CAD, and AI-ETD interrogation of the two most intense precursors from the MS¹ scan. At (AI-ETD) laser powers greater than 60 W, *b*- and *y*-type product ions resulting from precursor photo-dissociation are observed (data not shown).

In general, as laser power was increased, the degree of hydrogen abstraction we observed decreased; in practice this results in higher laser powers producing a greater proportion of odd electron z-type ions (z-), and even electron c-type product ions (c-) than lower laser powers. To quantify the effect of such hydrogen abstractions and also the overall product ion abundances, we considered AI-ETD performance as a function of laser power used (**Table 1**). PSM counts for both mixtures increase as laser power is increased from 12 to 48 W, followed by a mild decrease as power is increased to 60 W. Next, PSMs binned by precursor m/z (50 Th wide) were plotted for the 12, 36, and 60 W experiments, normalized to the most PSMs for each individual bin (**Fig. 2**). The use of 12 W generates the most PSMs for low m/z precursors (m/z = 300-400), with the most PSMs of moderate m/z precursors (m/z = 400-650) occurring using 36 W and 60W producing the most PSMs for high m/z peptides (m/z > 650).

To investigate this trend, we wrote software to search MS/MS spectra, of all PSMs (1% FDR) *en masse*, for the presence of c- and z•-type product ions. A product ion was considered present if the ion had S/N > 3 and the observed m/z value was within 0.25 Th of the theoretical value. We plotted the probability of observing the c_n - and z_n -type product ions as a function of n for ETD and AI-ETD at laser powers 12-60 W for all PSMs from the LysC dataset (**Fig. 3**). For smaller ions ($c_1/z_1 - c_2/z_2$), as laser power increases, the probability of observation decreases; intermediate laser powers produce the

Table 1. Peptide spectral matches as a function of AI-ETD laser power for both Tryptic and LysC digested peptides.

| | Lysine-C | Trypsin |
|---------------|----------|---------|
| AI-ETD (12 W) | 1354 | 982 |
| AI-ETD (24 W) | 1566 | 1180 |
| AI-ETD (36 W) | 1841 | 1304 |
| AI-ETD (48 W) | 2022 | 1377 |
| AI-ETD (60 W) | 1980 | 1308 |

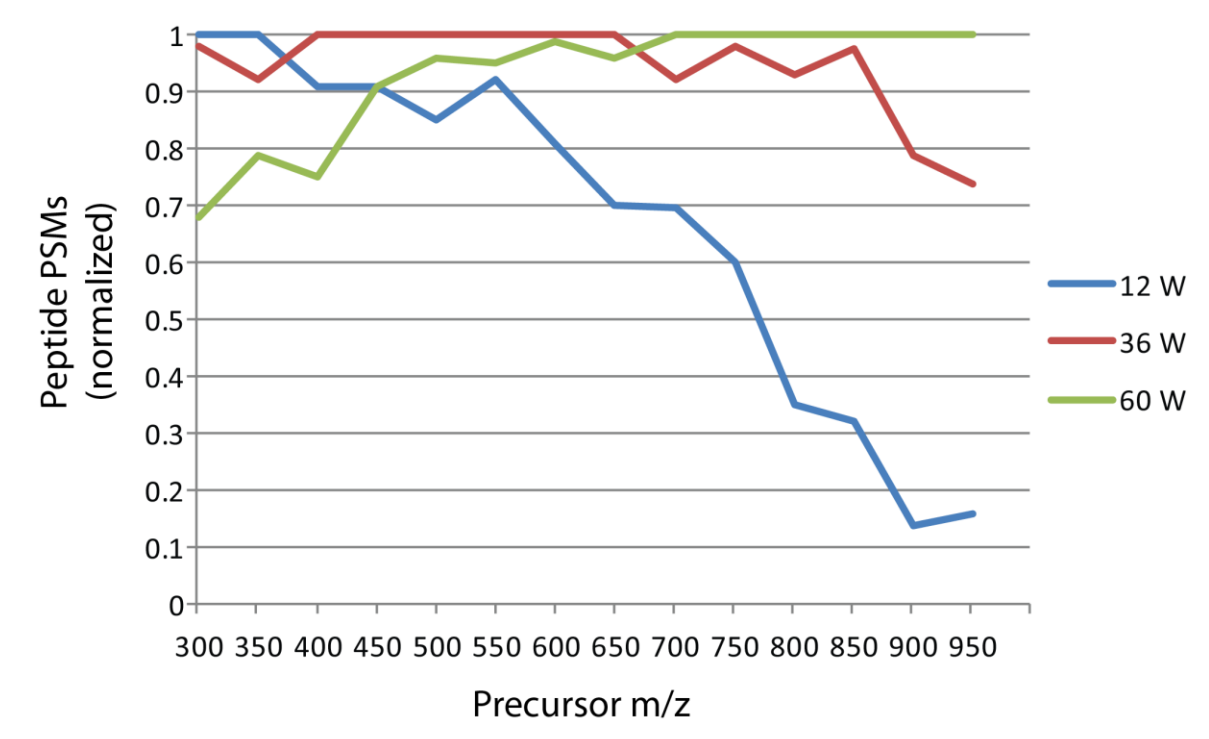


Figure 2. Peptide spectral matches as a function of precursor peptide m/z for AI-ETD at 12, 36, and 60 W AI-ETD laser power.

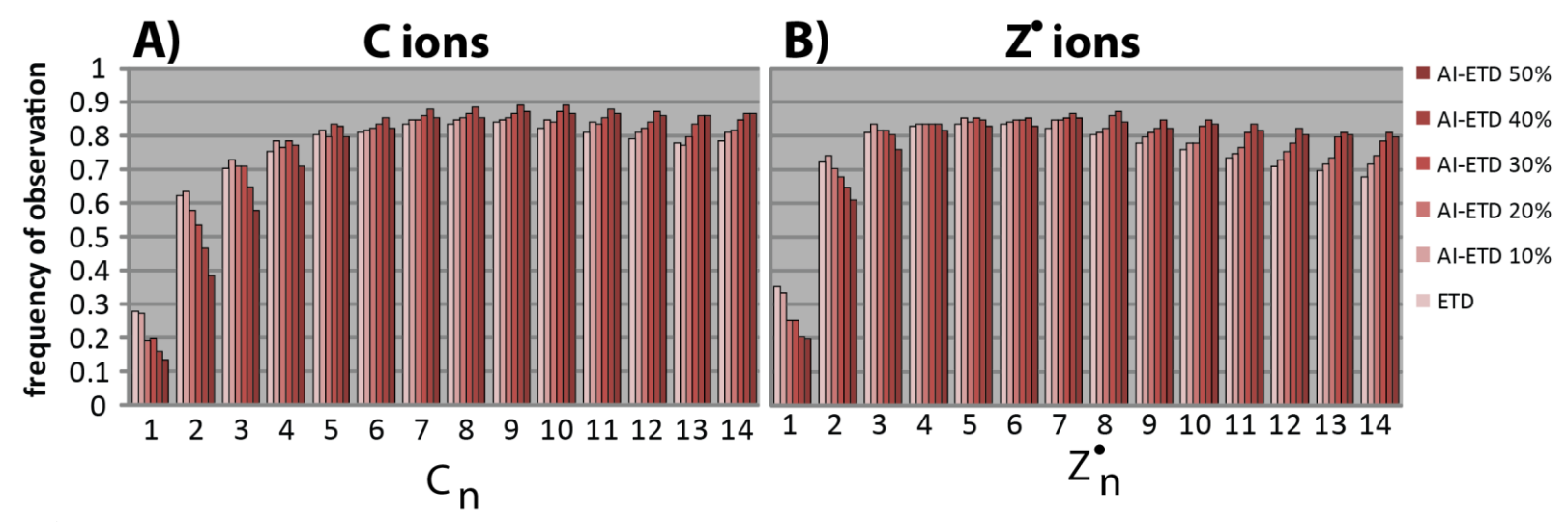


Figure 3. The probability of observing cn- (A) and zn- (B) as a function of n for ETD and AI-ETD at various laser powers. At low n values, low laser powers result in the greatest chance of observation, but with increasing n, higher laser powers lead to the highest probability of observation.

highest probability of observation for moderate sized product ions $(c_3/z_3 - c_6/z_6)$; larger product ions ($> c_0/z_6$) are most effectively generated using the highest laser powers. A recent study by Han *et al.* found that collisional activation of ETD product ions results mostly in a-, b-, y-, and x-type product ions.³² We anticipate IR activation of ETD product ions would have a similar effect. Thus secondary IR activation can decrease the probability of observing c- and z-type product ion, particularly for smaller product ions because (1) they have fewer degrees of molecular freedom, meaning there will be fewer channels to redistribute vibrational energy gained via infrared photons and (2) they have lower m/z values, in consequence the reduced Mathieu parameter (q-value) will be higher during the activation process. Glish, Brodbelt, and others have noted that the q-value influences ion position within an ion trap. Higher q-values can result in deeper pseudopotential wells, causing ions to spend a greater proportion of time in the center of the trap, and leading to a better overlap with the photon beam.^{33,34}

Larger ions have a higher probability of being formed at more intense laser powers because they come from large peptides (*i.e.*, c_{12} is only formed by peptides of at least 13 residues), which have greater magnitudes of gas phase secondary structure. Higher laser powers most effectively disrupt this secondary structure, enhancing the probability of their formation. For moderate-sized ions, intermediate powers achieve the highest probability of formation; though sufficient to disrupt peptide secondary structure, this level of heating does not induce extensive secondary IR activation.

The probabilities of c- and z-- type product ion formation are the primary factor determining PSM numbers at different AI-ETD laser powers. The small product ions

with less chance of being observed using AI-ETD conducted at high laser powers represent a relatively large percentage of all possible product ions for smaller precursors (m/z = 300-400), decreasing the probability of a PSM. Conversely, for peptide precursors with a high m/z value, the increased probability of observing the larger product ions more than compensates for the decreased probability of observing the first few ions, increasing the chance of a PSM. Because of this variability, we conclude that the most effective implementation of AI-ETD for shotgun proteomics is to set the laser power in a data-dependent manner, selecting modest laser powers for lower m/z peptide precursors and stronger laser powers for higher m/z peptide precursors.

Comparison of AI-ETD to ETD and CAD. The key motivation for this work was to evaluate the efficacy of AI-ETD as a fragmentation technique for interrogation of complex peptide mixtures as compared to current alternatives. Analyzing the data above and considering all three activation methods, AI-ETD (48 W) improves the numbers of PSMs relative to unassisted ETD for both tryptic and LysC analyses (**Table 2**). For LysC-digested peptides, the use of AI-ETD results in a substantial increase in PSMs relative to CAD; for trypsin-digested peptides, however, AI-ETD does not surpass CAD.

To determine which method is best for various types of peptide cations, we grouped the PSMs generated in these experiments based on precursor charge state (**Table 3**). These data show that for doubly protonated peptide precursors generated via either LysC or trypsin, CAD produces the most PSMs, although AI-ETD improves substantially upon ETD. For all other precursor charge states, for both tryptic and LysC peptides, AI-ETD identifies at least as many, and often more, peptides than either CAD or ETD.

Table 2. AI-ETD, ETD, and CAD peptide spectral match counts for both Tryptic and Lyscin-C derived peptides

| MS/MS Activation | Lysine-C | Trypsin |
|------------------|----------|---------|
| ETD | 1289 | 915 |
| CAD | 1366 | 2167 |
| AI-ETD | 2022 | 1377 |

Table 3. AI-ETD, ETD, and CAD peptide spectral match counts for both Tryptic and Lyscin-C derived peptides broken down by precursor charge state

| Lysine-C precursor Charge State IDs | | | Lysine-C precursor Charge State IDs | | | | | |
|-------------------------------------|-----|-----|-------------------------------------|-----|------|-----|-----|-----|
| | +2 | +3 | +4 | >+4 | +2 | +3 | +4 | >+4 |
| ETD | 3 | 506 | 493 | 287 | 2 | 605 | 248 | 60 |
| CAD | 360 | 624 | 287 | 95 | 1059 | 871 | 204 | 33 |
| AI-ETD | 73 | 819 | 677 | 453 | 140 | 860 | 299 | 78 |

SCX Fraction Analysis. Proteomic workflows often utilize two modes of separation prior to MS interrogation. To test the suitability of AI-ETD in this context, we next performed an experiment in which 12 SCX fractions of both LysC and tryptic digests were analyzed three times, using ETD, CAD, or AI-ETD. This experiment measures each activation technique based not only on the probability of PSM, but also on the duty cycle. AI-ETD laser power was set in a data-dependent manner, selecting laser power based upon precursor m/z and which power allowed for the highest probability of PSM for the whole cell lysate analyses (vide supra). Analysis of the tryptic SCX fractions revealed that while use of AI-ETD resulted in 9,130 PSMs, a considerable improvement over unassisted ETD (6,234), CAD (15,209) produced the most PSMs (Table 4). However, for the LysC fractions, AI-ETD produced 13,405 PSMs, eclipsing both ETD (7,968) and CAD (10,904). Further, while CAD interrogation of tryptic SCX fractions produced the most PSMs, AI-ETD analysis of LysC SCX fractions produced the greatest proteome coverage, reflecting the larger average size of peptides generated by LysC.

Early eluting SCX fractions contain mostly peptides which ionize in low charge states (*i.e.*, +2); thus, CAD generates the most PSMs for these analyses, although AI-ETD produces more PSMs than ETD. The middle fractions contain peptides which tend to ionize in moderate charge states, such that ETD often outperforms CAD. However, AI-ETD greatly extends the m/z range for which peptides can be successfully interrogated relative to ETD, meaning that for the middle fractions AI-ETD frequently improves over both CAD and ETD. The later fractions contain mostly peptides which ionize in high

Table 4. AI-ETD, ETD, and CAD peptide spectral match counts for both Tryptic and Lyscin-C derived peptides broken down by SCX fraction number. For higher number fractions (representing highly charged peptides), AI-ETD produced the most peptide identifications. Overall, AI-ETD analysis of Lysine-C derived peptides produces the greatest amino acid coverage of any pairing.

| | Lysine-C Peptide Identifications | | | Trypsin Peptide Identifications | | | |
|----------------|----------------------------------|---------|---------|---------------------------------|---------|---------|--|
| | ETD | AI-ETD | CAD | ETD | AI-ETD | CAD | |
| Fraction1-2 | 33 | 151 | 291 | 1 | 5 | 83 | |
| Fraction 3 | 247 | 444 | 1633 | 339 | 655 | 1544 | |
| Fraction 4 | 271 | 1050 | 2113 | 211 | 826 | 4443 | |
| Fraction 5 | 1073 | 1998 | 1789 | 763 | 1486 | 3044 | |
| Fraction 6 | 1454 | 1967 | 1400 | 1334 | 1535 | 2209 | |
| Fraction 7 | 1282 | 2354 | 1224 | 984 | 1323 | 1337 | |
| Fraction 8 | 870 | 1509 | 1035 | 935 | 1047 | 970 | |
| Fraction 9 | 776 | 1442 | 673 | 568 | 908 | 668 | |
| Fraction 10 | 386 | 563 | 200 | 621 | 789 | 609 | |
| Fraction 11 | 870 | 950 | 234 | 408 | 477 | 277 | |
| Fraction 12 | 706 | 977 | 312 | 70 | 79 | 25 | |
| Total Peptides | 7,968 | 13,405 | 10,904 | 6,234 | 9,130 | 15,209 | |
| Amino Acid | 146,343 | 281,120 | 212,834 | 96,779 | 150,485 | 241,070 | |
| Coverage | | | | | | | |

charge states; thus, though both ETD and AI-ETD are well suited, AI-ETD consistently improves over ETD.

The key distinction between the two datasets is the types of peptides produced by each enzyme; trypsin generates peptides which mostly elute in the earlier fractions for which CAD is best suited. In consequence, CAD is the superior method overall for the tryptic SCX fractions, although AI-ETD offers the best option for the later fractions. LysC, on the other hand, produces peptides which more evenly distribute across all fractions. CAD still generates the most PSMs for the early fractions, but AI-ETD produces the most PSMs overall, since the middle and later fractions contain a larger proportion of all peptides.

AI-ETD vs ETcaD. We next performed an experiment comparing AI-ETD (data-dependent laser power) with ETcaD using ES cell lysates generated via digestion with both trypsin and LysC (**Table 5**). AI-ETD results in improvement of ~50% (LysC) and ~80% (trypsin) in the number of PSMs generated over ETcaD. Because precursor charge state information is not available using a stand-alone ion trap, ETcaD was performed assuming a precursor charge state of +2, with the supplemental collisional activation step performed at an *m/z* value twice that of the precursor. An important comparison to make between AI-ETD and ETcaD, therefore, involves PSM numbers for doubly protonated peptides. By this metric, AI-ETD even more significantly improves over ETcaD, generating 2.4 (LysC) and 4.2 (Trypsin) times as many PSMs. We rationalize this improvement based on our previous observation that AI-ETD suffers less hydrogen abstraction than ETcaD; such abstractions produce even-electron *z*-type and

Table 5. AI-ETD and ETcaD peptide spectral matches for both Trypsin and Lysine-C derived peptides.

| | AI-ETD | ETcaD |
|----------------|--------|-------|
| Lys C; all z | 2978 | 1940 |
| Lys C; z=2 | 199 | 58 |
| Trypsin; all z | 2441 | 1344 |
| Trypsin; z=2 | 367 | 70 |

odd-electron c--type product ions, shifted by ~ 1 Da from their theoretically predicted value.²³

Shown in **Figure 4** are the AI-ETD and ETcaD scans of the doubly protonated precursor peptide ISSLLEEQFQQGK (m/z = 753). ETcaD and AI-ETD produce similar neutral loss patterns; this is expected as IRMPD and CAD are both considered 'slowheating' dissociation methods. 6 Secondary IR activation of the charge-reduced precursor would thus produce similar results as the CAD activation step of ETcaD. While both ETcaD and AI-ETD produce similar peptide sequence coverage, there is a marked difference between the types of product ions produced. AI-ETD produces nine z-type ions, eight of them odd electron (z·) and four c-type ions, all of them even electron. This near-complete sequence coverage and almost exclusive production of ions whose m/zvalues match those theoretically predicted yields a confident PSM (OMSSA e-value = 9.3x 10⁻⁴). In contrast, ETcaD also produces nine z-type ions, only five of which are odd electron $(z \cdot)$, and four c-type ions, only one of which are even electron, respectively. These shifted product ions result in a dubious PSM (OMSSA e-value of = 1.8), insufficient to identify the peptide within 1% FDR range. Different spectral search algorithms may lead to slightly different results when comparing AI-ETD and ETcaD; however, we conclude superior spectral specificity makes concomitant supplemental activation techniques such as AI-ETD superior to post ion-ion reaction techniques like ETcaD.

AI-ETD for Phosphopeptides. Because ETD is particularly well suited for the analysis of phosphopeptides, any method designed to augment ETD should be evaluated

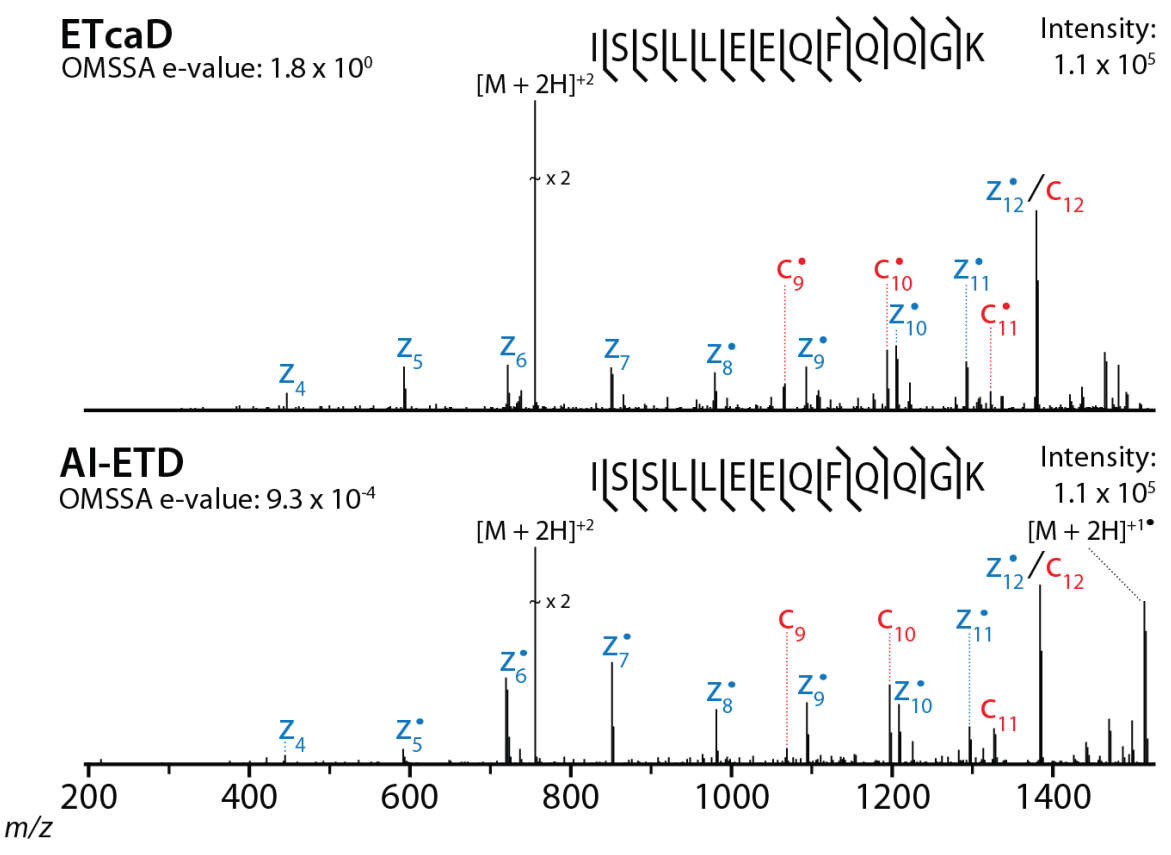


Figure 4. Spectra (single scan) resulting from either ETcaD (A) or AI-ETD (B) following dissociation of the doubly protonated peptide cation ISSLLEEQFQQGK. AI-ETD results almost exclusively in the formation of c- and z-type ions which match their theoretically predicted m/z values.

in this context.^{35,36} It is unclear whether the positive effects of AI-ETD will extend to phosphopeptides; Muddiman and others have noted that IRMPD of phosphopeptides results primarily in the neutral loss of the phosphoryl group.³⁷ The ETD, CAD, and AI-ETD spectra for doubly protonated peptide cation LRISSADsEK, (**Fig. 5**) however, reveal that AI-ETD greatly enhances the fragmentation of this peptide relative to ETD. ETD produces 22% peptide sequence coverage, insufficient to localize the serine phosphorylation; in contrast AI-ETD results in 89% sequence coverage and readily localizes the phosphorylation site. Application of CAD to this precursor produces a spectrum dominated by the neutral loss of H₃PO₄; however, sufficient backbone fragmentation is produced to generate 89% sequence coverage. This result, representing only a cursory evaluation, suggests that the efficacy of AI-ETD in the context of large-scale study of phosphopeptides is worth further evaluation. We note that more comprehensive studies of AI-ETD for phosphopeptides are ongoing.

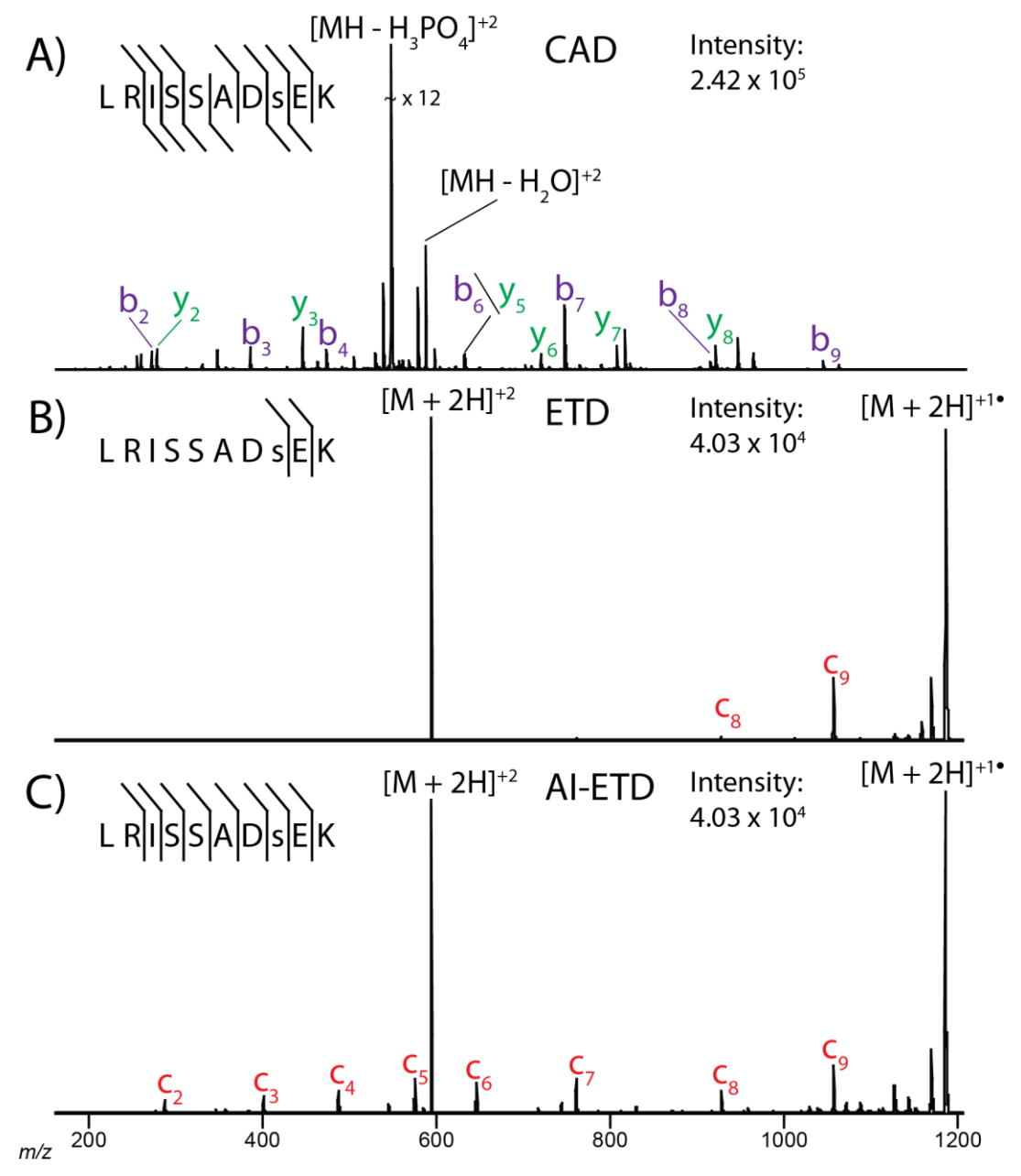


Figure 5. Spectra (single scan) resulting from either CAD (A), ETD (B), or AI-ETD (C) of the doubly protonated phosphopeptide cation LRISSADsEK

Discussion

We modified the hardware and firmware of an ETD-enabled QLT mass spectrometer, allowing for AI-ETD with upstream LC separations. Conducting a large-scale study, we conclude that for doubly protonated peptides, CAD is the most suitable activation method, although AI-ETD improves considerably over ETD. For all other peptide charge states, however, AI-ETD produces more PSMs (1% FDR) than both CAD and ETD. We evaluated the suitability of AI-ETD for large scale proteomics experiments by analyzing 12 SCX fractions generated with LysC and trypsin with ETD, CAD, and AI-ETD. For LysC, AI-ETD (13,405 PSMs), surpassed ETD (7,968) and CAD (10,904). Analysis of the tryptic SCX fractions reveals that while AI-ETD (9,130) improves upon the number of PSMs ETD produces (6,234), CAD generates the most PSMs (15,209) because more peptides are present in the earlier SCX fractions for which CAD is most effective.

We have demonstrated that the potential illustrated in our original description of AI-ETD (increased ETD fragmentation efficiency, little hydrogen abstraction) translates into a considerable boost in PSM numbers (1% FDR). Comparing AI-ETD to the previous ETD supplemental activation of choice, ETcaD, AI-ETD produces 80% (trypsin) and 50% (LysC) more PSMs. Improvements in AI-ETD duty cycle and implementation on hybrid MS platforms capable of providing precursor charge state information will improve AI-ETD further still. Implementation on such MS platforms will enable real-time selection of the activation technique allowing for the greatest probability of PSM between CAD and AI-ETD, based upon precursor m/z and charge state. We conclude that such incorporation with CAD in a decision tree fashion will

result in substantial improvements over either method individually, and would represent one of the most powerful peptide sequencing platforms described to date.

Methods

Cell Culture, Protein Harvest, and Protein Lysis: Human embryonic kidney (HEK) 293T cells were cultured to 90% confluency on 10cm plates containing high glucose (4.5g/L) DMEM (GIBCO) with 1% FBS (GIBCO). Cell pellets were collected after two washes in DPBS (GIBCO) and stored at -80°C. Upon lysis, the cell pellet was thawed and resuspended in 3mL of lysis buffer containing 8M urea, 75mM NaCl, 50mM Tris (pH 9), 50mM NaF, 1mM sodium orthovanadate, 6mM sodium pyrophosphate, complete mini EDTA-free protease inhibitor (Roche Diagonistics), and phosSTOP phophatase inhibitor (Roche Diagonotics). Lysis was accomplished via sonication. A 15 min room temperature spin at 3750 rpm allowed for collection of the supernatant.

Digestion: Approximately 3mL of lysis supernatant was subjected to 2.5mM DTT for 45 min at 37°C, followed by 7mM iodoacetamide for 30 min at room temperature to reduce and alkylate cysteine residues. Finally, an additional 2.5 mM DTT was added to the total volume for 15 min at room temperature. Two separate 500μg aliquots were isolated for subsequent digestion by sequencing grade modified trypsin (Promega) and lysyl endopeptidase LysC (Wako Chemicals). The first aliquot was diluted to 1.5M urea, 50mM Tris, and 10mM CaCl₂ and digested with 5 μg of trypsin overnight at 37°C. The second aliquot was diluted to 2M urea, 25mM Tris, and 1mM

CaCl₂ and digested with $5\mu g$ of LysC overnight at $37^{\circ}C$. The following morning, digestion reactions were quenched via addition of TFA to 0.5%. Each sample was desalted on a 50mg C₁₈ SepPak cartridge (Waters). The individual eluates underwent lyophilization followed by storage at $-20^{\circ}C$. For experimental use, eluates were resuspended in H₂O. SCX fractions of both trypsin- and LysC-digested whole cell lysates were prepared as previously described.³⁸

Mass Spectrometry, LC separation: All experiments were performed on a modified LTQ-XL (Thermo Fisher Scientific, San Jose CA) linear ion trap mass spectrometer (QLT) utilizing a nanoESI source for the generation of precursor peptide cations and NCI source for the generation of reagent anions as previously described.²³ For all experiments, azulene was used as the ETD reagent ion. Instrument modifications are detailed above. All AI-ETD experiments were performed using a Firestar T-100 Synrad 120-W CO₂ continuous wave laser (Mukilteo, WA).

LC separations were carried out using a NanoAcquity UPLC system (Waters, Milford, MA) as previously described, ^{39,40} using a 90 minute linear gradient from 1% to 35% acetonitrile followed by an additional 30 min at 1% acetonitrile for washing and equilibration for analysis of whole cell lysates and a similar 60 minute gradient for analysis of SCX fractions. For analysis of whole cell lysates, mass spectrometry methods consisted of an MS¹ scan followed by consecutive ETD, CAD, and AI-ETD data-dependent MS² scans of the two most intense precursors. For analysis of SCX fractions, an MS¹ scan was followed by MS² analysis of the six most intense precursors by ETD,

CAD, or AI-ETD. Precursors were dynamically excluded for 90 s using an exclusion window of +/- 1.5 Th. AGC target values were 40,000 for MS¹ and 10,000 for MS² analysis.

Database Searching and Data Analysis: Data reduction was performed with DTA Generator. OMSSA (version 2.1.7) was used to search spectra against the International Protein Index (IPI; http://www.ebi.ac.uk/IPI/) human database version 3.53.41 Average mass tolerances of +/- 5 Th and +/- 0.5 Th were used for precursor and product *m/z*, respectively, with carbaminomethylation of cysteine set as a fixed modification and oxidation of methionine set as a variable modification. False discovery rates (FDR) were determined using the concatenated forward-reverse database method determined false discovery rates (FDR).

References

- Hunt, D. F., Yates, J. R., Shabanowitz, J., Winston, S. & Hauer, C. R. PROTEIN SEQUENCING BY TANDEM MASS-SPECTROMETRY. *Proc. Natl. Acad. Sci. U. S. A.* **83**, 6233-6237, doi:10.1073/pnas.83.17.6233 (1986).
- Aebersold, R. & Mann, M. Mass spectrometry-based proteomics. *Nature* **422**, 198-207, doi:10.1038/nature01511 (2003).
- Coon, J. J., Syka, J. E. P., Shabanowitz, J. & Hunt, D. F. Tandem mass spectrometry for peptide and protein sequence analysis. *Biotechniques* **38**, 519-+, doi:10.2144/05384te01 (2005).
- de Godoy, L. M. F. *et al.* Comprehensive mass-spectrometry-based proteome quantification of haploid versus diploid yeast. *Nature* **455**, 1251-U1260, doi:10.1038/nature07341 (2008).
- Washburn, M. P., Wolters, D. & Yates, J. R. Large-scale analysis of the yeast proteome by multidimensional protein identification technology. *Nat. Biotechnol.* **19**, 242-247, doi:10.1038/85686 (2001).
- Sleno, L. & Volmer, D. A. Ion activation methods for tandem mass spectrometry. *J. Mass Spectrom.* **39**, 1091-1112, doi:10.1002/jms.703 (2004).

- Hunt, D. F., Buko, A. M., Ballard, J. M., Shabanowitz, J. & Giordani, A. B. Sequence-Analysis of Polypeptides by Collision Activated Dissociation on a Triple Quadrupole Mass-Spectrometer. *Biomedical Mass Spectrometry* **8**, 397-408 (1981).
- Mcluckey, S. A. Principles of Collisional Activation in Analytical Mass-Spectrometry. *Journal of the American Society for Mass Spectrometry* **3**, 599-614 (1992).
- 9 Verentchikov, A. N., Ens, W. & Standing, K. G. REFLECTING TIME-OF-FLIGHT MASS-SPECTROMETER WITH AN ELECTROSPRAY ION-SOURCE AND ORTHOGONAL EXTRACTION. *Anal. Chem.* **66**, 126-133, doi:10.1021/ac00073a022 (1994).
- Morris, H. R. *et al.* High sensitivity collisionally-activated decomposition tandem mass spectrometry on a novel quadrupole/orthogonal-acceleration time-of-flight mass spectrometer. *Rapid Commun. Mass Spectrom.* **10**, 889-896, doi:10.1002/(sici)1097-0231(19960610)10:8<889::aid-rcm615>3.3.co;2-6 (1996).
- Wysocki, V. H., Tsaprailis, G., Smith, L. L. & Breci, L. A. Special feature: Commentary Mobile and localized protons: a framework for understanding peptide dissociation. *J. Mass Spectrom.* **35**, 1399-1406, doi:10.1002/1096-9888(200012)35:12<1399::aid-jms86>3.0.co;2-r (2000).
- Dongre, A. R., Jones, J. L., Somogyi, A. & Wysocki, V. H. Influence of peptide composition, gas-phase basicity, and chemical modification on fragmentation efficiency: Evidence for the mobile proton model. *Journal of the American Chemical Society* **118**, 8365-8374 (1996).
- Schroeder, M. J., Shabanowitz, J., Schwartz, J. C., Hunt, D. F. & Coon, J. J. A neutral loss activation method for improved phosphopeptide sequence analysis by quadrupole ion trap mass spectrometry. *Anal. Chem.* **76**, 3590-3598, doi:10.1021/ac0497104 (2004).
- DeGnore, J. P. & Qin, J. Fragmentation of phosphopeptides in an ion trap mass spectrometer. *Journal of the American Society for Mass Spectrometry* **9**, 1175-1188 (1998).
- Olsen, J. V. & Mann, M. Improved peptide identification in proteomics by two consecutive stages of mass spectrometric fragmentation. *Proc. Natl. Acad. Sci. U. S. A.* **101**, 13417-13422, doi:10.1073/pnas.0405549101 (2004).
- Villen, J., Beausoleil, S. A. & Gygi, S. P. Evaluation of the utility of neutral-loss-dependent MS3 strategies in large-scale phosphorylation analysis. *Proteomics* **8**, 4444-4452, doi:10.1002/pmic.200800283 (2008).
- Ulintz, P. J. *et al.* Comparison of MS(2)-Only, MSA, and MS(2)/MS(3) Methodologies for Phosphopeptide Identification. *J. Proteome Res.* **8**, 887-899, doi:10.1021/pr800535h (2009).
- Zubarev, R. A., Kelleher, N. L. & McLafferty, F. W. Electron capture dissociation of multiply charged protein cations. A nonergodic process. *J. Am. Chem. Soc.* **120**, 3265-3266, doi:10.1021/ja973478k (1998).

- Syka, J. E. P., Coon, J. J., Schroeder, M. J., Shabanowitz, J. & Hunt, D. F. Peptide and protein sequence analysis by electron transfer dissociation mass spectrometry. *Proceedings of the National Academy of Sciences of the United States of America* **101**, 9528-9533 (2004).
- Coon, J. J., Syka, J. E. P., Schwartz, J. C., Shabanowitz, J. & Hunt, D. F. Anion dependence in the partitioning between proton and electron transfer in ion/ion reactions. *International Journal of Mass Spectrometry* **236**, 33-42 (2004).
- Good, D. M. & Coon, J. J. Advancing proteomics with ion/ion chemistry. *Biotechniques* **40**, 783-789 (2006).
- Good, D. M., Wirtala, M., McAlister, G. C. & Coon, J. J. Performance characteristics of electron transfer dissociation mass spectrometry. *Mol. Cell. Proteomics* **6**, 1942-1951, doi:10.1074/mcp.M700073-MCP200 (2007).
- Swaney, D. L. *et al.* Supplemental activation method for high-efficiency electron-transfer dissociation of doubly protonated peptide precursors. *Anal. Chem.* **79**, 477-485, doi:10.1021/ac061457f (2007).
- Du, Y., Parks, B. A., Sohn, S., Kwast, K. E. & Kelleher, N. L. Top-down approaches for measuring expression ratios of intact yeast proteins using Fourier transform mass spectrometry. *Anal. Chem.* **78**, 686-694, doi:10.1021/ac050993p (2006).
- Oh, H. *et al.* Secondary and tertiary structures of gaseous protein ions characterized by electron capture dissociation mass spectrometry and photofragment spectroscopy. *Proc. Natl. Acad. Sci. U. S. A.* **99**, 15863-15868, doi:10.1073/pnas.212643599 (2002).
- Breuker, K., Oh, H. B., Horn, D. M., Cerda, B. A. & McLafferty, F. W. Detailed unfolding and folding of gaseous ubiquitin ions characterized by electron capture dissociation. *J. Am. Chem. Soc.* **124**, 6407-6420, doi:10.1021/ja012267j (2002).
- 27 Senko, M. W., Speir, J. P. & McLafferty, F. W. COLLISIONAL ACTIVATION OF LARGE MULTIPLY-CHARGED IONS USING FOURIER-TRANSFORM MASS-SPECTROMETRY. *Anal. Chem.* **66**, 2801-2808, doi:10.1021/ac00090a003 (1994).
- Cooper, H. J., Hakansson, K. & Marshall, A. G. The role of electron capture dissociation in biomolecular analysis. *Mass Spectrom. Rev.* **24**, 201-222, doi:10.1002/mas.20014 (2005).
- Horn, D. M., Ge, Y. & McLafferty, F. W. Activated ion electron capture dissociation for mass spectral sequencing of larger (42 kDa) proteins. *Anal. Chem.* **72**, 4778-4784, doi:10.1021/ac000494i (2000).
- Xia, Y., Han, H. & McLuckey, S. A. Activation of intact electron-transfer products of polypeptides and proteins in cation transmission mode ion/ion reactions. *Analytical Chemistry* **80**, 1111-1117 (2008).
- Ledvina, A. R. *et al.* Infrared Photoactivation Reduces Peptide Folding and Hydrogen-Atom Migration following ETD Tandem Mass Spectrometry. *Angew. Chem.-Int. Edit.* **48**, 8526-8528, doi:10.1002/anie.200903557 (2009).

- Han, H. L., Xia, Y. & McLuckey, S. A. Ion trap collisional activation of c and z(center dot) ions formed via gas-phase ion/ion electron-transfer dissociation. *J. Proteome Res.* **6**, 3062-3069, doi:10.1021/pr070177t (2007).
- Remes, P. M. & Glish, G. L. Mapping the Distribution of Ion Positions as a Function of Quadrupole Ion Trap Mass Spectrometer Operating Parameters to Optimize Infrared Multiphoton Dissociation. *J. Phys. Chem. A* **113**, 3447-3454, doi:10.1021/jp808955w (2009).
- Gardner, M. W. *et al.* Infrared Multiphoton Dissociation of Peptide Cations in a Dual Pressure Linear Ion Trap Mass Spectrometer. *Anal. Chem.* **81**, 8109-8118, doi:10.1021/ac901313m (2009).
- Swaney, D. L., Wenger, C. D., Thomson, J. A. & Coon, J. J. Human embryonic stem cell phosphoproteome revealed by electron transfer dissociation tandem mass spectrometry. *Proc. Natl. Acad. Sci. U. S. A.* **106**, 995-1000, doi:10.1073/pnas.0811964106 (2009).
- Grimsrud, P. A., Swaney, D. L., Wenger, C. D., Beauchene, N. A. & Coon, J. J. Phosphoproteomics for the Masses. *ACS Chem. Biol.* 5, 105-119, doi:10.1021/cb900277e (2010).
- Flora, J. W. & Muddiman, D. C. Selective, sensitive, and rapid phosphopeptide identification in enzymatic digests using ESI-FTICR-MS with infrared multiphoton dissociation. *Anal. Chem.* **73**, 3305-3311, doi:10.1021/ac010333u (2001).
- Swaney, D. L., McAlister, G. C. & Coon, J. J. Decision tree-driven tandem mass spectrometry for shotgun proteomics. *Nat. Methods* 5, 959-964, doi:10.1038/nmeth.1260 (2008).
- Zhang, Y., Ficarro, S. B., Li, S. J. & Marto, J. A. Optimized Orbitrap HCD for Quantitative Analysis of Phosphopeptides. *J. Am. Soc. Mass Spectrom.* **20**, 1425-1434, doi:10.1016/j.jasms.2009.03.019 (2009).
- McAlister, G. C., Phanstiel, D., Wenger, C. D., Lee, M. V. & Coon, J. J. Analysis of Tandem Mass Spectra by FTMS for Improved Large-Scale Proteomics with Superior Protein Quantification. *Anal. Chem.* **82**, 316-322, doi:10.1021/ac902005s (2010).
- Geer, L. Y. *et al.* Open mass spectrometry search algorithm. *J. Proteome Res.* **3**, 958-964, doi:10.1021/pr0499491 (2004).
- Moore, R. E., Young, M. K. & Lee, T. D. Qscore: An algorithm for evaluating SEQUEST database search results. *J. Am. Soc. Mass Spectrom.* **13**, 378-386, doi:10.1016/s1044-0305(02)00352-5 (2002).
- Elias, J. E. & Gygi, S. P. Target-decoy search strategy for increased confidence in large-scale protein identifications by mass spectrometry. *Nat. Methods* **4**, 207-214, doi:10.1038/nmeth1019 (2007).

Chapter 4

A Segmented Cell for Expedient Activated-Ion ETD

Summary

Since its original description, Electron Transfer Dissociation (ETD) has become an important tool for biological researchers. While ETD has proven to be useful in a number of applications, there are nonetheless opportunities to improve ETD further; namely relatively slow activation time and diminishing effectiveness with increasing precursor m/z. To address these two shortcomings, we describe and characterize ETD performed in an RF device outfitted with an IR laser and distal from that used for precursor accumulation and isolation (segmented cell). Compared to the linear quadrupole ion trap (QLT), where ETD was previously conducted on this system, the segmented cell operates at a higher RF frequency (~2.37 MHz vs. 1.14 MHz), which increases the maximal number density of ions, and by proxy the maximal ETD reaction rate. Accordingly, the reaction time required to reach the optimal ETD product ion yield is reduced by greater ~ 2-fold. By equipping the segmented cell with an IR laser, we enable activated-ion ETD (AI-ETD), which we have previously shown increases the effectiveness of ETD for high m/z precursors. Using this arrangement, we find that as compared to previous ETD implementations (no IR photons, performed in the QLT) we identify more unique peptides (2,368 vs. 3,789) over the course of an LC-MS/MS experiment. This increase is due to both faster MS/MS duty cycle (afforded by the segmented cell) and a higher probability of peptide identification for each individual MS/MS event (due to IR activation). Using this instrument to interrogate a complex mixture of phosphopeptides, we identify nearly three times the number of unique phosphopeptides (647 vs. 1,575) compared to the previous ETD implementation. Finally, by differentiating the RF devices used for ion isolation and ion-ion reactions, we enable a multiple-fills scan function during which precursor cations are iteratively selected in the QLT and stored in the segmented cell. Following the accumulation of multiple loads of precursor ions, the summed population is dissociated and m/z analyzed. In so doing, we substantially increase the maximum number of precursor ions that we can interrogate in a single MS² event, increasing the number of dissociation channels which can be sufficiently populated, and thereby enhancing the utility of the segmented cell for whole protein analysis.

Introduction

In the last few years, mass spectrometer technology for proteomics has rapidly advanced. With the advent of new mass analyzers (i.e. the orbitrap),¹ novel hybrid instrument configurations (e.g., dual-cell ion trap designs),^{2,3} and new fragmentation techniques (e.g., ECD, ETD),^{4,5} the scope of biological questions which can be answered in a single experiment has expanded dramatically.^{6,7} Electron-based fragmentation methods ECD⁵ and ETD^{4,8} have become critical components of a number of high-impact proteomics workflows. Both of these dissociation techniques are unique in their tendency to cleave

the inter-residue N-C_a bonds of peptides with relative indifference to amino acid composition and the presence of labile post-translation modifications (PTMs). Because of these unique properties, ECD and ETD have allowed researchers to routinely investigate areas of proteomes that were previously difficult or impossible to characterize, including whole protein analysis, 9,10 combinatorial PTM patterns of histones, $^{11-13}$ localization and characterization of sites of glycosylation, $^{14-18}$ and global phosphorylation analysis, $^{19-21}$ to name a few. Nonetheless, there are still opportunities to improve aspects of ETD, (*i.e.*, fragmentation rate, the time required to accumulate reagent ions, fragmentation efficiency of high m/z precursors). The issue of low fragmentation efficiency has been somewhat addressed using a variety of techniques (*vide infra*), including the use of IR photons concomitant to ETD reaction (Activated-Ion ETD, AI-ETD; employed in the present study). Decreasing the required ETD reaction time, however, remains limited by the maximal reagent number density attainable in the region of the mass spectrometer tasked with conducting ion-ion reactions.

Many studies utilizing ETD has been somewhat limited by the fact that both the physical (e.g., ro, differential DC segment lengths) and operating parameters (e.g., RF amplitude and frequency) of the RF device designated for ETD were chosen to optimize functions unrelated to ETD; moreover the same RF device must retain the capability to perform other tasks associated with MS^2 scan functions (e.g., accumulation, isolation, energetic fragmentation, and <math>m/z analysis of ions). The optimal trapping conditions for ion-ion reactions differ greatly from the conditions best suited for other mass spectrometric tasks. In the context of ion-ion reactions, the optimal trapping conditions are essentially those

that allow for the fastest ion-ion reaction. Ignoring the role that the chemistry of participating ions plays (e.g., charge state, mass), ion-ion reaction rate is primarily determined by the density and overlap of the participating ion populations.²² The trapping conditions necessary to create dense ion populations (deep potential wells and strong ion dampening forces) negatively impact other mass spectrometric activities; for example ion ejection during m/z analysis is rendered more difficult as the strong dampening forces through which the ions must be removed tend to fragment the ions prior to detection. By divorcing the RF device used to conduct ion-ion reactions from the RF device used for other mass spectrometric activities, we can optimize the ion-ion reaction vessel without negatively impacting the other functionalities of the mass spectrometer.

Here, we describe a modified hybrid dual cell QLT-orbitrap mass spectrometer. In place of the standard RF device used to conduct beam-type collisional activation (HCD), we have installed a segmented ion trap which we have tailored for conducting ion-ion reactions (segmented cell). The segmented cell is outfitted with electronics which provide RF to both the rods and end lenses, allowing for the simultaneous trapping of ions of opposite polarity in the same spatial region, termed charge-sign independent trapping (CSIT). In this modified instrument, precursor ions are injected and isolated in the QLT and then transferred to the segmented cell. Once there, anions are injected from a distal CI source, ion-ion reactions are performed, and the resulting fragment ion population is transferred to either the low pressure QLT or the orbitrap for m/z analysis.

Our new trap design allows us to address the various fragmentation issues associated with ETD. As noted by ourselves and others, ETD suffers from poor fragmentation efficiency for high m/z peptides.²³⁻²⁷ Ideally, each ETD event results in the transfer of an electron to the precursor, followed by a radical rearrangement that ultimately results in the production of c- and z- ions. Sometimes, however, precursor peptides capture an electron but fail to separate into c- and z-type ions. The probability of precursor peptides undergoing non-dissociative electron transfer (ETnoD)²⁷ is elevated for high precursor m/z peptides. Shortly after the inception of ECD, McLafferty observed similar effects for ECD, positing that non-covalent interactions bind the dissociation c- and z- ion pairs together.²⁸ Practitioners of ECD devised a number of techniques to mitigate the detrimental effects of non-dissociative electron transfer. Termed "activated-ion ECD" (AI-ECD), these techniques shared the common strategy of disruption of non-covalent cation peptide interactions.²⁹⁻³⁴ This disruption leads to more efficient generation of cand z- type ions, and consequently higher fragmentation efficiency and bond heterogeneity.

Similar efforts have been undertaken for ETD. Increasing the bath gas temperature of a quadrupole ion trap during ETD results in some disruption of peptide secondary structure, allowing for improved ETD efficiency. Alternatively ETnoD products can be coaxed apart into the respective c- and z- type ions using either resonant excitation or beam-type collisional activation, termed ETcaD. Though effective for increasing peptide sequence coverage, ETcaD techniques produce primarily odd electron c-type ions (c^{\bullet} -) and even electron z-type ions. These product ions, both of which are shifted ~1 Da from

their theoretical value, are believed to result from the abstraction of a hydrogen atom from the c-type ion by the z- type ion while the two ions are bound together by noncovalent interactions.³⁶ ETcaD spectra thus contain product ion isotopic envelopes comprising both odd and even electron species, complicating both manual and automated Recently, we have developed a technique involving the spectral interpretation. bombardment of participating ions using IR photons concomitant to ETD reactions, termed activated-ion ETD (AI-ETD).^{24,37} By continually disrupting peptide secondary structure, we not only increase ETD fragmentation efficiency, but do so while minimizing the opportunities for hydrogen abstraction, resulting in the near-exclusive production of even electron c- and odd electron z- type ions. We have combined our segmented cell with the AI-ETD approach by installing a window in the segmented cell manifold and excavating a line of sight through the reagent anion transfer multipole. Taken together, these technologies represent a next generation ETD implementation, an implementation on par with other rapidly advancing areas of mass spectrometer technology.

In addition to facilitating faster ion-ion reactions, the segmented cell enables advanced scan functions. For example, multiple loads of precursor ions can be injected into the segmented cell, allowing for very large ion populations to be accumulated prior to ETD activation. Similar scan functions have recently been described during which multiple loads of precursor cations were injected into an FT-ICR prior to ECD activation. These scan functions are particularly well suited for top-down analysis, as analysis of even modest-sized whole proteins typically necessitates spectral averaging or microscans,

requiring long acquisition times. Using the segmented cell, it is possible to instead use iterative ion injection, isolation, and transfer to the segmented cell to accumulate a large ion population. Following this, ETD activation and m/z analysis are performed, decreasing the time requirement to obtain high quality top-down ETD spectra. We have demonstrated that using this scan function results in a linear increase in product ion S/N, and also demonstrate the application of this approach to whole-protein characterization with very encouraging first results.

Results

Characterization of the Segmented Cell

A primary goal of this work is to decrease the activation time required to perform ETD. This activation time leads to a comparatively long duty cycle for ETD MS^2 relative to alternatives (*e.g.*, CAD, HCD). By performing ETD in an RF segmented cell, tasked solely with conducting ion-ion reactions, we can optimize the trapping parameters of this device (*e.g.*, trap dimensions, RF settings) for ETD. The pseudo first order ion-ion reaction rate as described by McLuckey²² is shown in **Equation. 1**:

$$[\mathbf{MH_n}^{n+}]_t = [\mathbf{MH_n}^{n+}]_0 \exp^{(-Nk(z)t)}$$
 (Equation 1)

Where $[MH_n^{n+}]_t$ is the time dependent precursor cation population, $[MH_n^{n+}]_0$ is the initial precursor cation population, k(z) is the charge (z) dependent ion-ion rate constant, t is reaction time, and N is the number density of the anion population. The parameters k and z are primarily determined by the physical characteristics of the precursor and reagent ions (**Eqn. 2**):

$$K = v (\pi/2)[Z_1 Z_2 e^2/\mu v^2]^2$$
 (Equation 2)

Where v is the relative velocity and μ is the reduced mass of the two participating ions and Z_1 and Z_2 are the charge states of the cation and anion, respectively. The relative velocity is influenced somewhat by the bath gas pressure. We manually adjusted the nitrogen flow into the segmented cell to allow for efficient trapping and ion transfer into and out of the segmented cell. We therefore estimate that the relative velocity of ETD participant ions is roughly equivalent for both the QLT and segmented cell. The parameter which is independent of precursor or reagent chemistry and susceptible to manipulation using the segmented cell is the number density, N, of the reagent anions. The most straightforward way to consider relevant parameters is to use the pseudopotential well model of ion behavior (Eqn. 3):

$$N = 3/64\pi * (m\Omega^2/z^2)*q^2$$
 (Equation 3)

where Ω is the RF frequency, m is the mass of the ion, z is the charge state of the ion, and q is the reduced Mathieu parameter. At a fixed reduced Mathieu parameter (q), number density of the reagent population increases roughly proportional to the square of the RF frequency. To explicitly evaluate the effect of higher RF frequency, we treated the q-value as an independent variable. By default, ETD activation takes place at a q-value of 0.40 relative to m/z 202. This places the low mass cutoff at approximately m/z = 90. We injected calibration solution into the segmented cell and slowly increased the RF amplitude. When we observed that the low mass cutoff reached $m/z \sim 90$, we inferred that the q-value relative to m/z 202 at this level was roughly equal to 0.4 (Fig. 1). Holding the q-value constant for both devices, the time-resolved ETD product ion

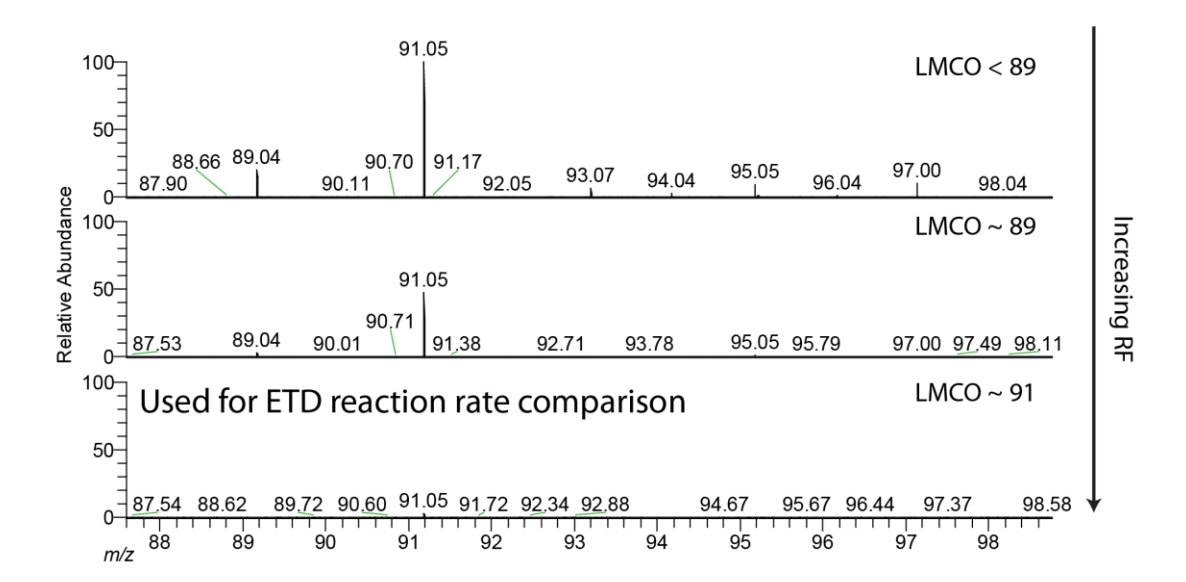


Figure 1. Determination of q-value in segmented cell. By injecting a mixture of ions into the segmented cell, raising the RF amplitude, and observing the low mass cutoff the q-value relative to m/z 202 can be inferred.

abundance plot of triply-protonated angiotensin reveals that the optimal reaction time using the segmented cell (~18 ms) is less than half of that using QLT (~40 ms) (Fig. 2). Assuming that optimal ETD reaction time scales with the square of precursor charge state, this translates to optimal reaction times of ~90 ms in the QLT vs. ~40 ms in the segmented cell for doubly protonated peptides. Excluding cation accumulation time (set dynamically depending upon precursor ionization efficiency), the 50ms activation time difference translates to ~15% of the MS²duty cycle. Moreover, the ETD reaction time required for quadrupoly charged or higher peptides (< 10 ms) is almost negligible. Besides increasing the density of a fixed population of reagent anions, an alternative method to increasing the ion/ion reaction rate is to accumulate more reagent ions in the trap prior to the reaction. Increasing the number of reagent ions contained within the fixed dimensions of the RF device increases the number density, up to the point at which the storage space charge capacity is exceeded. The reagent anion population, like the precursor cation population, is regulated using AGC. The flux of anions from the CI source is estimated using the quadrupole ion trap analyzer (due to its faster m/z analysis speed), allowing for an accurate estimation of the injection time required to accumulate a given number of reagent ions in the ion traps to be easily determined. When reagent anions leave the CI source they first pass through a long multipole before reaching the segmented cell. IF ETD reactions are to be conducted in the segmented cell, they are trapped in the back section of that device. If ETD is to be conducted in the QLT, the ions continue to travel onwards, passing through the segmented cell, the C-Trap, an additional multipole ion guide, and the low-pressure quadrupole ion trap before they are trapped in

| technique: | LTQ | Segmented cell |
|------------|------------------|------------------|
| maximum: | 40 ms | 18 ms |
| υ: | ~ 1.14 MHz | ~ 2.37 MHz |
| q-value: | 0.40 @ m/z = 202 | 0.40 @ m/z = 202 |

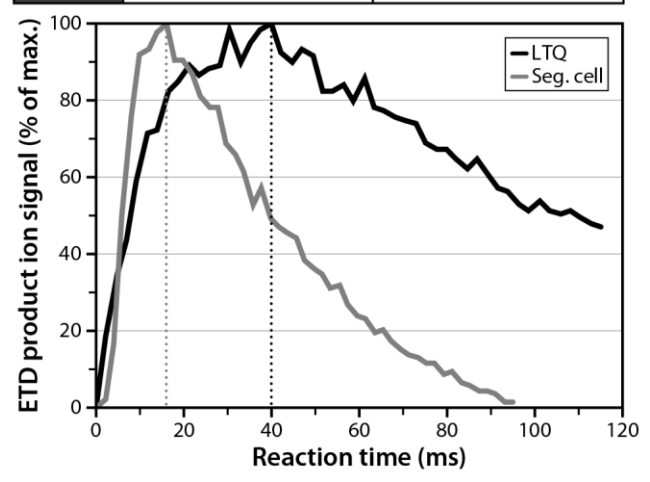


Figure 2. Time-resolved ETD product ion yields for the segmented cell and QLT ion trap. The segmented cell operates at a higher RF frequency; the result of which is higher ion density and concomitantly higher ion-ion reaction rates (>2 fold faster).

the high-pressure quadrupole ion trap. In consequence, reagent ions have to travel a much shorter distance to reach the segmented cell (relative to the high-pressure quadrupole ion trap). This results in shorter ion flight times and more efficient ion transfers; the consequence of which is generally shorter injection times for the segmented cell compared to the high-pressure trap (when accumulating the same number of ions) (**Fig. 3**).

The two plots were collected performing ETD of doubly protonated Substance P in both the QLT (75 ms) and the segmented cell (40 ms), with total product ion intensity divided by unreacted precursor intensity monitored as a function of the reagent AGC target, normalized to one. In each case, as reagent ion AGC target is increased, eventually a saturation point is reached, reflecting the approximate storage space charge capacity of the RF device used for ETD. Using the segmented cell, 80% saturation is achieved at a reagent AGC accumulation time of ~ 9 ms. In contrast, the QLT reaches 80% saturation at a reagent AGC accumulation time of ~ 17 ms. In addition to faster ETD reaction rates, the segmented cell therefore also requires less time devoted to the accumulation of anions as compared to the QLT.

Using multiple precursor fills for top-down proteomics

Large (> 10 kDa) whole protein analysis is challenging because as protein size increases:

1) So does the number of possible fragment ions, dividing limited precursor signal into increasing numbers of fragment channels, 2) Higher average charge states mean fewer absolute numbers of precursor ions at a given AGC target (space-charge is dictated by charges, not molecules), and 3) Isotopic envelopes of product ions become larger, further

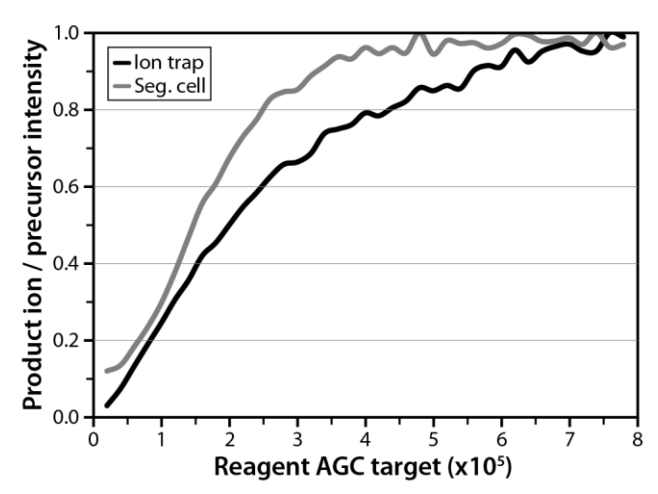


Figure 3. ETD product Ion intensity divided by unreacted precursor intensity vs. Reagent AGC target. The segmented cell is located closer to the reagent CI source than the QLT, with substantially fewer ion optical elements for anions to traverse. Because of this proximity, the segmented cell reaches $\sim 80\%$ saturation at a target of $\sim 2 \times 10^5$, approximately half the value associated with the QLT. In consequence, less anion accumulation time is required for ETD performed in the segmented cell vs. ETD performed in the QLT.

diluting the signal associated with the product ions. 41,42 This cadre of limitations results in an inverse relationship between average product ion S/N and protein size. Most practicioners of top-down proteomics utilize spectral averaging to mitigate the low S/N associated with large protein MS^2 spectra. This is not the ideal solution; statistics dictate that S/N increases proportional to \sqrt{n} , where n is the number of spectra averaged. The diminishing rate of return associated with this approach means that to obtain spectra having acceptable S/N, prohibitively long acquisition times may be required for very large precursors, rendering the overall approach incompatible with the online separations which dominate modern proteomics.

The more ideal solution is to interrogate higher numbers of precursor peptides during each MS² event; the S/N will in this case increase in direct proportion with the number of precursor ions sampled. The caveat with this approach for standard ion trap instrumentation is that the isolation space charge capacity of the trap ultimately imposes the limit of how many precursor charges may be isolated and fragmented in a single MS² event. An advantage of using the segmented cell is that the RF device used for isolation is divorced from the the one used for ion-ion reactions. In consequence, we can iteratively isolate precursor cations followed by transmission to the segmented cell, building up a large population of precursor cations, followed by a single set of activation and analysis events (**Fig. 4**). By using this scan function, the maximum number of precursor charges that can be sampled in a single scan sequence is liberated from the isolation space charge limit of the ion traps (~ 5x10⁵). The limit to how many precursor

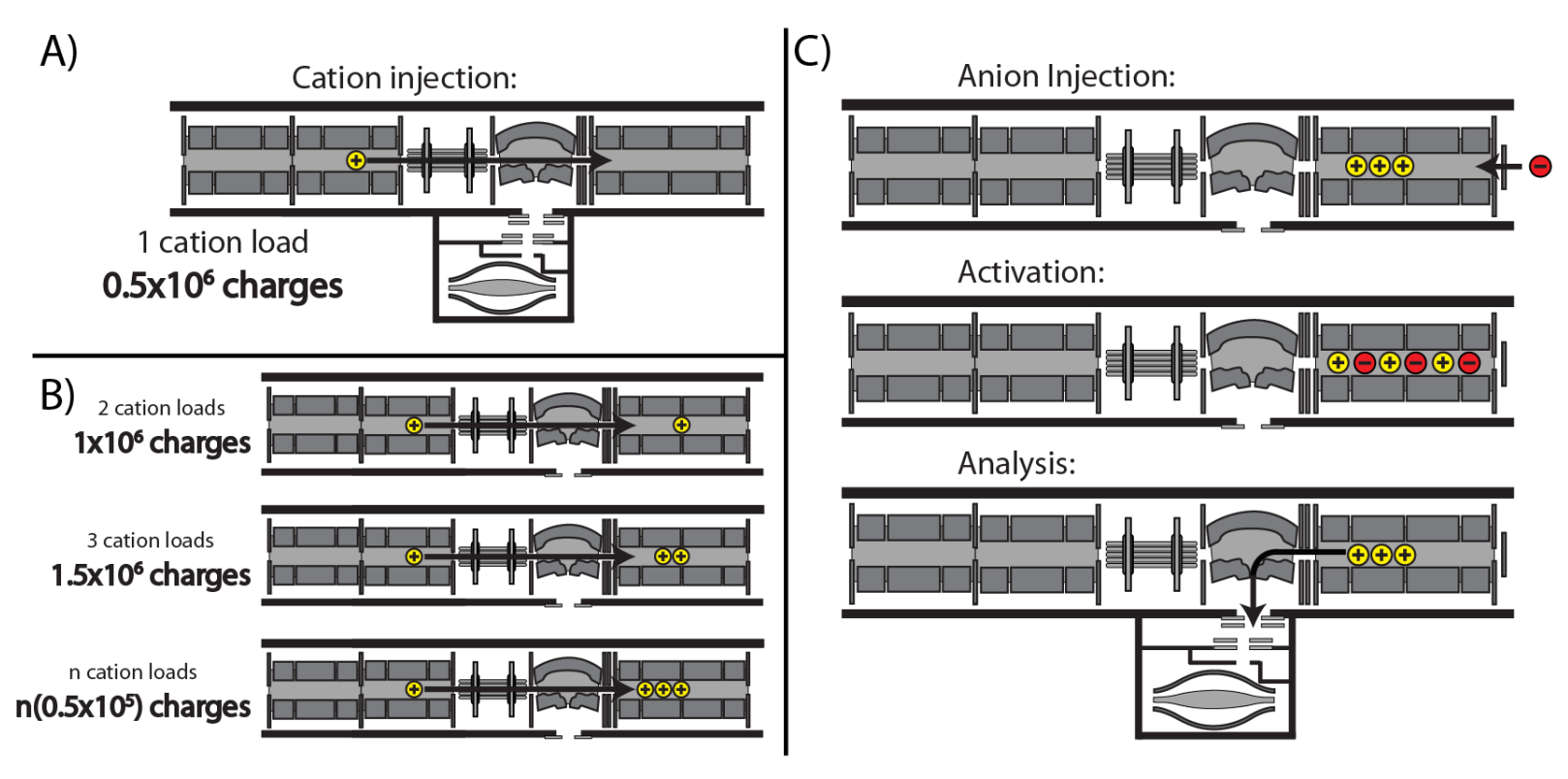


Figure 4. Multiple fills scan function. Cation precursors are accumulated and isolated in the QLT, followed by transfer to the segmented cell (A). This process can be repeated iteratively, building a large population of isolated precursor cations in the segmented cell (B). Finally, anions are injected into the segmented cell, followed by ionion reaction and m/z analysis in the orbitrap.

charges can be sampled in a single scan is likely impossed by the storage space charge capacity of the C-trap ($\sim 1.5 \times 10^6$ charges) upon transfer of ETD product ions from the segmented cell. Since ETD by its nature neutralizes precursor charge, 1.5×10^6 product ion charges likely correspond to $3-4 \times 10^6$ precursor charges. Thus, by using the segmented cell the mass range of the proteins which can be effectively characterized in a single scan is increased. Using this scan function, the S/N increases in direct proportion to the number of precursor injections (**Fig. 5**).

To evaluate the efficacy of this strategy for online protein separations, we conducted three LC-MS/MS experiments in which a mixture of intact yeast whole cell lysate proteins was separated using a reversed-phase LC column and interrogated using ETD. In one experiment, the ion trap was used as the ETD reaction vessel, followed by m/z analysis in the orbitrap with each MS^2 event conducted using FT transient averaging (n=6). In separate experiments, the segmented cell was used to conduct ETD, using six precursor fills and either collection of a single FT transient (\sim same number of precursor ions sampled as conventional ETD) or using the average of 3 FT transients (\sim same acquisition time as conventional ETD). Shown in **Figure 6** are example spectra of 60s Ribosomal Protein L30, identified in each of the three experiments.

Theoretically, averaging 6 FT transients (used for the LTQ ETD activation) increases S/N by a factor of $\sqrt{6}$ relative to a single transient while increasing the number of precursor cations used for ETD activation by 6x using multiple fills increases S/N by a factor of 6. Concomitantly, the 6 individual ion injections and six individual FT transients

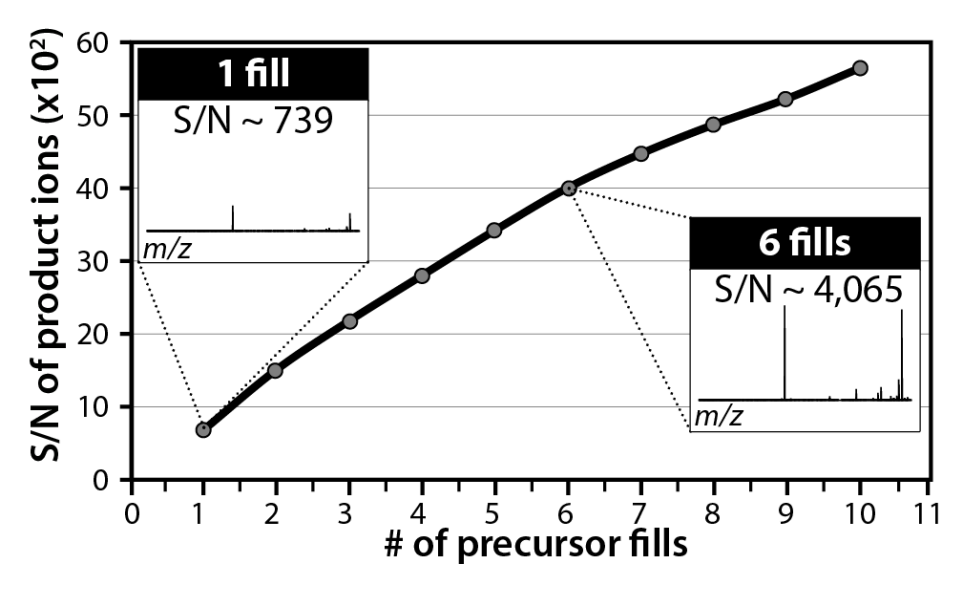


Figure 5. Signal to noise of ETD product ions vs. number of precursor cation fills. For ETD of doubly-protonated Angiotensin, increasing the number of precursor multiple fills used to populate the segmented cell linearly increases the summed ETD fragment ion S/N. Shown in the lift-outs are the ETD spectra for 1 and six fills, shown on the same intensity scale. Use of multiple fills greatly enhances the overall spectral S/N. Precursor AGC target was set to 1E5. S/N represent the summed S/N of major product ions (c₇, c₈, c₉, and z₉).

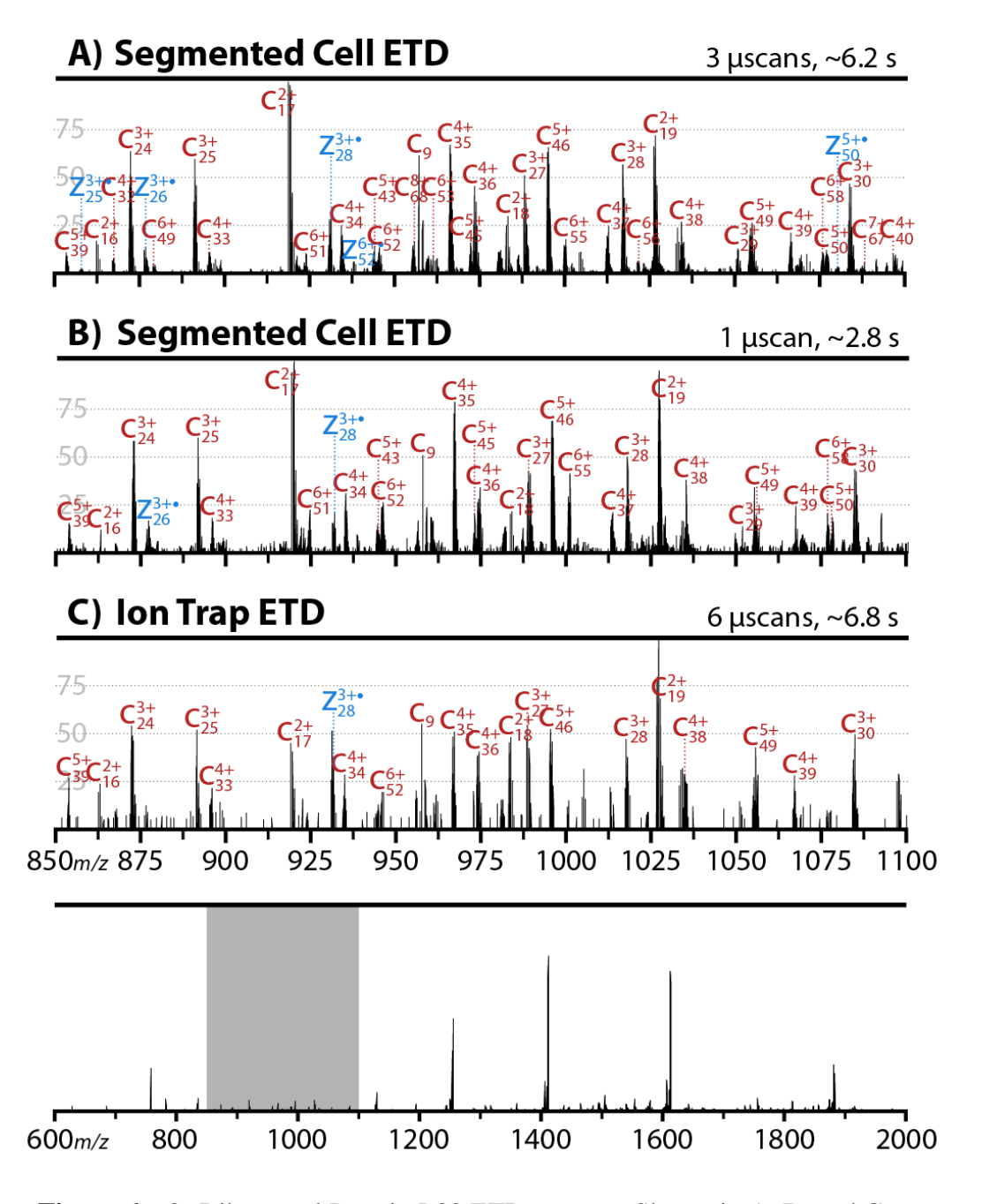


Figure 6. 60s Ribosomal Protein L30 ETD spectra. Shown in A, B, and C are spectral liftouts of ETD conducted in the segmented cell using the average of 3 (A) and 1 (B) FT transients, both of which offer substantial improvement in fragment ion diversity and S/N over ETD conducted in the QLT using an average of 6 FT transients (C).

acquisitions associated with spectral averaging requires substantially more time than the 6 precursor injections and single FT transient. From a theoretical standpoint, this means that the use of multiple fills enables the acquisition of spectra having superior S/N in less time than what is possible using spectral averaging. The data we collected demonstrate the utility of multiple fills relative to spectral averaging (**Fig 6.**).

60s Ribosomal Protein L30 was identified by Prosight PC 2.0 in each of the three LC-MS/MS analyses. Using the QLT to perform ETD with 6 transient averages, 27 c- ions and 11 z- ions are identified, with a spectral acquisition time of \sim 6.8 s. Use of the segmented cell with 6 precursor fills and a single transient acquisition results in the identification of 41 c- ions and 24 z- ions and requires \sim 2.8 s. Using the segmented cell with 6 precursor fills and and averaging 3 transients, the spectral acquisition time is 6.2 s, and we identify 55 c- type and 30 z-type product ions. These data provide a cogent example of the great utility provided by the segmented cell combined with multiple fills for whole protein analysis; multiple fills of ETD in the segmented cell enables the acquisition of superior whole protein MS² spectra in less time or vastly superior MS² spectra in the same time as compared to spectral averaging of ETD MS² conducted in the QLT.

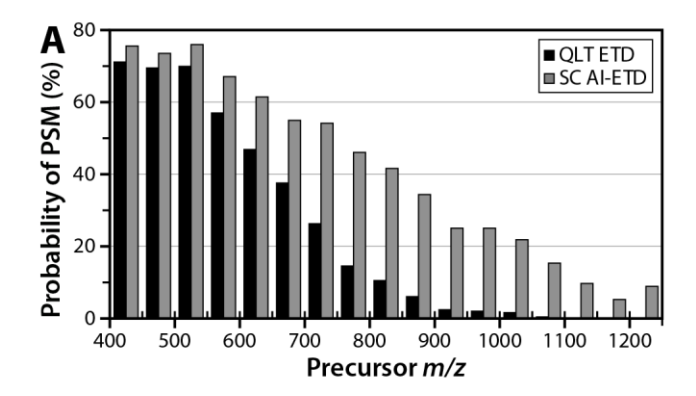
Compatibility with Activated-Ion ETD

Traditionally, ETD has underperformed when interrogating precursors with high m/z values (i.e., low charge densities). Peptide secondary structure, more prevalent with increasing precursor m/z, can bind newly formed c- and z- type product ions following electron transfer, preventing the formation of sequence informative fragment ions

(ETnoD). Early work in our group sought to address this shortcoming through the use of resonant-excitation of the ETnoD species to induce separation of the bound c- and z- type product ions (ETcaD). The major deficiency associated with the ETcaD approach is that while they are bound by peptide secondary structure, the z- type ion may abstract a hydrogen atom from the c- type ion, shifting the m/z value of each product ion by ~ 1 Da and confounding spectral interpretation. An alternative approach is to immerse precursor peptides in IR photons during the ETD reaction (Activated-Ion ETD, AI-ETD). In so doing, we continually disrupt secondary structure and improve ETD fragmentation efficiency. Moreover, AI-ETD spectra show little evidence of hydrogen abstraction, leading to improved amenability with automated searching algorithms. 37

Prior to the present study, AI-ETD has been limited to implementation on standalone ion trap systems. For many applications, particularly whole protein characterization and large-scale peptide analysis, high resolution m/z analysis has had a transformative effect.² Moreover, the combination of AI-ETD with the segmented cell results in a powerful, next generation ETD. To enable this combination, we modified the mass spectrometer to introduce photons to the segmented cell by placing a ZnSe window on the segmented cell manifold. Next, we excavated a hole in the transfer multipole which conducts anions from the CI source to either the LTQ or the segmented cell. This modification enables the immersion of ion-ion participants in IR photons, allowing for AI-ETD. The instrument firmware was modified to trigger the external IR laser upon commencement of ETD within the segmented cell.

We ran two LC-MS/MS experiments using a ~120 LC gradient to separate a limited tryptic digest of yeast protein extract. In one experiment, we used the QLT to conduct ETD; in the other experiment, we used the segmented cell to conduct AI-ETD. We produced 4643 peptide spectral matches (PSMs) at a 1% false-discovery rate (FDR), corresponding to 2368 unique peptides using QLT ETD. Using the segmented cell and conducting AI-ETD, we obtained 8256 PSMs, correlating to 3789 unique peptides. Using our next generation ETD system, we identified nearly all unique peptides obtained using conventional ETD, and also a large number of peptides that we didn't identify using conventional ETD (**Fig. 7a**). The ~80% increase in the number of PSMs is due to 1) the use of the segmented cell increasing the number of MS² scans, and 2) IR activation increasing the probability of peptide identification for each individual MS² event. Use of the segmented cell enables faster ETD reactions and requires less time to accumulate reagent anions relative to the QLT; the result is that the average scan time for segmented cell AI-ETD events is ~ 40 ms faster than QLT ETD events. This in turn enables the collection of ~1500 more MS² scans. To examine the difference in identification rate, we next binned each individual PSM by precursor m/z and divided by the total number of spectral features sampled over the course of the analysis. The resulting data provide a 'batting average' for both conventional ETD and segmented cell AI-ETD in each precursor m/z bin (Fig 7b). ETD performance drops quickly as precursor m/z increases, a phenomenon previously described in the literature.²⁶ This diminishing performance is attributed to decreased peptide charge density and higher magnitudes of gas-phase secondary structure which impairs separation of c- and z- type ions. By disrupting the



| В | QLT ETD | SC AI-ETD |
|-------------------|---------|-----------|
| Unique peptides: | 2,368 | 3,789 |
| Avg. MS/MS time: | 652 ms | 616 ms |
| # of MS/MS scans: | 16,230 | 17,661 |

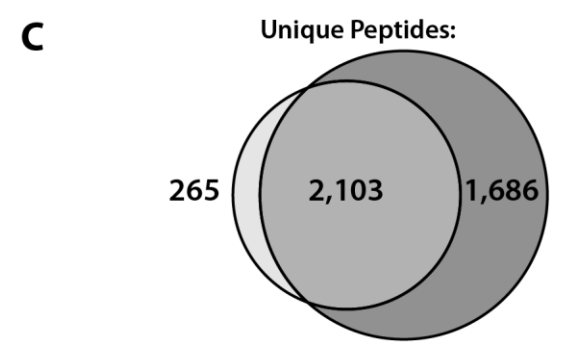


Figure 7. Comparison of QLT-based ETD and Segmented Cell-based AI-ETD. Using laser activation, the probability of producing a peptide spectral match (PSM) is greatly increased, particularly for peptide precursors having a high m/z value (A). Use of the segmented cell further augments our implementation of ETD because the reduced reaction time and reagent accumulation time requirements result in a shorter MS/MS time and more MS/MS scans over the course of the LC-MS/MS analysis (B). The cumulative effect of the segmented cell and laser activation is a substantial improvement in unique peptide identifications over previous ETD implementation using the QLT.

secondary structure using AI-ETD, performance still diminishes somewhat with increasing precursor m/z, but, in general, is far more uniform across a wide range of precursor m/z values. An example of the advantages offered by AI-ETD as compared with ETD for precursor peptides with high (> 800) m/z values is shown in **Figure 8**. ETD of triply protonated peptide SVEMHHEQLEQGVPGDNVGFNVK produces only two sequence informative ions, translating to 9% peptide sequence coverage. AI-ETD, in addition to requiring only 40% of the ion-ion reaction time relative to the QLT, results in the generation of 27 product ions, with peptide sequence coverage of 82%. Use of the segmented cell and IR photons ultimately results in superior fragmentation in less time than conventional ETD performed in the QLT.

Segmented Cell AI-ETD for phosphopeptide interrogation

There has been tremendous interest in the application of ETD to the analysis of phosphopeptides; the initial description of ETD included multiple MS² spectra demonstrating the ability to localize sites of phosphorylation.⁴ A number of high-profile phosphorylation studies utilizing ETD have verified its importance to the field.¹⁹⁻²¹ It is therefore important to evaluate the segmented cell and AI-ETD in the context of phosphopeptide analysis. Our previous description of AI-ETD demonstrated improvement over ETD for the interrogation of phosphopeptides, but the analysis was limited to a small sample set, (n=1).³⁷ While useful to verify the potential of AI-ETD, ultimately the utility of AI-ETD for the analysis of phosphopeptides remained somewhat ambiguous.

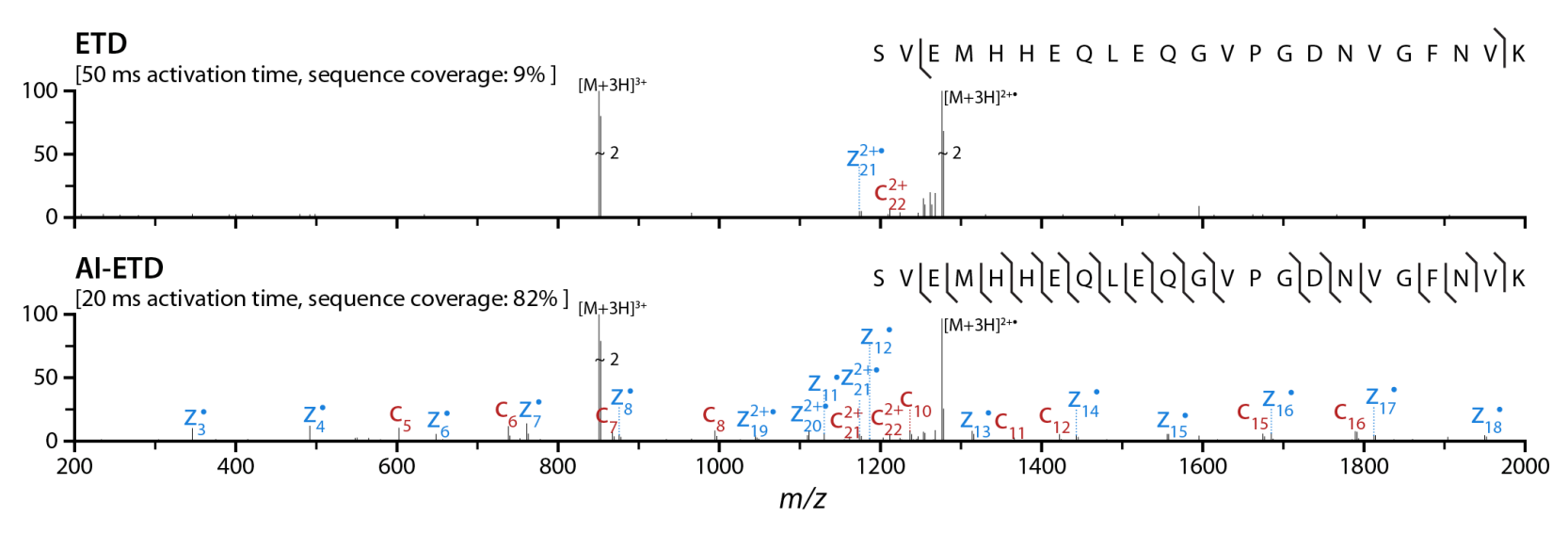
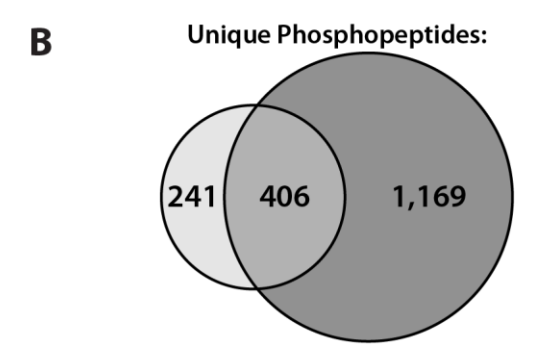


Figure 8. ETD and AI-ETD of triply protonated SVEMHHEQLEQGVPGDNVGFNVK. AI-ETD performed in the segmented cell drastically improves the fragmentation efficiency relative to ETD conducted in the QLT. An additional benefit is that the ETD activation time required in the segmented cell is less than half of that required for QLT activation.

To investigate the efficacy of segmented cell AI-ETD for large-scale phosphopeptide experiments, we conducted two LC-MS/MS experiments. In one experiment, we used the QLT to conduct ETD; in the other experiment, we used the segmented cell and performed AI-ETD. Using the QLT, we produced 1164 PSMs, corresponding to 980 phosphopeptides, 647 of them unique. In contrast, use of segmented cell AI-ETD results 3271 PSMs, corresponding to 2736 phosphopeptides and 1575 unique phosphopeptides. The resulting data were treated similarly to the large scale experiment using unmodified peptides (vide supra). Data were again searched using OMSSA, and PSMs within a 1% FDR were binned by precursor m/z and divided by the number of spectral features sampled, providing a measure of success for both ETD and AI-ETD as a function of precursor m/z (Fig. 9). AI-ETD produces more phosphopeptide PSMs than ETD, particularly for high m/z precursors. Increasing precursor m/z has a detrimental effect on the ability of ETD to generate PSMs. While AI-ETD is likewise less effective for high m/z precursors than low m/z precursors, the difference in overall performance is far less dramatic. An example of the improvement segmented cell AI-ETD offers over conventional ETD conducted in the LTQ is shown in **figure 10**. AI-ETD results in much higher ETD fragmentation efficiency, and concomitantly a much greater diversity of product ions. An apparent caveat associated with AI-ETD of phosphopeptides is the unintended production of b- and y- type ions. Such ions result from vibronic excitation and are not typically observed in the AI-ETD spectra of unmodified peptides. We rationalize that this because phosphopeptides have much higher IR photon absorption efficiencies than unmodified peptides. 43,44 We attempted AI-ETD at a number of

| Α | QLT ETD | SC AI-ETD |
|-------------------------|---------|-----------|
| Pep. spectral matches: | 1,164 | 3,271 |
| Phosphopeptides: | 980 | 2,736 |
| Unique phosphopeptides: | 647 | 1,575 |



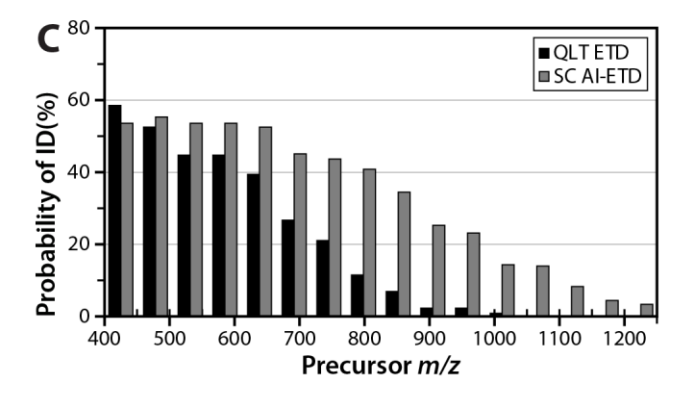


Figure 9. Comparison of QLT-based ETD and segmented cell-based AI-ETD for phosphopeptide analysis. Use of the segmented cell AI-ETD results in a greater number of PSMs, phosphopeptide PSMs, and unique phosphopeptides identified (A), while retaining a high proportion of the unique phosphopeptides obtainable using QLT-based ETD. This is largely due to greatly enhanced probability of PSM, particularly for high m/z precursors (C) afforded by the IR activation of precursors during ETD.

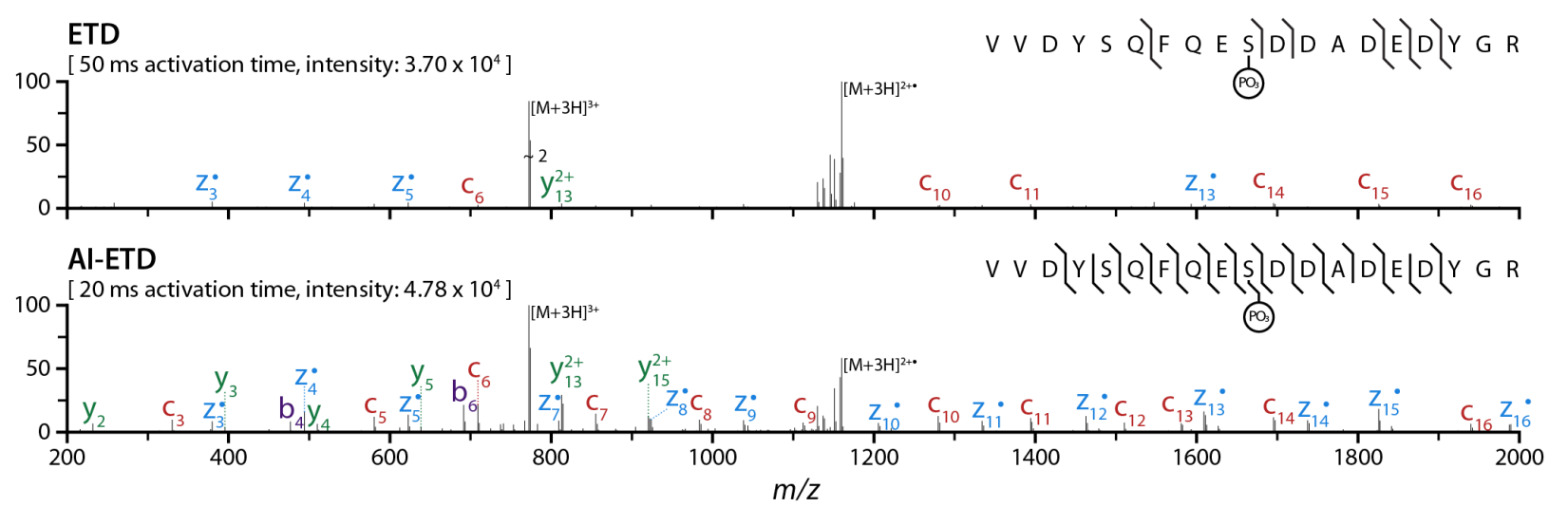


Figure 10. ETD and AI-ETD of the triply protonated phosphopeptide VVDYSQFQEsDDADEDYGR. AI-ETD results in a much greater diversity of fragment ions. In addition to enhancing ETD fragmentation, *b*- and *y*- type ions indicate direct photo-dissociation of the peptide precursor as well, presumably due to the presence of the phospho-moiety, which enhanced the coefficient of IR photon absorption.

different laser powers. At powers lower than the ~35 W used, there was insufficient disruption of non-covalent secondary structure, leading to minimal improvement over ETD. At powers higher than 35 W, formation of collisional fragment ions and precursor neutral losses dominate the spectra. We therefore conclude that this power represents an effective compromise between detrimental formation of vibronic-type products and effective peptide secondary structure disruption.

Discussion

By relocating the ETD reactions from the multi-function ion trap to a device specifically tailored to performing ETD (namely operation at a higher RF frequency), we have reduced ETD fragmentation time requirements by over 50%. The amount of time required to accumulate sufficient numbers of reagent anions is likewise reduced. Taken together, these advancements reduce the overall scan time required to perform ETD by nearly 50 ms/scan, enabling ~1500 more MS² scans to be collected over a typical LC-MS/MS experiment. Moreover, we have demonstrated that simple instrument modifications allow the introduction of IR photons to the segmented cell, enabling the use of IR photon activation concomitant to ETD (AI-ETD). Use of AI-ETD substantially enhances ETD fragmentation efficiency for unmodified peptides and, importantly, phosphopeptides as well. Finally, we have demonstrated an advanced scan function comprising iterative isolation and accumulation of precursor ions followed by a single activation and mass analysis. Use of such a scan function shows significant promise to increase the utility of ETD for whole-protein analysis. Taken as a whole, the

implementation of a segmented cell for ETD with the availability of IR photon activation represents a next generation implementation of ETD. Use of the segmented cell to conduct AI-ETD resulted in nearly a two-fold increase in the number of unique unmodified peptides identified (2,368 vs. 3,789) and almost three times as many unique phosphopeptides (647 vs. 1,575) over an LC-MS/MS experiment as compared to unassisted ETD performed in the QLT.

Since the implementation of this work, a new generation of orbitraps has been released allowing for a 4x improvement in the spectral resolution for a fixed transient acquisition time (Orbitrap Elite, Thermo Fisher Scientific, Bremen, Germany). This new technology promises to improve the overall utility of all associated analyses, but in particular whole-protein analysis. The complex nature of top-down MS/MS spectra necessitates high resolution mass analysis; in consequence the time required for m/z analysis is proportionally large relative to the overall MS/MS duty cycle. We predict that a 4x reduction in this time in tandem with the segmented cell for whole protein analysis should represent a boon to the top-down community.

Finally, while we have replaced the pre-existing RF cell used for beam-type activation of precursor peptides (HCD), the presence of the segmented cell does not preclude the ability to perform such activation using the segmented cell; indeed preliminary data suggest that HCD is readily performed in the segmented cell. Hence, we anticipate that the cumulative effect of modifications we have made (incorporation of the segmented cell, allowances made to introduce IR photons to the segmented cell) adds significant utility to the mass spectrometer without compromising other instrument functionalities.

Methods

Samples

All peptides and chemicals were purchased from Sigma-Aldrich (St. Louis, MO). Standard peptides were prepared by diluting stock solutions to ~ 5 pmol/uL in 70:29.9:0.1 ACN/H₂O/acetic acid. Peptide and protein solutions were ionized using a static tip.

Wild-type yeast (*Saccharomyces cerevisiae*) was grown in YPD medium at 30 °C to an optical density (OD₆₀₀) of ~0.6. Cells were collected and centrifuged at 8000 rpm for 10 min at 4 °C. The resulting cell pellet was washed twice with sterile water and centrifuged at 5000 rpm for 5 min at 4 °C. Lysis buffer of approximately three times the cell pellet volume was added. The lysis buffer contained 8 M urea, 75 mM NaCl, 50 mM Tris (pH 8), 1 mM sodium orthovanadate, 100 mM sodium butyrate, complete mini EDTA-free protease inhibitor (Roche Diagnostics) and phosSTOP phosphatase inhibitor (Roche Diagnostics). Drops of yeast lysate were flash frozen in liquid nitrogen to form lysis popcorn. Equal volumes of lysis popcorn and acid-washed glass beads (Sigma) were added to the grinding jar. Cells were ruptured by bead-beating on a Restek MM4000 Mixer Mill using 3 x 4 min. cycles at 30 Hz. Lysates were transferred to fresh tubes and centrifuged at 5000 rpm for 15 min at 4 °C. Cysteine residues were reduced and alkylated by incubating lysate with 5 mM DTT (final concentration) for 45 min at 37 °C followed by incubation in 15 mM IAA for 1 h at room temperature in the dark. The alkylation

reaction was capped by incubating the reaction with DTT for 15 min at room temperature. Proteins were digested for ~ 60 min at ~5 °C after the addition of 1 mM CaCl₂, 50 mM Tris (to decrease urea to 1 M) and adjusting to pH 8 at an enzyme:substrate ratio of 1:200 of trypsin (Promega, Madison, WI). The digest was quenched by the addition of TFA to a final concentration of 0.5% (pH 2), and desalted via solid phase extraction on a 50-mg tC₁₈ SepPak cartridge (Waters, Milford, MA).

To prepare phosphopeptides, human embryonic stem cells were lysed in ice-cold 8M urea, 40 mM NaCl, 50 mM tris (pH 8), 2 mM MgCl₂, 50 mM NaF, 50 mM β–glycero phosphate, 1 mM sodium orthovanadate, 10 mM sodium pyrophosphate, 1X mini EDTA-free protease inhibitor (Roche Diagnostics), and 1X phosSTOP phosphatase inhibitor (Roche Diagnostics). To solubilize protein and ensure complete lysis, samples were sonicated three times for 15 seconds with 30 second pauses. Total protein was then quantified using a BCA protein assay kit (Thermo Scientific Pierce), reduced by adding DTT to a final concentration of 5 mM, and alkylated with 10 mM iodoacetamide. Digestion was carried out by adding trypsin (Wako Chemicals) at a 1:100 emzyme-to-protein ratio and incubating at 37 degrees C for 2 hours. At this time, the lysate was diluted with 25 mM tris (pH 8) to a final urea concentration of 1.5 M and further digested for 12 hours at 37 degrees C with trypsin (Promega) at a 1:100 enzyme to protein ratio. Peptides were then acidified with TFA to quench the reaction and de-salted using C-18 solid phase extraction (SPE) columns (Waters).

Phosphopeptides were enriched from 1 mg of protein *via* immobilized metal affinity chromatography (IMAC) using magnetic beads (Qiagen). Following equilibration with

water, the beads were treated with 40 mM EDTA (pH 8.0) for 30 minutes with shaking, and washed 3x with water again. The beads were then incubated with 100 mM FeCl₃ for 30 minutes with shaking and finally were washed 3 times with 80% acetonitrile/0.1% TFA. Samples were likewise re-suspended in 80% acetonitrile/0.15% TFA and incubated with beads for 45 minutes with shaking. The resultant mixture was washed 3 times with 1 mL 80% acetonitrile/0.1% TFA, and eluted using 1:1 acetonitrile:0.7% NH_4OH in water. Eluted phosphopeptides were acidified immediately with 4% formic acid and lyophilized to ~5 μ L.

To prepare whole protein samples for top-down mass spectrometry, wild-type *Saccharomyces cerevisiae* was cultured and lysed as previously described. Samples were desalted using a C2 SepPak (Waters Corp., Milford, MA), lyophilized, and stored at -80°C or reconstituted in 10% ACN/0.2% formic acid for immediate analysis.

Mass Spectrometry and LC separation

All experiments were performed on an ETD-enabled hybrid dual-cell quadrupole ion trap - orbitrap mass spectrometer (Velos-Orbitrap, Thermo Fisher Scientific, San Jose, CA). The primary modification was the installation of a custom ion/ion reaction cell in place of the pre-existing HCD cell (**Fig. 11**). The segmented cell retains the basic layout of the HCD cell, with four hyperbolic rods of the same length. However, in the case of the segmented cell the four rods have been divided up into four sections, with each section being powered by a separate filer of the RF coil, so each section retains independent control of its RF DC offset. Also of note, r₀ was decreased to 2.75 mm (relative to the

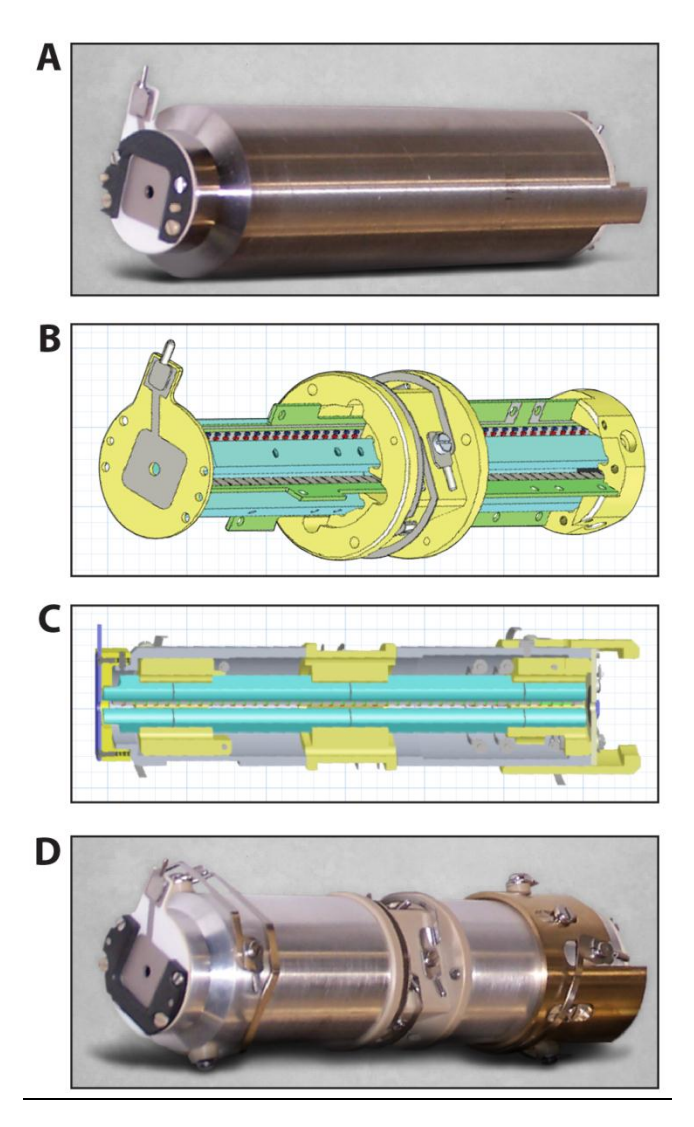


Figure 11. In place of the pre-existing HCD cell (A), we have installed a custom ion-ion reaction vessel (segmented cell, B-D). The segmented cell comprises four separate sections, allowing for axial manipulation of ion populations. The segmented cell possesses an inscribed radius (r_o) of 2.75 mm.

QLT which has an r_0 of 4.00 mm). To support the segmented cell, external RF electronics were installed which delivered high-RF amplitudes (> 1500 V_{0-P}) and high RF frequencies (~3 MHz) to both the rods and end lenses. In this manner RF voltages trapped ions both radially as well as axially, enabling charge-sign independent trapping (CSIT). Additionally, to support the new devices and the associated scan functions, we extensively modified the instrument control code. With this new instrument configuration, ETD reagent anions are still formed in a distal CI source and transmitted to the segmented cell *via* a transfer multipole.

We also modified the instrument to allow for concurrent excitation of the ETD precursor population by IR photon irradiation. IR photons were generated with an external Firestar T-100 Synrad 100-W CO₂ continuous wave laser (Mukilteo, WA), which was triggered on and off through the mass spectrometer firmware. To create a line of sight between our IR photon source and the segmented cell, we installed a ZnSe window concentric with the trapping volume of the segmented cell (**Fig. 12**). We also excavated a photon passage through the ETD reagent anion transfer multipole which conducts ions to the segmented cell. This enables the introduction of IR photons to the trapping volume of the segmented cell.

During MS² events, the LTQ performs most of its traditional functions, namely trapping and isolation of precursor cations. Subsequent to isolation, cations are transmitted to the segmented cell. This process can be repeated, during which precursor cations of interest are sequentially isolated and transferred to the segmented cell, iteratively increasing the overall number of precursor charges present for ETD fragmentation. Following

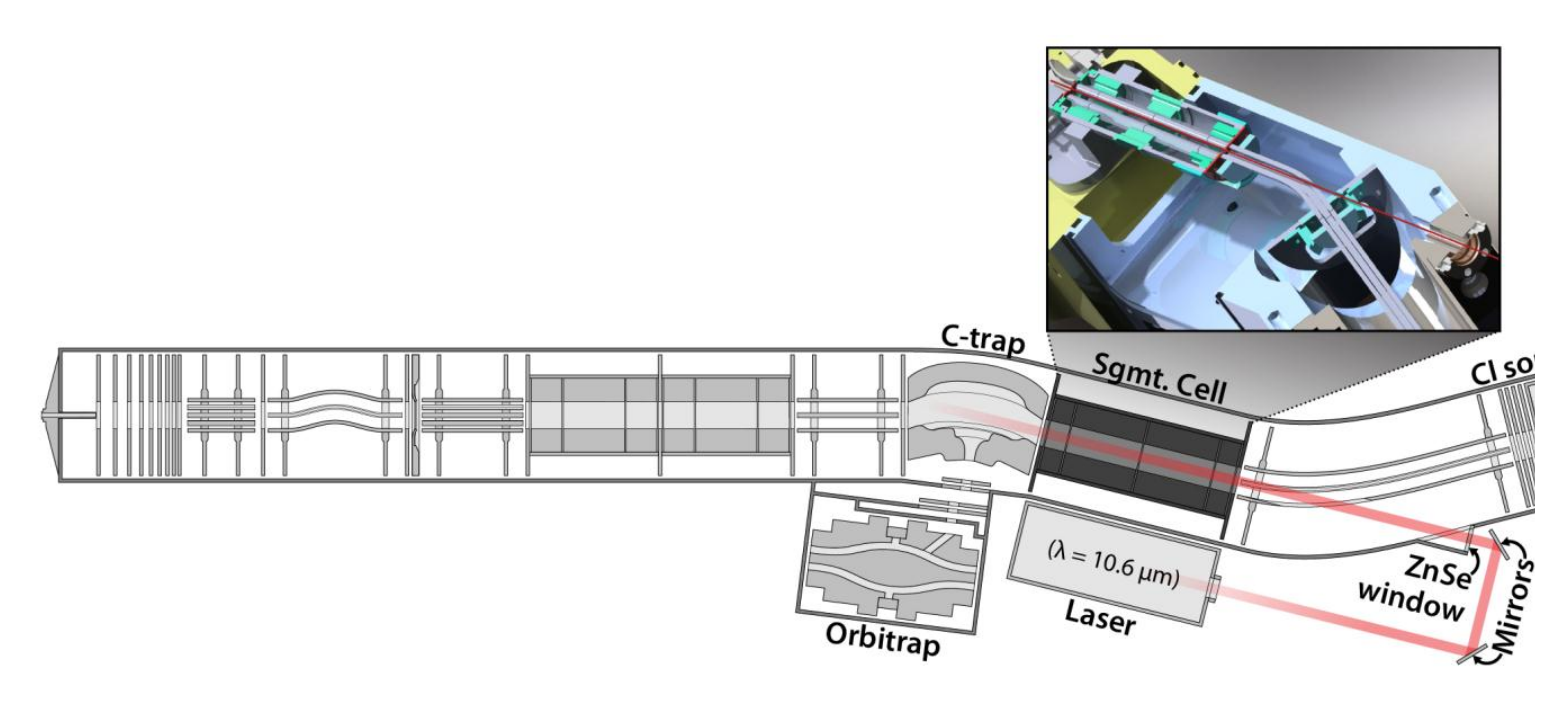


Figure 12. Modified LTQ-velos orbitrap hybrid mass spectrometer. In addition to the installation of the segmented cell, we have excavated a photon passage through the transfer multipole which conducts anions from the chemical ionization (CI) source to forward sections of the mass spectrometer. Using external mirrors and a ZnSe window, we enable the irradiation of the trapping volume of the segmented cell with IR photons generated using an external laser.

accumulation, cation precursors are sequestered in the front of the segmented cell, while the DC voltages of the back sections are set to positive values suitable for accumulation of ETD reagent anions. The chemical ionization (CI) source then forms and the associated ion optics transmit reagent anions to the rear sections of the segmented cell. ETD is initiated by applying an axial RF voltage to the end lenses of the segmented cell, and by setting all the DC offsets within the segmented cell to 0 V. The ETD reaction is quenched by setting the center two sections to negative offsets, follow by m/z analysis using the orbitrap.

LC separations of unmodified and phosphopeptides were carried out using a NanoAcquity UPLC system (Waters, Milford, MA) as previously described, using a 90 minute gradient of 2% to 10% B (0.2% formic acid in ACN) over 30 seconds followed by a linear gradient increasing buffer B to 28% over 60 minutes, followed by a ramp up to 70% B over 2 minutes and held for 5 minutes. The gradient was dropped back to 98% A (0.2% formic acid in H2O) over a period of 2 minutes and allowed to re-equilibrate for 20 minutes. During the LC- MS^2 analysis of unmodified and phosphopeptide complex mixtures, mass spectrometry methods consisted of an MS^1 scan followed by consecutive ETD and AI-ETD data-dependent MS^2 scans of the five most intense precursors. Precursors were dynamically excluded for 45 s using an isolation window of \pm 1.5 Th. Unless otherwise specified, AGC target values were 1 x 10^6 for MS^1 , 1 x 10^5 for MS^2 analysis, and an ETD reagent AGC target of 2 x 10^5 .

Database Searching and Data Analysis

For phosphopeptide and unmodified peptide LC- MS² analyses, data reduction was performed with COMPASS, 46 a program which converts output files to searchable text files, as described previously. OMSSA (version 2.1.8, www.yeastgenome.org) was used to search spectra against the concatenated target-decoy SGD yeast database (downloaded 01-05-2010). Average mass tolerances of +/- 5 Th and +/- 0.01 Th were used for precursor and product m/z respectively, with carbaminomethylation of cysteine set as a fixed modification and oxidation of methionine set as a variable modification. All analyses were independently filtered to 1% false discovery rate at the unique peptide level using the concatenated forward-reverse database method as previously described. 47-⁴⁹ C- and z- type fragment ions were searched for both ETD and AI-ETD spectra. For LC-MS/MS analysis of the unmodified, limited tryptic digest, up to eight missed cleavages were considered; for LC-MS/MS analysis of the complex mixture of phosphopeptides, up to three missed cleavages were considered. Phosphopeptide site localization and assignment of peptides (both unmodified and phosphorylated) to corresponding proteins was carried out as previously described.⁶ For LC-MS/MS analyses of yeast whole protein mixtures, ProsightPC 2.0 was used to evaluate the MS² spectra in both absolute mass and biomarker modes with the delta mass option enabled to find PTMs.⁵⁰

References

- Makarov, A., Denisov, E. & Lange, O. Performance Evaluation of a High-field Orbitrap Mass Analyzer. *J. Am. Soc. Mass Spectrom.* **20**, 1391-1396, doi:10.1016/j.jasms.2009.01.005 (2009).
- McAlister, G. C., Phanstiel, D., Wenger, C. D., Lee, M. V. & Coon, J. J. Analysis of Tandem Mass Spectra by FTMS for Improved Large-Scale Proteomics with Superior Protein Quantification. *Anal. Chem.* **82**, 316-322, doi:10.1021/ac902005s (2010).
- Olsen, J. V. *et al.* A Dual Pressure Linear Ion Trap Orbitrap Instrument with Very High Sequencing Speed. *Mol. Cell. Proteomics* **8**, 2759-2769, doi:10.1074/mcp.M900375-MCP200 (2009).
- Syka, J. E. P., Coon, J. J., Schroeder, M. J., Shabanowitz, J. & Hunt, D. F. Peptide and protein sequence analysis by electron transfer dissociation mass spectrometry. *Proc. Natl. Acad. Sci. U. S. A.* **101**, 9528-9533, doi:10.1073/pnas.0402700101 (2004).
- Zubarev, R. A., Kelleher, N. L. & McLafferty, F. W. Electron capture dissociation of multiply charged protein cations. A nonergodic process. *J. Am. Chem. Soc.* **120**, 3265-3266, doi:10.1021/ja973478k (1998).
- Phanstiel, D. H. *et al.* Proteomic and phosphoproteomic comparison of human ES and iPS cells. *Nat. Methods* **8**, 821-U884, doi:10.1038/nmeth.1699 (2011).
- de Godoy, L. M. F. *et al.* Comprehensive mass-spectrometry-based proteome quantification of haploid versus diploid yeast. *Nature* **455**, 1251-U1260, doi:10.1038/nature07341 (2008).
- 8 Coon, J. J., Syka, J. E. P., Schwartz, J. C., Shabanowitz, J. & Hunt, D. F. Anion dependence in the partitioning between proton and electron transfer in ion/ion reactions. *Int. J. Mass Spectrom.* **236**, 33-42, doi:10.1016/j.ijms.2004.05.005 (2004).
- 9 Kelleher, N. L. Top-down proteomics. *Anal. Chem.* **76**, 196A-203A, doi:10.1021/ac0415657 (2004).
- 10 Chi, A., Bai, D. L., Geer, L. Y., Shabanowitz, J. & Hunt, D. F. Analysis of intact proteins on a chromatographic time scale by electron transfer dissociation tandem mass spectrometry. *Int. J. Mass Spectrom.* **259**, 197-203, doi:10.1016/j.ijms.2006.09.030 (2007).
- 11 Coon, J. J. *et al.* Protein identification using sequential ion/ion reactions and tandem mass spectrometry. *Proc. Natl. Acad. Sci. U. S. A.* **102**, 9463-9468, doi:10.1073/pnas.0503189102 (2005).
- Phanstiel, D. *et al.* Mass spectrometry identifies and quantifies 74 unique histone H4 isoforms in differentiating human embryonic stem cells. *Proc. Natl. Acad. Sci. U. S. A.* **105**, 4093-4098, doi:10.1073/pnas.0710515105 (2008).
- Young, N. L. *et al.* High Throughput Characterization of Combinatorial Histone Codes. *Mol. Cell. Proteomics* **8**, 2266-2284, doi:10.1074/mcp.M900238-MCP200 (2009).

- 14 Chalkley, R. J., Thalhammer, A., Schoepfer, R. & Burlingame, A. L. Identification of protein O-GlcNAcylation sites using electron transfer dissociation mass spectrometry on native peptides. *Proc. Natl. Acad. Sci. U. S. A.* **106**, 8894-8899, doi:10.1073/pnas.0900288106 (2009).
- Khidekel, N. *et al.* Probing the dynamics of O-GlcNAc glycosylation in the brain using quantitative proteomics. *Nat. Chem. Biol.* **3**, 339-348, doi:10.1038/nchembio881 (2007).
- Hogan, J. M., Pitteri, S. J., Chrisman, P. A. & McLuckey, S. A. Complementary structural information from a tryptic N-linked glycopeptide via electron transfer ion/ion reactions and collision-induced dissociation. *J. Proteome Res.* **4**, 628-632, doi:10.1021/pr049770q (2005).
- Darula, Z., Chalkley, R. J., Baker, P., Burlingame, A. L. & Medzihradszky, K. F. Mass spectrometric analysis, automated identification and complete annotation of O-linked glycopeptides. *Eur. J. Mass Spectrom.* **16**, 421-428, doi:10.1255/ejms.1028 (2010).
- Scott, N. E. *et al.* Simultaneous Glycan-Peptide Characterization Using Hydrophilic Interaction Chromatography and Parallel Fragmentation by CID, Higher Energy Collisional Dissociation, and Electron Transfer Dissociation MS Applied to the N-Linked Glycoproteome of Campylobacter jejuni. *Mol. Cell. Proteomics* **10**, doi:M000031
- 10.1074/mcp.M000031-MCP201 (2011).
- Swaney, D. L., Wenger, C. D., Thomson, J. A. & Coon, J. J. Human embryonic stem cell phosphoproteome revealed by electron transfer dissociation tandem mass spectrometry. *Proc. Natl. Acad. Sci. U. S. A.* **106**, 995-1000, doi:10.1073/pnas.0811964106 (2009).
- 20 Chi, A. *et al.* Analysis of phosphorylation sites on proteins from Saccharomyces cerevisiae by electron transfer dissociation (ETD) mass spectrometry. *Proc. Natl. Acad. Sci. U. S. A.* **104**, 2193-2198, doi:10.1073/pnas.0607084104 (2007).
- Molina, H., Horn, D. M., Tang, N., Mathivanan, S. & Pandey, A. Global proteomic profiling of phosphopeptides using electron transfer dissociation tandem mass spectrometry. *Proc. Natl. Acad. Sci. U. S. A.* **104**, 2199-2204, doi:10.1073/pnas.0611217104 (2007).
- Stephenson, J. L. & McLuckey, S. A. Ion/ion reactions in the gas phase: Proton transfer reactions involving multiply-charged proteins. *J. Am. Chem. Soc.* **118**, 7390-7397, doi:10.1021/ja9611755 (1996).
- Swaney, D. L. *et al.* Supplemental activation method for high-efficiency electron-transfer dissociation of doubly protonated peptide precursors. *Anal. Chem.* **79**, 477-485, doi:10.1021/ac061457f (2007).
- Ledvina, A. R. *et al.* Infrared Photoactivation Reduces Peptide Folding and Hydrogen-Atom Migration following ETD Tandem Mass Spectrometry. *Angew. Chem.-Int. Edit.* **48**, 8526-8528, doi:10.1002/anie.200903557 (2009).

- Ben Hamidane, H. *et al.* Electron Capture and Transfer Dissociation: Peptide Structure Analysis at Different Ion Internal Energy Levels. *J. Am. Soc. Mass Spectrom.* **20**, 567-575, doi:10.1016/j.jasms.2008.11.016 (2009).
- Good, D. M., Wirtala, M., McAlister, G. C. & Coon, J. J. Performance characteristics of electron transfer dissociation mass spectrometry. *Mol. Cell. Proteomics* **6**, 1942-1951, doi:10.1074/mcp.M700073-MCP200 (2007).
- Han, H. L., Xia, Y. & McLuckey, S. A. Beam-type collisional activation of polypeptide cations that survive ion/ion electron transfer. *Rapid Commun. Mass Spectrom.* **21**, 1567-1573, doi:10.1002/rcm.2994 (2007).
- Horn, D. M., Ge, Y. & McLafferty, F. W. Activated ion electron capture dissociation for mass spectral sequencing of larger (42 kDa) proteins. *Anal. Chem.* **72**, 4778-4784, doi:10.1021/ac000494i (2000).
- Cooper, H. J., Hakansson, K. & Marshall, A. G. The role of electron capture dissociation in biomolecular analysis. *Mass Spectrom. Rev.* **24**, 201-222, doi:10.1002/mas.20014 (2005).
- Oh, H. *et al.* Secondary and tertiary structures of gaseous protein ions characterized by electron capture dissociation mass spectrometry and photofragment spectroscopy. *Proc. Natl. Acad. Sci. U. S. A.* **99**, 15863-15868, doi:10.1073/pnas.212643599 (2002).
- Oh, H. B. & McLafferty, F. W. A variety of activation methods employed in "activated-ion" electron capture dissociation mass spectrometry: A test against bovine ubiquitin 7+ions. *Bull. Korean Chem. Soc.* **27**, 389-394 (2006).
- Senko, M. W., Speir, J. P. & McLafferty, F. W. COLLISIONAL ACTIVATION OF LARGE MULTIPLY-CHARGED IONS USING FOURIER-TRANSFORM MASS-SPECTROMETRY. *Anal. Chem.* **66**, 2801-2808, doi:10.1021/ac00090a003 (1994).
- Breuker, K., Oh, H. B., Horn, D. M., Cerda, B. A. & McLafferty, F. W. Detailed unfolding and folding of gaseous ubiquitin ions characterized by electron capture dissociation. *J. Am. Chem. Soc.* **124**, 6407-6420, doi:10.1021/ja012267j (2002).
- Horn, D. M., Breuker, K., Frank, A. J. & McLafferty, F. W. Kinetic intermediates in the folding of gaseous protein ions characterized by electron capture dissociation mass spectrometry. *J. Am. Chem. Soc.* **123**, 9792-9799, doi:10.1021/ja003143u (2001).
- Pitteri, S. J., Chrisman, P. A. & McLuckey, S. A. Electron-transfer ion/ion reactions of doubly protonated peptides: Effect of elevated bath gas temperature. *Anal. Chem.* **77**, 5662-5669, doi:10.1021/ac050666h (2005).
- O'Connor, P. B. *et al.* Long-lived electron capture dissociation product ions experience radical migration via hydrogen abstraction. *J. Am. Soc. Mass Spectrom.* **17**, 576-585, doi:10.1016/j.jasms.2005.12.015 (2006).
- Ledvina, A. R. *et al.* Activated-Ion Electron Transfer Dissociation Improves the Ability of Electron Transfer Dissociation to Identify Peptides in a Complex Mixture. *Anal. Chem.* **82**, 10068-10074, doi:10.1021/ac1020358 (2010).

- Schaub, T. M. *et al.* High-performance mass spectrometry: Fourier transform ion cyclotron resonance at 14.5 tesla. *Anal. Chem.* **80**, 3985-3990, doi:10.1021/ac800386h (2008).
- Tsybin, Y. O., Witt, M., Baykut, G. & Hakansson, P. Electron capture dissociation Fourier transform ion cyclotron resonance mass spectrometry in the electron energy range 0-50 eV. *Rapid Commun. Mass Spectrom.* **18**, 1607-1613, doi:10.1002/rcm.1525 (2004).
- Hakansson, K. *et al.* Combined electron capture and infrared multiphoton dissociation for multistage MS/MS in a Fourier transform ion cyclotron resonance mass spectrometer. *Anal. Chem.* **75**, 3256-3262, doi:10.1021/ac030015q (2003).
- 41 McAlister, G. C. in 56th ASMS Conference on Mass Spectrometry and Allied Topics.
- 42 Compton, P. D., Zamdborg, L., Thomas, P. M. & Kelleher, N. L. On the Scalability and Requirements of Whole Protein Mass Spectrometry. *Anal. Chem.* **83**, 6868-6874, doi:10.1021/ac2010795 (2011).
- Flora, J. W. & Muddiman, D. C. Selective, sensitive, and rapid phosphopeptide identification in enzymatic digests using ESI-FTICR-MS with infrared multiphoton dissociation. *Anal. Chem.* **73**, 3305-3311, doi:10.1021/ac010333u (2001).
- Crowe, M. C. & Brodbelt, J. S. Infrared multiphoton dissociation (IRMPD) and collisionally activated dissociation of peptides in a quadrupole ion trap with selective IRMPD of phosphopeptides. *J. Am. Soc. Mass Spectrom.* **15**, 1581-1592, doi:10.1016/j.jasms.2004.07.016 (2004).
- Swaney, D. L., McAlister, G. C. & Coon, J. J. Decision tree-driven tandem mass spectrometry for shotgun proteomics. *Nat. Methods* **5**, 959-964, doi:10.1038/nmeth.1260 (2008).
- Wenger, C. D., Phanstiel, D. H., Lee, M. V., Bailey, D. J. & Coon, J. J. COMPASS: A suite of pre- and post-search proteomics software tools for OMSSA. *Proteomics* 11, 1064-1074, doi:10.1002/pmic.201000616 (2011).
- Moore, R. E., Young, M. K. & Lee, T. D. Qscore: An algorithm for evaluating SEQUEST database search results. *J. Am. Soc. Mass Spectrom.* **13**, 378-386, doi:10.1016/s1044-0305(02)00352-5 (2002).
- Elias, J. E. & Gygi, S. P. Target-decoy search strategy for increased confidence in large-scale protein identifications by mass spectrometry. *Nat. Methods* **4**, 207-214, doi:10.1038/nmeth1019 (2007).
- Wenger, C. D. *et al.* Gas-phase purification enables accurate, multiplexed proteome quantification with isobaric tagging. *Nat. Methods* **8**, 933-935, doi:10.1038/nmeth.1716 (2011).
- Zamdborg, L. *et al.* ProSight PTM 2.0: improved protein identification and characterization for top down mass spectrometry. *Nucleic Acids Res.* **35**, W701-W706, doi:10.1093/nar/gkm371 (2007).

Chapter 5

Implementing Photodissociation in an Orbitrap Mass Spectrometer

Summary

We modified a dual pressure linear ion trap Orbitrap to permit infrared multiphoton dissociation (IRMPD) in the higher energy collisional dissociation (HCD) cell for high resolution analysis. A number of parameters, including the pressures of the C-trap and HCD cell, the radio frequency (RF) amplitude applied to the C-trap, and the HCD DC offset, were evaluated to optimize IRMPD efficiency and maintain a high signal-to-noise ratio. IRMPD was utilized for characterization of phosphopeptides, supercharged peptides, and N-terminal modified peptides, as well as for top-down protein analysis. The high resolution and high mass accuracy capabilities of the Orbitrap analyzer facilitated confident assignment of product ions arising from IRMPD.

Introduction

Over the past decade, both electron- and photon-based activation methods have emerged as versatile alternatives to collision-activated dissociation for fragmentation of peptides in proteomics applications ¹⁻⁵. Both infrared and ultraviolet photodissociation have proven successful tools for proteomic analysis using quadruple ion traps (QITs) ¹, time-of-flight mass spectrometers ^{6,7}, and Fourier transform ion cyclotron resonance (FT ICR) instruments ^{8,9}; in the latter the high resolving power and mass accuracy has been

particularly valuable for assignment of sequence ions. Implementation of photodissociation on other high performance mass spectrometers is a compelling objective, especially with the growing adoption of Q-TOF ¹⁰ and Orbitrap ¹¹ platforms for high throughput proteomics applications. Here we present the modification of an Orbitrap mass spectrometer to allow infrared multiphoton dissociation (IRMPD). We demonstrate a variety of applications that highlight the utility of IRMPD in combination with high resolution and mass accuracy Orbitrap mass analysis.

Results

To evaluate the potential utility of IRMPD performed on an orbitrap mass spectrometer, we modified a hybrid mass spectrometer comprising both linear ion trap (QLT) and orbitrap mass analyzers (**Fig. 1**). Briefly, a ZnSe window was installed on the manifold housing the RF device using to conduct beam-type collisional activation (HCD). Further, we installed gas lines to both the c-trap and HCD cell, allowing for substantially independent control of the N₂ gas flow to both devices.

The optimization of nitrogen flow to the HCD cell and C-trap is important for a number of reasons. IRMPD efficiency typically diminishes at higher pressures due to greater competition from collisional cooling 12,13 . The trapping efficiencies of both the C-trap and HCD cells are pressure-dependent; with improved trapping efficiencies occurring at higher pressures, particularly for high m/z ions. To evaluate the overall effects of gas flow (*i.e.*, pressure) to both the HCD cell and C-trap on photodissociation

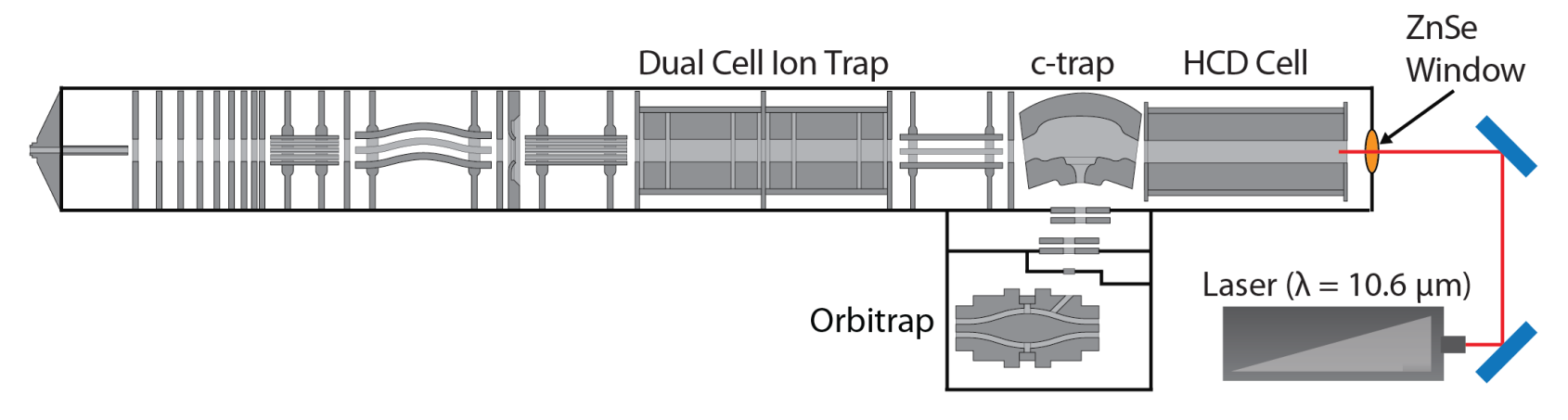


Figure 1. Schematic showing implementation of IRMPD in the HCD cell of a dual-cell linear ion trap-Orbitrap.

efficiency, we evaluated three flow settings, one with reduced gas flow to both the C-trap and the HCD cell (P1), a second with a slightly increased flow to the C-trap while maintaining the reduced flow to the HCD cell (P2), and a third with no flow to the HCD cell and with the same increased flow to the C-trap as P2 (P3). Each flow setting led to corresponding changes in the pressures of the C-trap and HCD cell, and we observed notable changes in IRMPD signal levels and photodissociation efficiencies (**Fig. 2**). The P1 setting led to the lowest absolute signal levels, nearly one order of magnitude lower than those observed using the P2 setting, but with the highest photodissociation efficiency (*i.e.*, conversion of precursor ions to fragment ions). For the P2 setting, the photodissociation efficiency was relatively low due to collisional cooling, but the absolute signal levels were high. The P3 setting represented a compromise in the gas flow (and resulting pressures) that led to satisfactory precursor-to-product conversion efficiency and best product ion sensitivity, and therefore was used for all subsequent experiments.

In addition to pressure, the C-trap RF amplitude and HCD cell DC offset can influence overall IRMPD performance. As one parameter that defines the low-mass cut off, the C-trap RF amplitude is set as a function of the lower limit for the mass range selected through the user interface (also termed "first m/z"). The C-trap RF amplitude also influences the efficiency with which product ions are trapped prior to injection into the Orbitrap for mass analysis. Optimization of this parameter was needed in response to the pressure changes in the C-trap and HCD cell. As the C-trap RF amplitude varied from $600-2300 \text{ V}_{p-p}$ (*i.e.*, corresponding to a first m/z range of 50-250 Th), the signal-to-noise

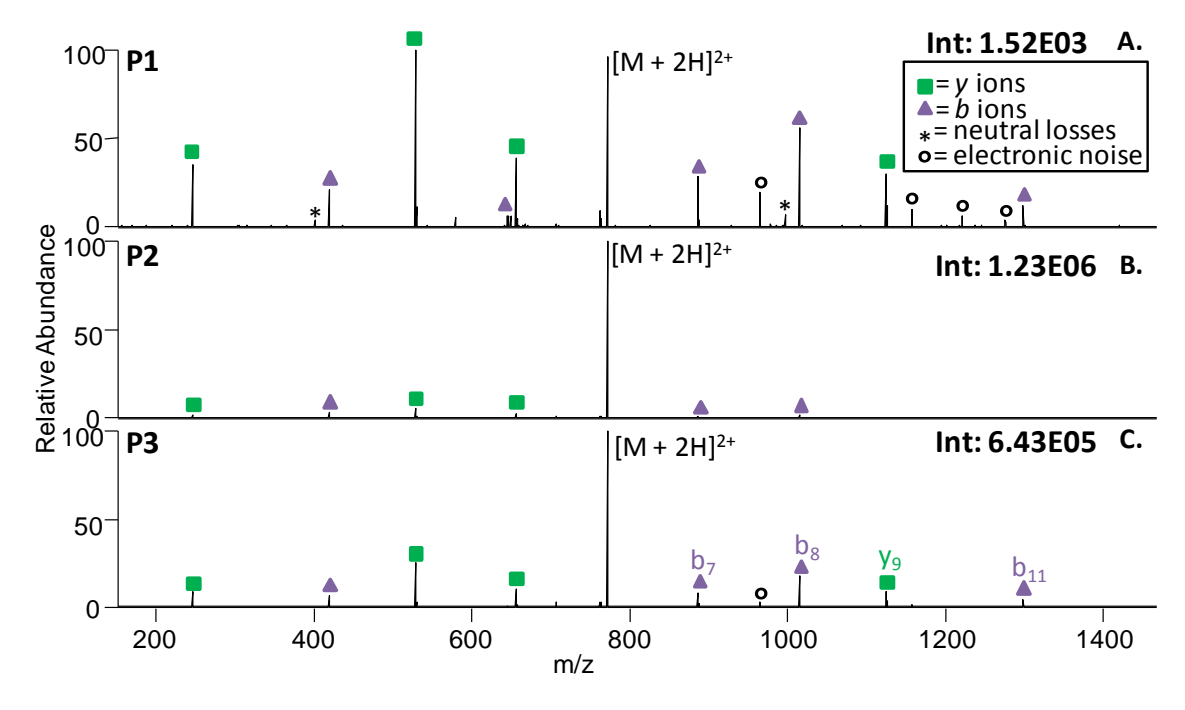


Figure 2. Effect of pressure on photodissociation efficiency and signal intensity. IRMPD of doubly protonated phosphorylated peptide TSTEPQpYQPGENL, following 1 ms of 48 W irradiation at P1 (A), P2 (B), and P3 (C). C-trap RF amplitude was set to 1180 V_{pk-pk} , with the DC offset of the HCD cell placed at -11V.

(S/N) ratio increased substantially until leveling off at RF amplitudes above 1800 V_{p-p} (Fig. 3). S/N was recorded for the most abundant fragment ion upon photoirradiation of a series of peptide precursor ions, and the averaged results are reported in **Figure 3**. To allow trapping of as many of the low m/z product ions as possible during IRMPD while still maintaining a high S/N ratio, a C-trap RF amplitude of 1180 $V_{p\text{-}p}$ was used for most of the remaining experiments. We varied the HCD cell RF amplitude from $100 - 500 \text{ V}_{p-}$ p, but observed no significant changes in photodissociation efficiency (data not shown); indicating that the ion cloud has a diameter smaller that the laser beam diameter. Additionally, the HCD cell DC offset, the potential difference between the C-trap and HCD cell, plays a significant role in IRMPD performance as a result of the reduced pressures in the HCD cell. The HCD cell DC offset determines the kinetic energy with which ions are transferred from the C-trap to the HCD region. Under normal instrument operating conditions, this parameter modulates the collision energy during beam-type CAD, with greater HCD cell DC offsets providing greater collisional activation. At the reduced HCD cell pressures needed for efficient IRMPD, trapping of ions in the HCD cell is less effective. The HCD cell DC offset is normalized relative to precursor mass; as a result, no single HCD cell DC offset was optimal for the transfer of precursor ions. For the mass range of precursor ions utilized in this IRMPD study, HCD cell DC offsets of -8 to -11 V relative to the QLT provided the best results in terms of the S/N ratio of isolated precursor (results not shown). For HCD cell DC offsets greater than -8V, the ions were not efficiently removed from the c-trap, and at offsets less than -11 V, ions underwent

C Trap rf Amplitude (Vp-p) 600 870 1180 **S** 300 First m/z

Figure 3. Variation of S/N with C-trap RF amplitude. S/N was measured for the most abundant fragment ion arising from several different peptide precursor ions as the C-trap rf amplitude was varied.

collisional activation upon injection to the HCD cell. At HCD cell DC offsets of -8 to -11 V, collisional activation prior to IRMPD was avoided while still efficiently extracting ions from the c-trap.

After optimization of the parameters summarized above, we utilized IRMPD in the hybrid Orbitrap system for a number of applications. Although conventional peptide cations exhibit relatively low IRMPD efficiencies, due to significant competition with collisional cooling, phosphopeptides display ample IRMPD efficiencies even at mTorr pressures due to the high photoabsorptivities of P-O bonds at 10.6 µm. 14,15 Phosphorylated peptides can be fully characterized and distinguished in a complex mixture with the phosphorylation site easily pinpointed through IRMPD following short irradiation times. 16 As shown in Figure 2C, the phosphorylated peptide TSTEPpYQPGENL yielded an array of diagnostic sequence ions after just 1 ms of irradiation. Production of b_7 , b_8 , b_{11} and y_9 sequence ions, all of which retained the phosphoryl group, allowed facile localization of the site of phosphorylation. In addition to phosphorylated peptides, peptides specifically derivatized via attachment of an IR chromophore can likewise be dissociated with high efficiency. As we described previously, peptides can be derivatized at their N-terminus using a phosphono derivatization agent, PPITC, which attaches a strong IR chromophore.¹⁷ Upon IRMPD, PPITC derivatized peptides dissociated into b and y ions with preferential cleavage at the y_{n-1} bond, as previously reported, using as little as 5-10 ms of IR irradiation (**Fig. 4**).

Ions in higher charge states undergo photodissociation more efficiently than those in lower charge states ¹⁸, an outcome largely attributed to the greater number of mobile

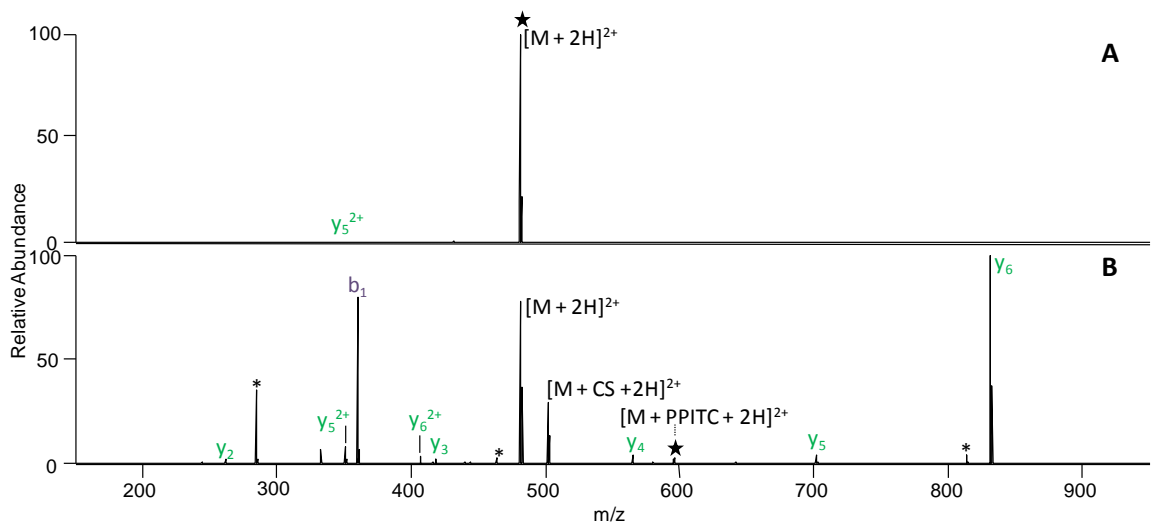


Figure 4. IRMPD of unmodified (**A**) MEHFRWG (2+) and (**B**) PPITC-derivatized MEHFRWG (2+) (10 μ M in 49.5/49.5/1 methanol/water/acetic acid) following 10 ms of 48 W irradiation, C-trap rf amplitude = 1180 V_{p-p}, (corresponding to first m/z = 100), collision energy = -11V, * = neutral losses such as H₂O and NH₃, \star = precursor, [M + CS + 2H]²⁺ represents the ion arising after partial loss of the derivatization reagent.

protons in highly charged peptide ions. The abundances of ions in higher charge states can be enhanced via a "super-charging" method in which a small amount of a solvent additive, like m-nitrobenzyl alcohol, alters the charging dynamics of ESI droplets and the resulting ions.^{19,20} This super-charging method also proved to be beneficial for improving the IRMPD efficiencies, as illustrated in figure 5 for supercharged peptide ADSGEGDFLAEGGGVR in the 3+ charge state. A large array of b and y ions was generated after 8 ms of irradiation. The expected masses of the b_3 ion, 274.1042 Da, and y_2 ion, 274.1882 Da, (a difference of 306 ppm from each other and 2.9 ppm from the experimental values) make them indistinguishable in lower resolution ion traps. IRMPD in the HCD cell with subsequent mass analysis in the Orbitrap allowed unambiguous assignment of these ions. In some but not all cases, IRMPD results in a greater array of fragment ions than observed upon HCD, presumably due to consecutive IRMPD of primary fragment ions.

The enhanced resolution and mass accuracy is particularly beneficial for assignment of sequence ions upon IRMPD of whole proteins. **Figure 6** shows the IRMPD spectrum of the 12+ charge state of ubiquitin in which many of the fragment ions are highly charged, ranging from a singly-charged b2 ion to the multi-charged y_{70}^{11+} ion. With the increased resolution afforded by Orbitrap mass analysis, all photodissociation product ions were confidently distinguished and assigned. For example, in the inset of **Figure 4**, the y_{58}^{10+} ion was baseline-resolved with 3.5 ppm mass accuracy. Interestingly, IRMPD also resulted in a greater degree of backbone cleavage selectivity compared to that obtained upon HCD with particular enhancement N-terminal to proline and C-

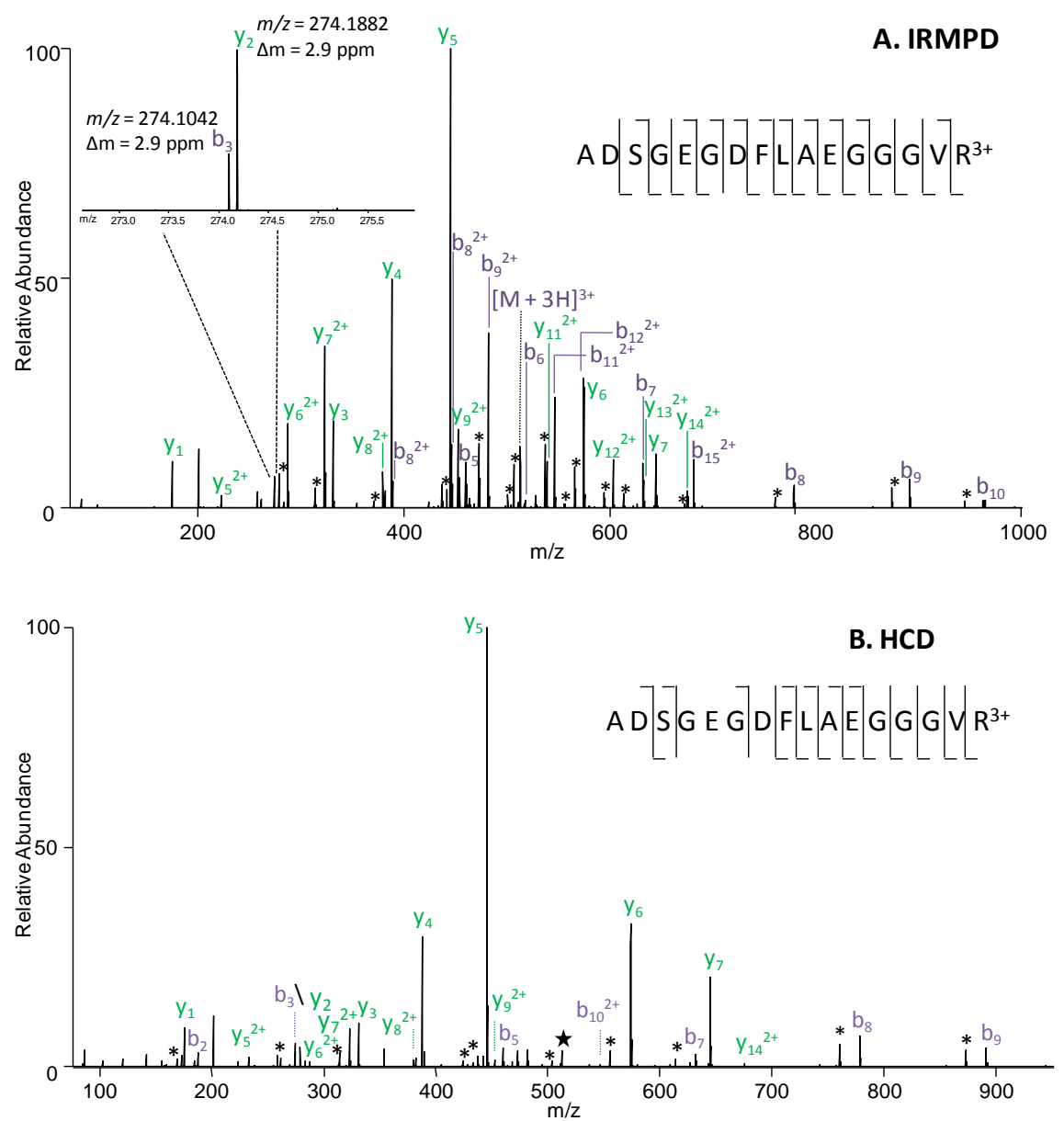


Figure 5. MS/MS of supercharged fibrinopeptide A (3+, sequence ADSGEGDFLAEGGGVR, 10 μ M in 49.5/49.5/1 methanol/water/acetic acid with 1% *m*-nitrobenzyl alcohol) (A) IRMPD using 8 ms of 48 W irradiation. * = neutral losses such as H₂O and NH₃, C-trap rf amplitude = 1180 V_{p-p} (corresponding to first m/z = 100), collision energy = -11V, and (B) HCD DC offset ~ -18 V and C-trap rf amplitude = 870 V_{p-p} (corresponding to first m/z = 75).

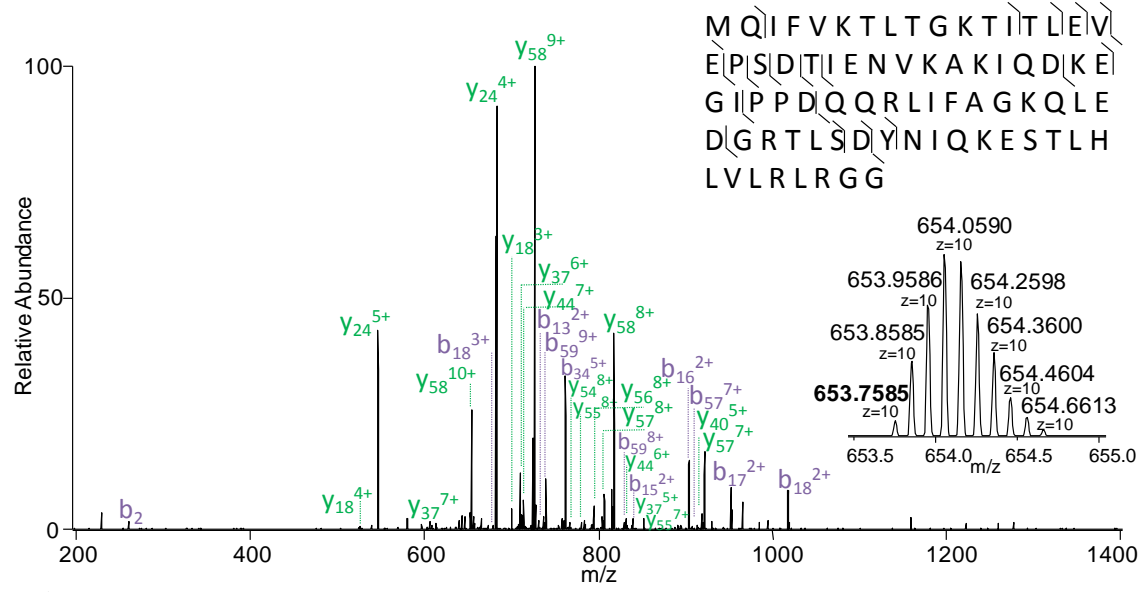


Figure 6. IRMPD of the 12+ charge state of ubiquitin following 25 ms of 48 W irradiation. Inset shows baseline resolution of the y_{58}^{10+} ion with a mass accuracy of 3.5 ppm relative to the theoretical m/z of 653.7562

terminal to glutamic acid residues. This phenomenon has been noted previously upon application of IRMPD in a dual pressure linear ion trap,²¹ albeit without high resolution or highmass accuracy ion assignments. A comparison of cleavage selectivity obtained upon IRMPD versus HCD for the 10+, 11+, and 12+ charge states of ubiquitin is shown in **Figure 7**.

Discussion

The results summarized here illustrate the practical rewards of photodissociation in an Orbitrap hybrid mass spectrometer. Photodissociation was accomplished in the HCD cell in which a decrease in its gas flow (and pressure), along with a concomitant increase in the gas flow to the C-trap, most effectively balancing IRMPD efficiency and overall ion abundance (S/N). Maximizing both photodissociation and sensitivity requires further optimization of many of the parameters discussed.

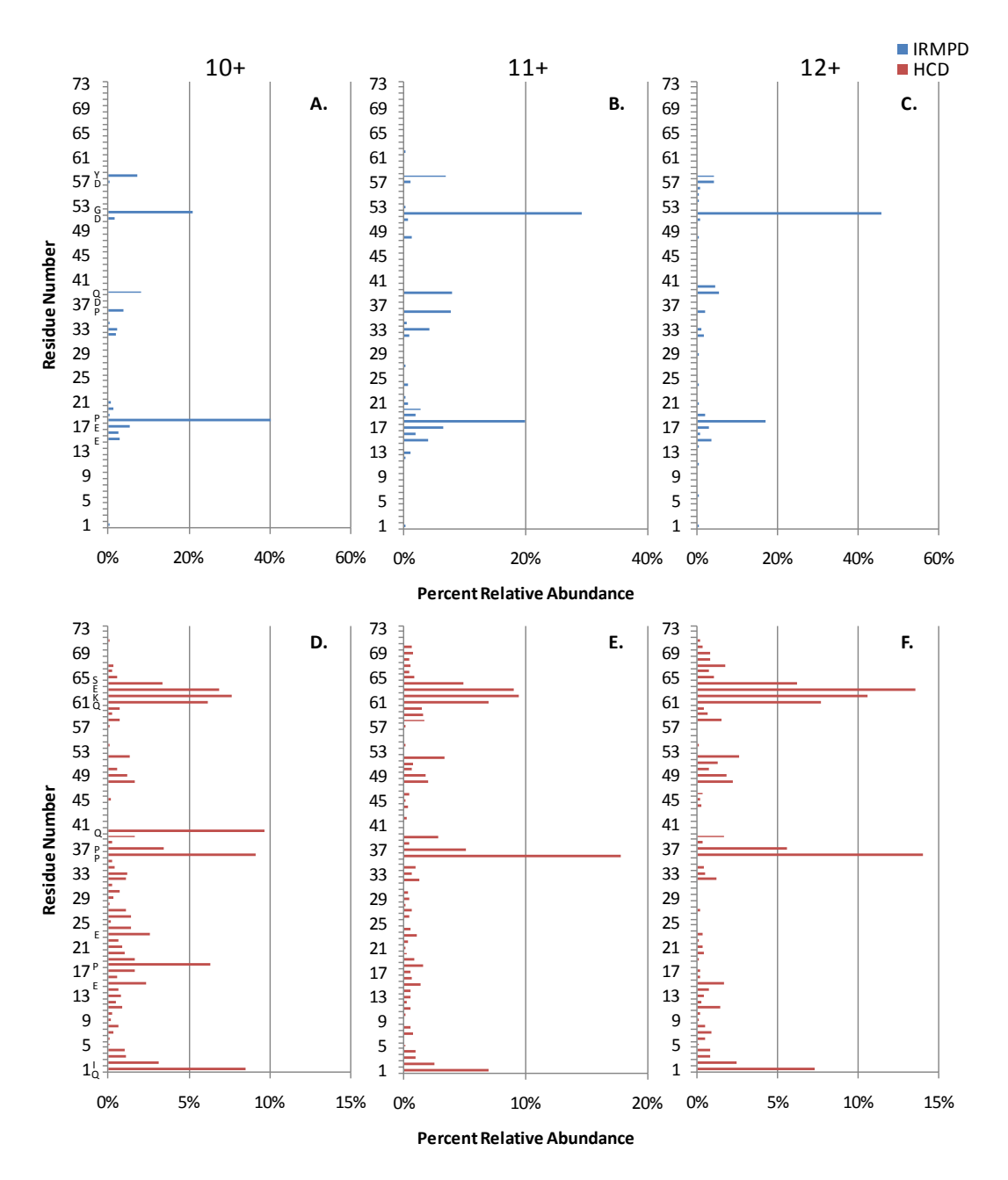


Figure 7. Summed b- and y- abundances for complementary ion pairs as a function of residue number from resulting cleavages of ubiquitin with IRMPD for (A) $[M+10H]^{10+}$, (B) $[M+11H]^{11+}$, and (C) $[M+12H]^{12+}$; and with HCD for the (D) $[M+10H]^{10+}$, (E) $[M+11H]^{11+}$, and (F) $[M+12H]^{12+}$ ions.

Methods

IRMPD was performed in the HCD cell of a modified hybrid mass spectrometer comprising both linear ion trap and orbitrap mass analyzers (Fig. 1). Typically utilized for beam-type CAD, the HCD cell provides a convenient region for photoexcitation of ions that have been mass-selected in the forward linear ion trap and transferred to the HCD cell ²². Briefly, the HCD manifold was modified via the addition of a ZnSe window concentric with the HCD cell and opened up its end lens ($d = \sim 2.54$ mm), allowing the irradiation of the HCD trapping region with IR photons (Fig. 8). Additionally, a nitrogen gas line was installed in the C-trap (a region normally used for spatial compression and temporally compact transfer of the ion bundle into the Orbitrap), and the top and bottom of the C-trap were fitted with ceramic plates to decrease gas conductance out of the Ctrap, reducing the gas flow needed to achieve desired trapping efficiencies in the C-trap while minimizing the N₂ partial pressure in the QLT. Taken as a whole, these modifications allowed substantially independent control of nitrogen gas flow to both the C-trap and HCD cell. A 100 W Synrad CO₂ laser was directed in the HCD cell using two optic mirrors mounted behind the HCD cell as shown in Figure 8. The beam width of the laser is 2.2 mm with a beam divergence of 7mR.

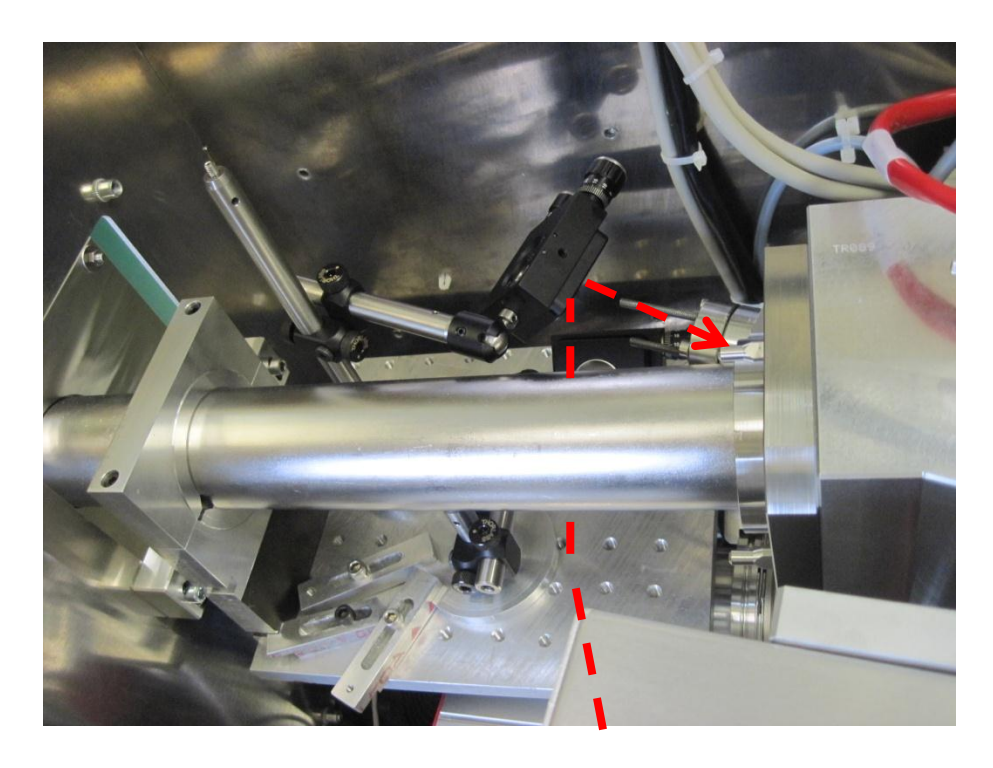


Figure 8. Introduction of laser into HCD cell; laser directed into HCD manifold through addition of a ZnSe window concentric with the HCD cell and two mirrors mounted through the use of a toe clamp.

References

- Brodbelt, J. S. & Wilson, J. J. Infrared multiphoton dissociation in quadrupole ion traps. *Mass Spectrom. Rev.* **28**, 390-424 (2009).
- Wiesner, J., Premsler, T. & Sickmann, A. Application of electron transfer dissociation (ETD) for the analysis of posttranslational modifications. *Proteomics* **8**, 4466-4483 (2008).
- Zubarev, R. Electron capture dissociation and other ion-electron fragmentation reactions. *Principles of Mass Spectrometry Applied to Biomolecules*, 475-517 (2006).
- 4 Ly, T. & Julian, R. R. Ultraviolet Photodissociation: Developments towards Applications for Mass-Spectrometry-Based Proteomics. *Angew. Chem., Int. Ed.* **48**, 7130-7137 (2009).
- Coon, J. J. Collisions or Electrons? Protein Sequence Analysis in the 21st Century. *Anal. Chem.* **81**, 3208-3215 (2009).
- Zhang, L. & Reilly, J. P. Peptide photodissociation with 157 nm light in a commercial tandem time-of-flight mass spectrometer. *Anal. Chem.* **81**, 7829-7838 (2009).
- Reilly, J. P. Ultraviolet photofragmentation of biomolecular ions. *Mass Spectrom. Rev.* **28**, 425-447 (2009).
- 8 Mann, M. & Kelleher, N. L. Precision proteomics: the case for high resolution and high mass accuracy. *Proc. Natl. Acad. Sci. U. S. A.* **105**, 18132-18138 (2008).
- 9 Eyler, J. R. Infrared multiple photon dissociation spectroscopy of ions in Penning traps. *Mass Spectrom. Rev.* **28**, 448-467 (2009).
- 10 Chernushevich, I. V., Loboda, A. V. & Thomson, B. A. An introduction to quadrupole-time-of-flight mass spectrometry. *J. Mass Spectrom.* **36**, 849-865 (2001).
- Hu, Q. et al. The Orbitrap: A new mass spectrometer. J. Mass Spectrom. 40, 430-443 (2005).
- Black, D. M., Payne, A. H. & Glish, G. L. Determination of Cooling Rates in a Quadrupole Ion Trap. *J. Am. Soc. Mass Spectrom.* **17**, 932-938 (2006).
- Gardner, M. W. *et al.* Infrared Multiphoton Dissociation of Peptide Cations in a Dual Pressure Linear Ion Trap Mass Spectrometer. *Anal. Chem.* **81**, 8109-8118 (2009).
- Flora, J. W. & Muddiman, D. C. Selective, Sensitive, and Rapid Phosphopeptide Identification in Enzymatic Digests Using ESI-FTICR-MS with Infrared Multiphoton Dissociation. *Anal. Chem.* **73**, 3305-3311 (2001).
- Flora, J. W. & Muddiman, D. C. Gas-phase ion unimolecular dissociation for rapid phosphopeptide mapping by IRMPD in a Penning ion trap: An energetically favored process. *J. Am. Chem. Soc.* **124**, 6546-6547 (2002).
- 16 Crowe, M. C. & Brodbelt, J. S. Differentiation of Phosphorylated and Unphosphorylated Peptides by High-Performance Liquid Chromatography-

- Electrospray Ionization-Infrared Multiphoton Dissociation in a Quadrupole Ion Trap. *Anal. Chem.* **77**, 5726-5734 (2005).
- Vasicek, L. A., Wilson, J. J. & Brodbelt, J. S. Improved Infrared Multiphoton Dissociation of Peptides through N-Terminal Phosphonite Derivatization. *J. Am. Soc. Mass Spectrom.* **20**, 377-384 (2009).
- Madsen, J. A. & Brodbelt, J. S. Comparison of Infrared Multiphoton Dissociation and Collision-Induced Dissociation of Supercharged Peptides in Ion Traps. *J. Am. Soc. Mass Spectrom.* **20**, 349-358 (2009).
- Iavarone, A. T., Jurchen, J. C. & Williams, E. R. Supercharged protein and peptide ions formed by electrospray ionization. *Anal. Chem.* **73**, 1455-1460 (2001).
- Iavarone, A. T. & Williams, E. R. Supercharging in electrospray ionization: effects on signal and charge. *Int. J. Mass Spectrom.* **219**, 63-72 (2002).
- Madsen, J. A. *et al.* Top-Down Protein Fragmentation by Infrared Multiphoton Dissociation in a Dual Pressure Linear Ion Trap. *Anal. Chem.* **81**, 8677-8686, doi:10.1021/ac901554z (2009).
- Olsen, J. V. *et al.* Higher-energy C-trap dissociation for peptide modification analysis. *Nat. Methods* **4**, 709-712 (2007).

Chapter 6

Infrared Multiphoton Dissociation for Quantitative Shotgun Proteomics

Summary

We modified a dual-cell linear ion trap (dual cell QLT) mass spectrometer to perform infrared multiphoton dissociation (IRMPD) for large-scale analyses of complex peptide mixtures. Upon optimization of activation parameters (precursor *q*-value, irradiation time, and photon flux), IRMPD subtly, but significantly outperforms resonant excitation CAD by generating more peptide identifications (1% false-discovery rate, FDR) from a yeast tryptic digest (95% confidence, p = 0.019). We further demonstrate that IRMPD is compatible with the large-scale analysis of isobaric-tagged peptides. A direct comparison between IRMPD and beam-type collisional activation shows that IRMPD converts a greater proportion of precursor charge to TMT reporter tag. We conclude that IRMPD offers an expedient and effective route to achieve large-scale quantitative proteomics on bench top ion trap instrumentation.

Introduction

With the advent of large-scale proteomics, ¹⁻⁴ a number of techniques have been developed to enable quantitation of proteins, including label-free methods (*e.g.*, spectral counting), ⁵ metabolic labeling, ⁶⁻¹⁰ and chemical labeling. ¹¹⁻¹⁴ Isobaric tagging strategies

(i.e., TMT and iTRAQ) have proven highly useful mainly for their ability to multiplex and compatibility with tissues and biofluids. 15,16 The success of an isobaric tagging experiment, however, depends heavily on the dissociation method; the ideal method routinely produces MS/MS spectra which are informative of both peptide sequence and relative abundance. While resonant-excitation collisional-activated dissociation (CAD) is a common form of peptide dissociation for discovery proteomics, ¹⁷⁻¹⁹ the inefficiency of the CAD process at low RF amplitudes, required for retention of reporter ions, precludes its use for isobaric tagging experiments. This shortcoming has inspired the development of alternatives. Pulsed-q dissociation and high amplitude short time excitation (HASTE) are modifications of the resonant-excitation process in which the ion trap RF amplitude is pulsed high for efficient energy deposition and then quickly lowered to retain low m/z ions. 20,21 Though amenable to the study of isobaric-tagged peptides, PQD and HASTE suffer from low precursor-to-product ion conversion efficiencies. Beam-type collisional activation is efficiently performed at low RF amplitudes, enabling the successful interrogation of isobaric-tagged peptides. 17,22-25 The pre-requisite for a dedicated, external RF device to serve as the collision cell, however, renders many ion trap systems unable to perform beam-type collisional activation. Work from our group has recently demonstrated that the ESI ion injection optics of stand-alone ion traps can serve this function effectively (iHCD).²⁶ While this work cogently demonstrated that stand-alone ion traps in most cases possess the hardware to perform beam-type collisional activation, the efficiency peptide dissociation using any beam-type collisional activation scheme is limited by ion loss due to scattering, a problem exacerbated under the activation conditions (high collision energy) optimal for the generation of isobaric reporter tags.

Photon-based fragmentation techniques (*e.g.*, UVPD, IRMPD) are efficiently performed at low RF amplitudes in QLT ion traps, do not induce ion scattering, and require only a single RF device.²⁷⁻²⁹ The utility of IRMPD has been somewhat limited because the activation efficiency of peptide cations, at typical ion trap operating pressures (~1 mTorr), is relatively low.³⁰ Efforts made to improve the efficiency include dynamic adjustment of ion trap pressure, ^{31,32} increased photon flux, ³³ pre-activation prior to or during IRMPD *via* either resonant excitation of elevated bath gas temperature. ³⁵ Other approaches involve chemical modification of peptides through the attachment of chromogenic moieties. ³⁶⁻³⁹ Though each of these approaches enables efficient IRMPD, an attractive and straightforward solution is to perform IRMPD on a dual-cell quadrupole linear ion trap (dual-cell QLT). ^{40,41} This approach requires no chemical modification of peptides. Further, the hardware modifications are simple, just the addition of a viewport to the rear flange of the instrument.

Here we build on the initial description of IRMPD performed in a dual-cell ion trap by demonstrating marginally superior effectiveness compared to CAD for shotgun sequencing of complex peptide mixtures. Further, we evaluate IRMPD as a means to interrogate isobaric-tagged peptides. We report conditions which simultaneously provide good quantitative accuracy and effective peptide sequencing. Moreover, IRMPD shows strong potential to improve upon existing methods for the generation of TMT reporter

ions *via* sequential dissociation of primary b- and y- fragments to accumulate ions in the TMT reporter channel.

Results

Evaluation of IRMPD for shotgun proteomics

CAD is a common peptide activation method used for large-scale proteomics due to 1) high efficiency of activation and 2) ease of use. Both of these traits are in large part because primary b- and y- type fragment ions formed from precursor activation are not susceptible to further activation; this obviates the need to optimize activation conditions to avoid excessive secondary activation events that exist for other dissociation techniques (e.g., HCD, ETD). Primary product ions formed via IRMPD dissociation, however, are susceptible to secondary activation. Secondary fragmentation events can produce product ions having analytical value (e.g., diagnostic side chain losses, immonium ions), though excessive secondary fragmentation can confound spectral interpretation. potentiate the utility of IRMPD for shotgun peptide sequencing, it is critical to control and optimize the degree of secondary activation. The primary variables influencing the magnitude of secondary fragmentation (and precursor-to-product ion conversion efficiency) are the photon flux (laser power), the reduced Mathieu parameter (q-value) precursors are placed at, and the duration of time ions are subjected to IR activation. We performed a series of nLC-MS/MS analyses, investigating several combinations of irradiation times (3, 5, 10, 15, and 25 ms), q-values (0.10, 0.15, 0.20, and 0.25), and laser powers (36 W, 48 W, and 60 W). For each experiment, an MS¹ survey scan was

followed by MS/MS activation of the top three most intense precursors using IRMPD (conditions varied for each analysis) and resonant-excitation CAD (NCE = 35, 10 ms activation time).

In total, 60 nLC-MS/MS analyses were conducted (Fig. 1). For 6 of the 60 IRMPD conditions considered, IRMPD produced a slightly greater number of PSMs (1% False-discovery rate, FDR) than CAD. The conditions under which IRMPD performed the best relative to CAD was at a precursor q-value of 0.10, laser power of 48W, and irradiation time of 10 ms. To determine the reproducibility of this result we performed two additional experiments, again subjecting each precursor to CAD and IRMPD (Fig. 2). In each of the three trials, IRMPD produced subtly more PSMs than CAD (7,223 vs. 6,969; 6,617 vs. 6,432; 6,909 vs. 6,747); these data lead us to conclude that IRMPD is marginally, but significantly, more effective than CAD (> 95% confidence, paired students t-test, p = 0.019). In each trial, CAD and IRMPD largely identified similar subsets of the peptide complex mixture (Fig. 2), likely due to the similar 'slow heating' dissociation mechanisms of both CAD and IRMPD.⁴² While CAD is a common MS/MS technique for large-scale proteomics, there are well-known shortcomings associated with CAD, including inefficient energy deposition at low RF amplitudes, leading to a relatively high low-mass cutoff (LMCO). Here we have demonstrated that IRMPD is at least as effective as CAD for shotgun sequencing of peptides derived from protein digestion from trypsin. Unlike CAD, however, IRMPD is efficiently performed at low RF amplitudes, ²⁸ alleviating LMCO issues and allowing for

IRMPD Peptide Identifications under various conditions

| | | 36 W laser power | | 48 W lase | 48 W laser power | | 60 W laser power | |
|-----------------|--------------|------------------|---------------------|---------------------|---------------------|---------------------|---------------------|--|
| <i>q</i> -value | IR Time (ms) | IRMPD IDs | CAD IDs | IRMPD IDs | CAD IDs | IRMPD ID | s CAD IDs | |
| 0.10 | 3 | 2926 | 6821 | 4977 | 6782 | 5862 | 6364 | |
| | 5 10 | 5143 6788 | 6946 | 6717 7223 | 7003 6969 | 6242 6017 | 6224 6263 | |
| | 15 | 6960 | 6834 6742 | 6634 | 6763 | 4721 | 6315 | |
| | 25 | 4224 | 5965 | 3627 | 6489 | 915 | 6480 | |
| 0.15 | 3 | 4000 | 7015 | 5968 | 6907 | 6237 | 6416 | |
| | 5 | 5950 | 6723 | 6667 | 6648 | 6306 | 6222 | |
| | 10 | 6937 | 6862 | 6350 | 6868 | 4959 | 6824 | |
| | 15 | 6001 | 6721 | 4201 | 6731 | 603 | 6243 | |
| | 25 | 866 | 5962 | 163 | 6576 | 30 | 6363 | |
| 0.20 | 3 | 4881 | 7005 | 6172 | 6953 | 6204 | 6486 | |
| | 5 | 6582 | 6945 | 6676 | 6886 | 5937 | 6479 | |
| | 10 | 6533 | 6756 | 5043 | 6670 | 2224 | 6377 | |
| | 15 | 4470 | 6868 | 1191 | 6799 | 106 | 6382 | |
| 0.25 | 25 | 106 | 6134 | 5 | 6620 | (272 | 6356 | |
| 0.25 | 3 5 | 5505 | 6840 | 6481 | 6786 | 6272 | 6649 | |
| | _ | 6628 | 6941 | 6320 | 6557 | 5778 | 6444 | |
| | 10 15 | 5318 | 6875 | 3288 | 6756 | 663 | 6364 | |
| | 25 | 1517 | 6317 | 147 0 | 6454 | 16 0 | 6522 | |
| | 25 | 29 | 6288 | 0 | 6543 | U | 6207 | |

Figure 1. Results of parametric optimization of IRMPD for large-scale LC-MS/MS analysis. We varied photon flux, irradiation time, and *q*-value for IRMPD activation. For each experiment, CAD activation conditions were held constant to provide an internal benchmark of success. Shown in bold are IRMPD conditions which resulted in more peptide spectral matches (PSMs) than activation with CAD.

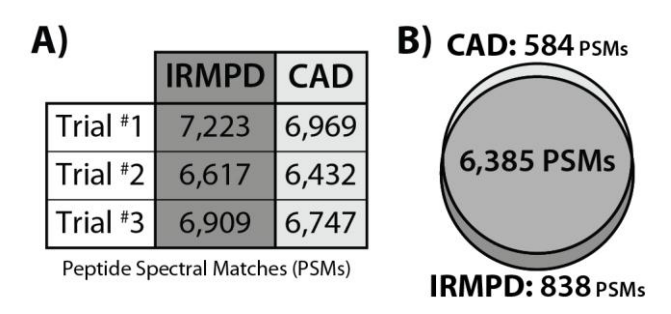


Figure 2: Replicate test for IRMPD vs. CAD. IRMPD conditions were 10 ms irradiation time, *q*-value of 0.10, and laser power of 48 W. Using these IRMPD conditions we were able to consistently produce a greater number of peptide-spectral matches (PSMs) at a 1% FDR than CAD (A). Comparing IMRPD PSMs with corresponding CAD PSMs indicates very high overlap between peptides identified by CAD and IRMPD (B).

the observation of potentially important low m/z product ions, namely isobaric reporter tags.

Compatibility with isobaric tagging techniques

Isobaric tagging techniques (*i.e.*, iTRAQ and TMT) have become increasingly widespread and important for quantitative proteomics owing to compatibility with tissues and biofluids and the ability to multiplex several samples in a single experiment. To investigate the use of IRMPD for MS/MS analysis of isobaric-tagged peptides, a synthetic peptide, WAAAKAAAK, was divided into six aliquots and labeled with TMT six-plex in 1:5:2:1.5:1:3 ratios, and subjected to IRMPD (**Fig. 3**). In addition to producing a near-complete series of both *b*- and *y*-type product ions, IRMPD also generates substantial reporter ion signal. The observed channels are within ~ 10% of the purity-corrected theoretical values (indicated by black dots), comparable to the accuracy that can be expected using beam-type collisional activation (HCD).²⁵ We conclude that IRMPD conducted within a dual pressure QLT mass spectrometer is compatible with peptide quantitation using isobaric tags.

An interesting observation was that the partitioning between reporter and b- / ytype product ions was dependent upon the irradiation time. To explore we generated an
irradiation time-resolved plot of product ions derived from doubly protonated
WAAAKAAAK. These data indicate that the optimal IRMPD activation time for the
generation of b- and y- type product ions is shorter than that required to optimize
production of TMT reporter ions (**Fig. 4**). To determine whether reporter tag can be
harvested from a primary product ion, we dissociated WAAAKAAAK precursor using

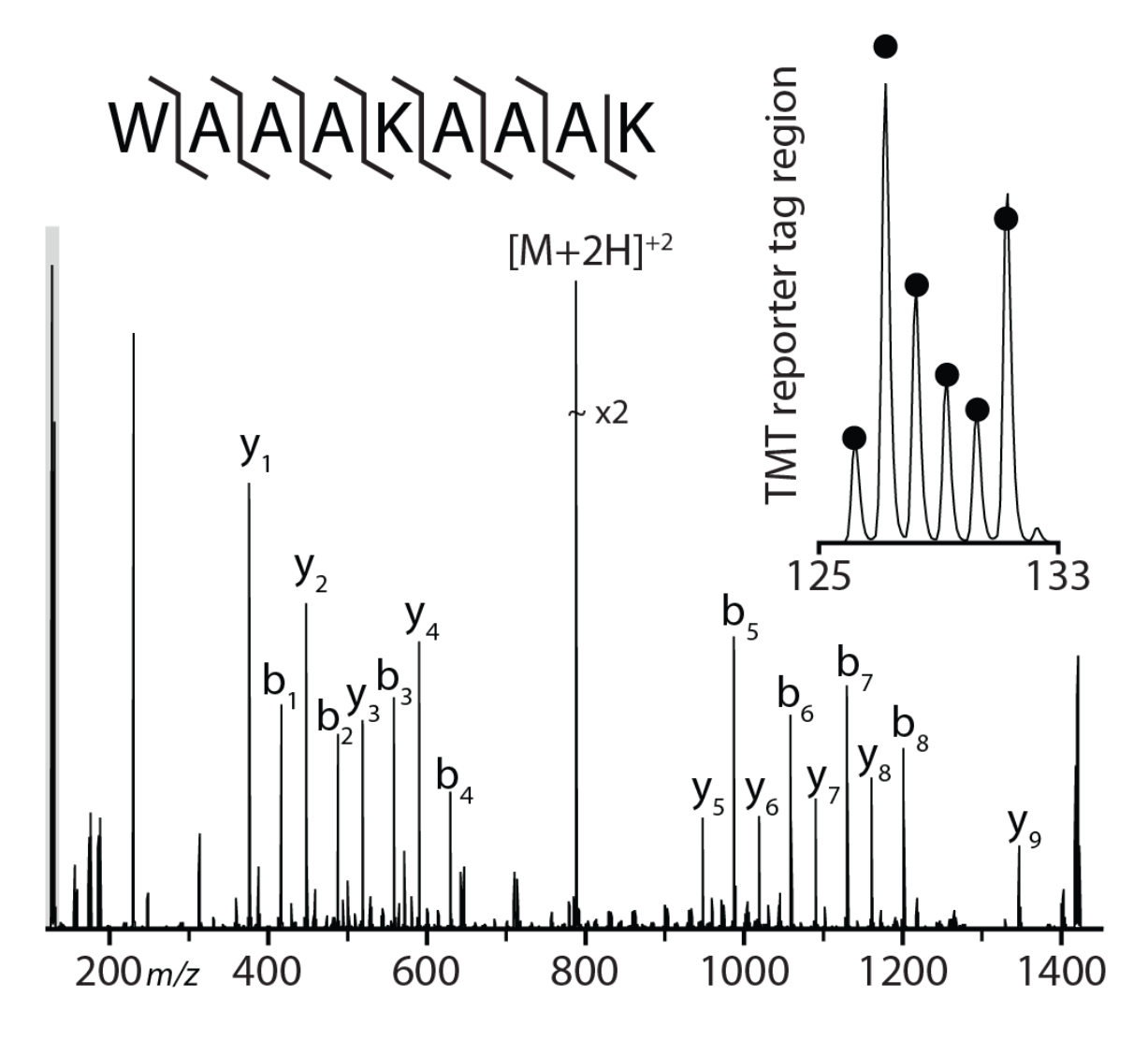


Figure 3. Single scan IRMPD MS/MS spectrum of the doubly protonated peptide cation, WAAAKAAAK, performed at a q=0.13 relative to the precursor for 7 ms at 60 W laser power. The labeled peptides were mixed in ratios of 1:5:2:1.5:1:3. The black dots indicate purity corrected theoretical ratios.

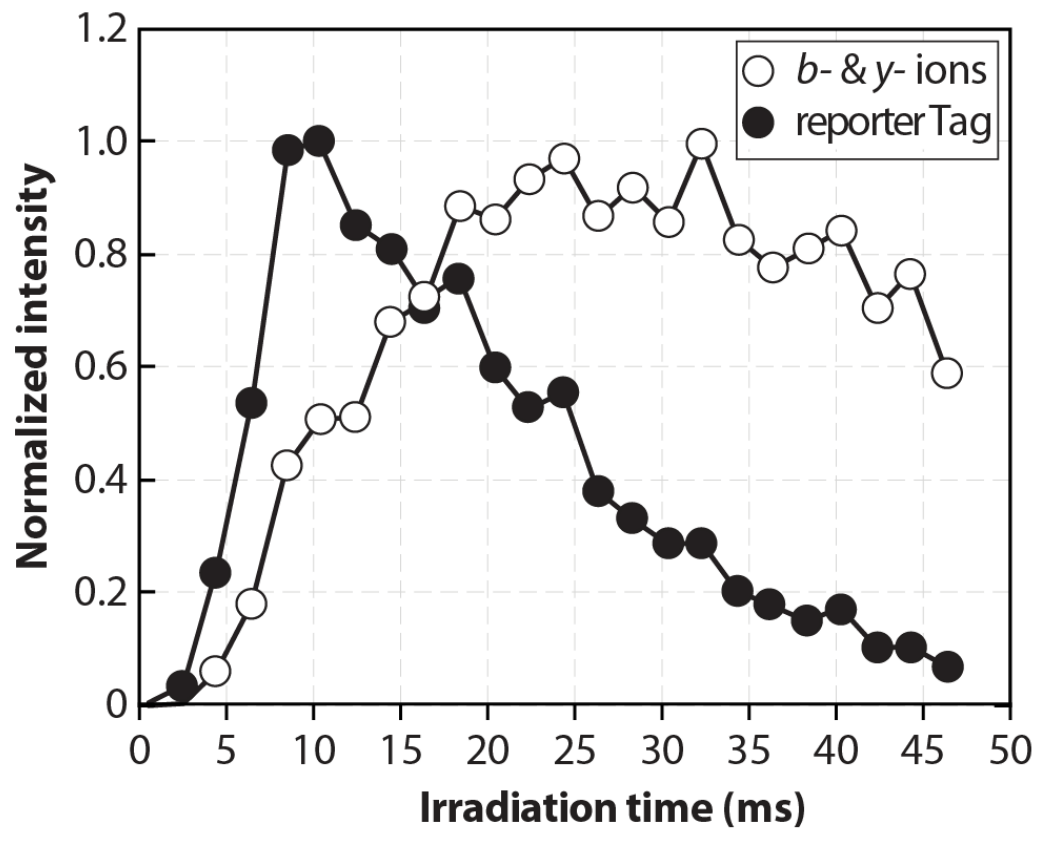


Figure 4. IRMPD time-resolved plot of b-/y- type and isobaric reporter tag intensities. The maximum yield of b- and y- type product ions occurs and a shorter time than the maximum yield of TMT reporter tag.

CAD, isolated of the y_6 product ion, and activated y_6 by IRMPD (**Fig. 5**). Intriguingly, photo-activation of the y_6 product ion primarily produces TMT reporter products. IRMPD of the peptide precursor generates b- and y- type product ions along with the TMT reporter ion; continued exposure of the b- and y-type products to photons induces secondary fragmentation and concentrates signal in TMT reporter regions. This is of importance because maximizing TMT reporter ion intensity likewise improves quantitative accuracy.

LC-MS/MS isobaric tagging experiments

Encouraged by the results of our shotgun analyses of unmodified peptides and the apparent compatibility of IRMPD for MS/MS of TMT-tagged peptides, we investigated IRMPD for shotgun analysis of complex, TMT-tagged peptide mixtures. To ensure that the reporter ions necessary for peptide quantitation are retained for all peptide precursors, we set the QLT RF amplitude to a fixed value during IRMPD (low-mass cutoff was ~ m/z 100). We interrogated un-fractionated yeast whole-cell lysate digested with trypsin and labeled with TMT in the known ratios (1:5:2:1.5:1:3). In each experiment, IRMPD was performed on the ten most abundant precursors identified from the MS¹ survey scan; we performed six individual analyses using irradiation times from 3 to 25 ms.

By fixing the RF amplitude during IRMPD the optimal irradiation time roughly scales with precursor m/z (**Fig. 6**). To evaluate quantitative accuracy, the intensity of each individual TMT quantitation channel was compared to the individual intensity of all the other channels (*e.g.*, TMT₁₂₆ was compared to TMT₁₂₇-TMT₁₃₁; TMT₁₂₇ was compared to TMT₁₂₆ and TMT₁₂₈-TMT₁₃₁, *ect.*). We averaged the absolute

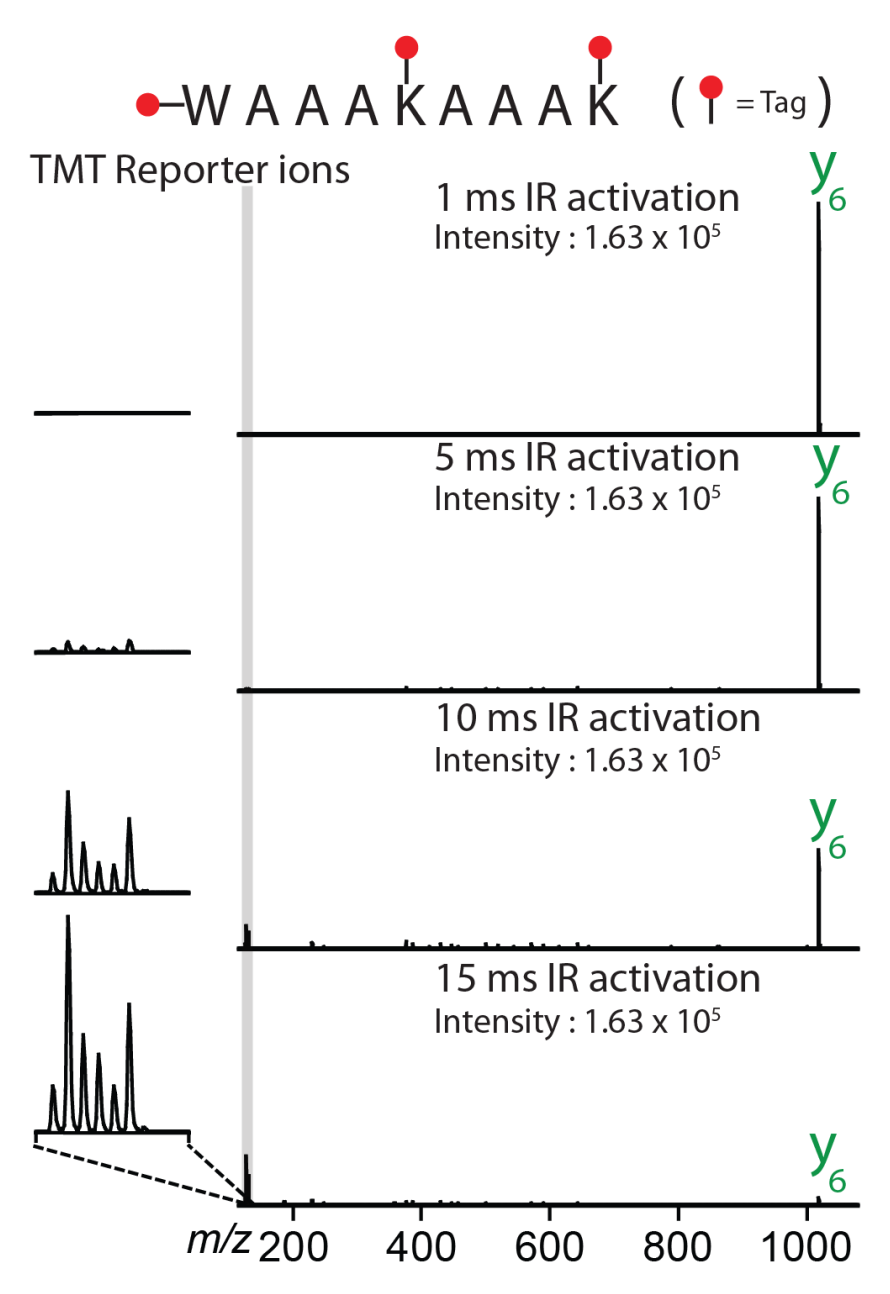


Figure 5. Single-scan IRMPD MS3 spectra of the y6 ion generated via CAD from the doubly protonated peptide WAAAKAAAK. The isolated y6 ion was subjected to IRMPD for 1, 5, 10, and 15 ms at 60W laser power. Increasing IR activation times produces increasingly intense reporter ions.

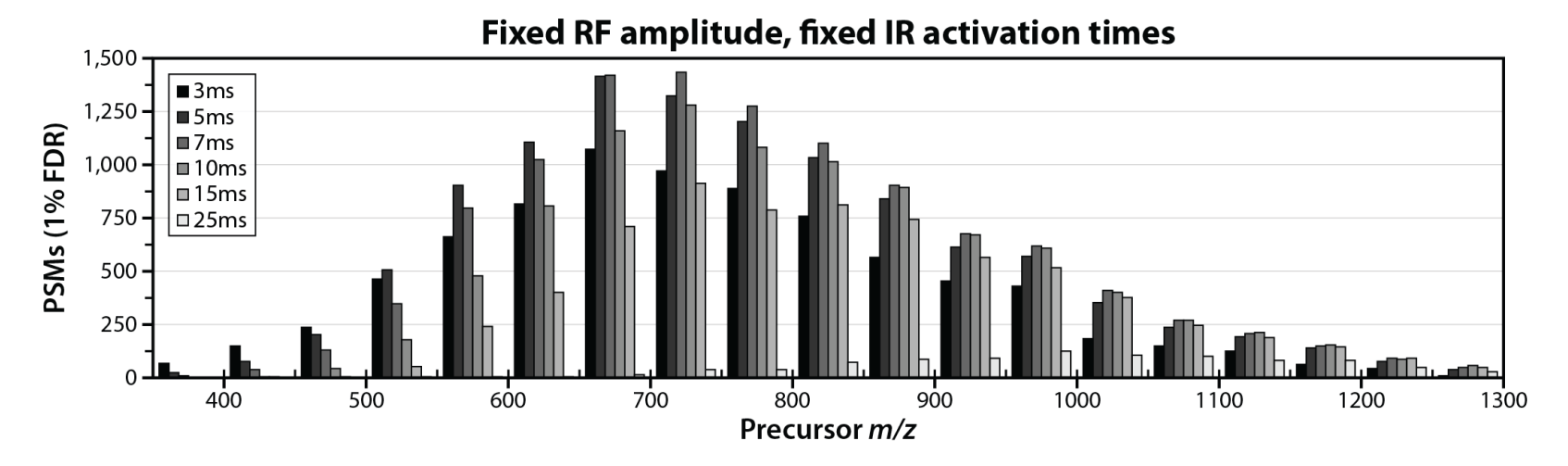


Figure 6: PSMs binned by precursor m/z value for IRMPD experiments. For each experiment, the RF amplitude was held constant, resulting in a fixed low-mass cutoff (LMCO) and dynamic precursor *q*- value. IRMPD activation times were varied from 3 to 25 ms. The resulting data indicate that setting the RF in this manner results in optimal IRMPD activation times varying strongly as a function of precursor *m/z* value.

value of the percentage deviation between theoretical (*e.g.*, TMT₁₂₆/TMT₁₂₇ should be 0.2) and observed ratios for each of the 15 comparisons, producing a metric of approximate quantitative accuracy for each MS/MS spectrum. We conclude that quantitative accuracy is likewise dependent on precursor m/z, with accuracy generally superior for peptide precursors having low m/z values (**Fig. 7**), although this can be remedied (*vide infra*). High quantitative accuracy generally correlated with high TMT reporter tag intensity (**Fig. 8**).

We reason that the uneven PSM production and quantitative accuracy across the precursor m/z range is largely a result of performing IRMPD at fixed QLT RF amplitude; by using this strategy, precursor q-value is inversely related to precursor m/z. The precursor q-value influences the proportion of time that precursor peptides spend in the center of QLT, exerting a strong influence over the magnitude of secondary dissociation and optimal irradiation time. To make IRMPD performance for both PSM production and quantitative accuracy uniform for precursors having a wide range of m/z values, we executed a set of nLC-MS/MS experiments where IRMPD time was set in a data-dependent manner, depending on precursor m/z. The general strategy we employed was to normalize the degree of secondary dissociation for all peptide precursors by manipulating the IRMPD irradiation time. Low m/z precursors (having a high q-value) require short irradiation times; in contrast, high m/z precursors (having a low q-value) require longer times (**Fig. 6**). For precursor m/z \sim 550, 5 ms represents the optimal irradiation time for production of PSMs. To produce similarly favorable

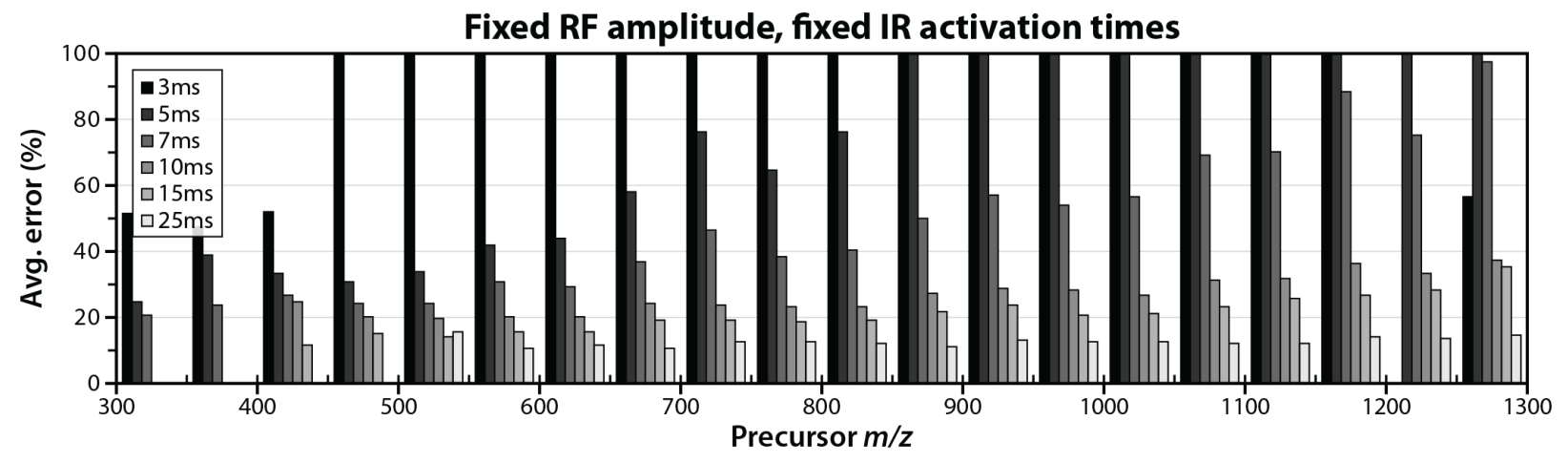


Figure 7: PSMs binned by precursor m/z value for IRMPD experiments. For each experiment, the RF amplitude was held constant, resulting in a fixed low-mass cutoff (LMCO) and dynamic precursor q- value. IRMPD activation times were varied from 3 to 25 ms. The resulting data indicate that setting the RF in this manner results in optimal IRMPD activation times varying strongly as a function of precursor m/z value.

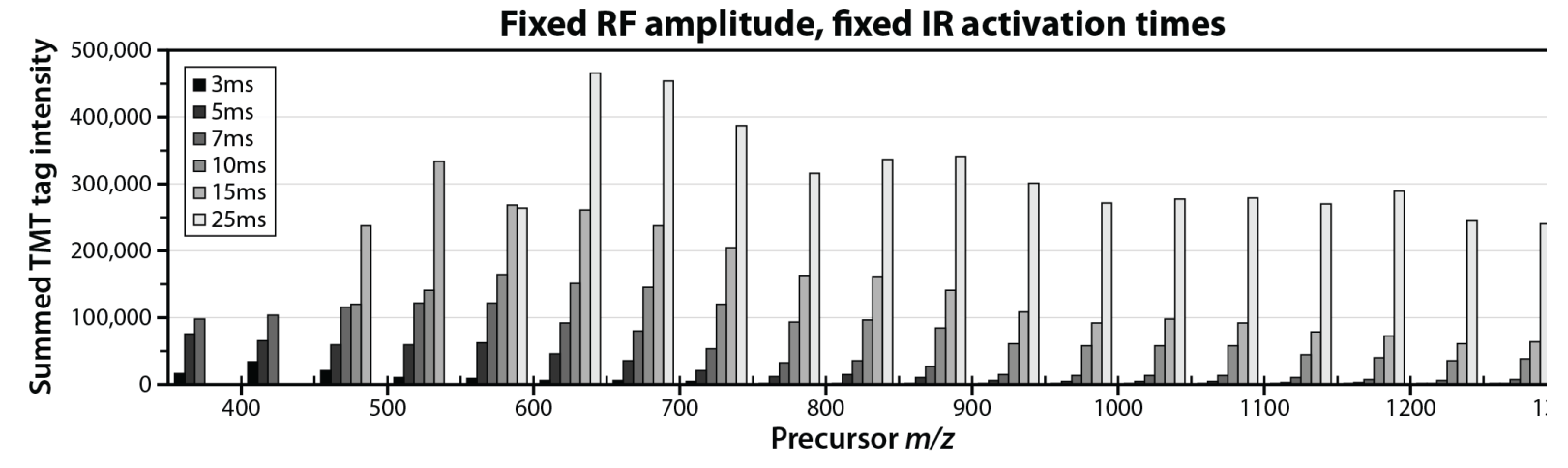


Figure 8: Average quantitative accuracy for PSMs binned by precursor m/z value for IRMPD experiments. For each experiment, the RF amplitude was held constant, resulting in a fixed low-mass cutoff (LMCO) and dynamic precursor q-value. IRMPD activation times were varied from 3 to 25 ms. At a given precursor m/z value, increasing the irradiation time decreases the metric score (reflecting better quantitative accuracy). At a given IRMPD irradiation time, quantitative accuracy is the best for precursors having a low m/z value.

results for all precursor m/z values, we varied the irradiation time as shown below (**Eqn.** 1).

$$t = t_0 \cdot \frac{precursor m/z}{550}$$
 Eq. 1

where t is the IRMPD irradiation time, and t_0 is 5 ms. Reducing this equation further results in a straightforward, data-dependent IRMPD irradiation time set by a single normalized IRMPD irradiation time coefficient multiplied by the precursor m/z value (**Eqn. 2**).

$$t = c_i \cdot precursor m/z$$
 Eq. 2

where t is the IRMPD irradiation time (ms) and c_i is the coefficient. In our initial experiment (designed to optimize PSM production), this coefficient is 0.0091. To investigate conditions more favorable for TMT reporter tag generation and higher quantitative accuracy, we also conducted experiments in which this coefficient was set to 0.0136, 0.0182, 0.0227, and 0.0273; these coefficients correspond to irradiation times of between 5 and 15 ms for precursor m/z = 550. We term these coefficients 1, 2, 3, 4, and 5 respectively.

By setting the IRMPD irradiation time dynamically, depending on precursor m/z, we successfully normalized the magnitude of secondary dissociation, ensuring homogenous IRMPD quantitative accuracy (**Fig. 9**) and PSM production across a wide range of precursor m/z values. Peptide precursors possessing higher m/z values are subjected to longer irradiation times, compensating for lower *q*-values (and slower IRMPD reaction kinetics); conversely, low m/z peptides having higher *q*-values are

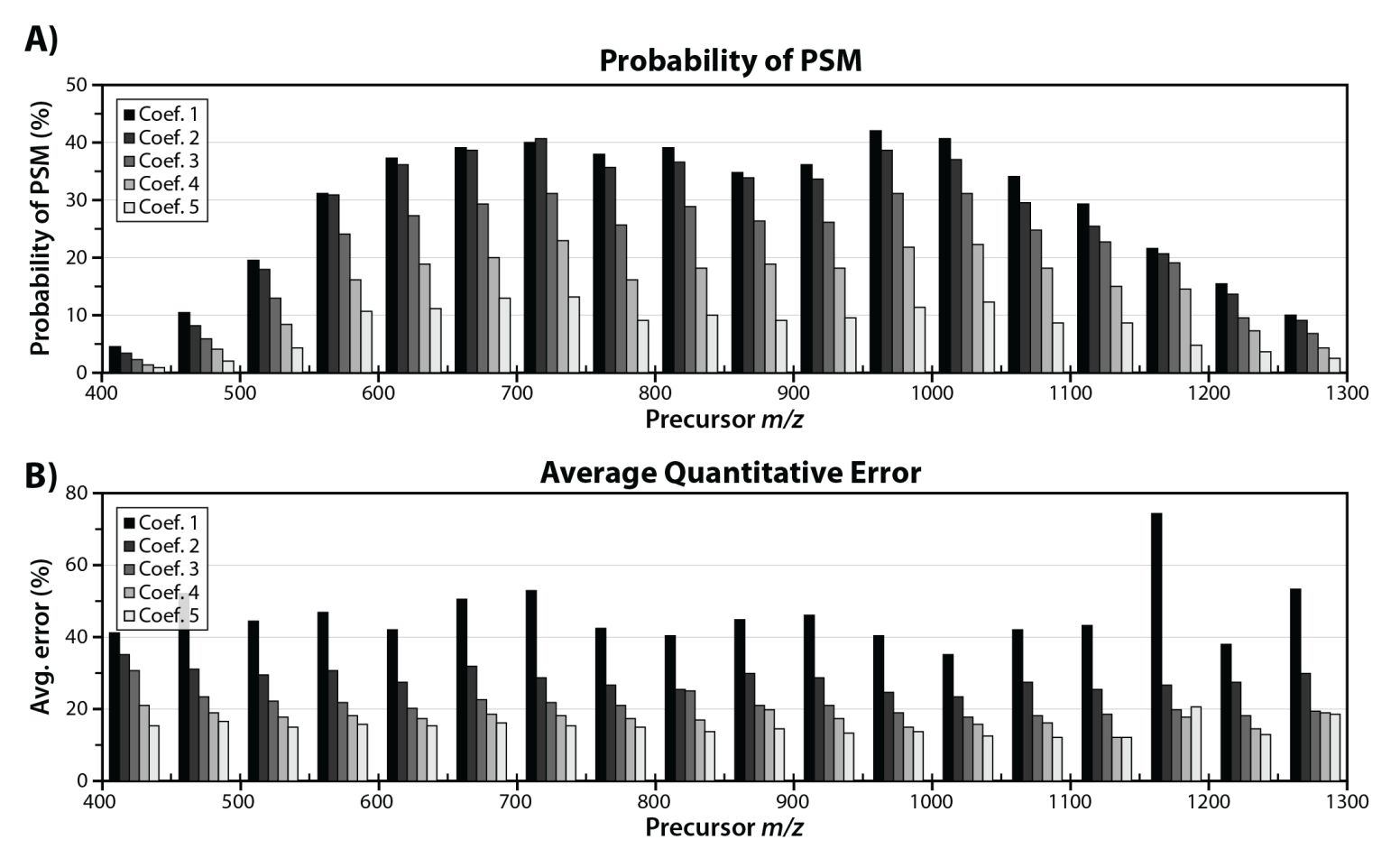


Figure 9. Average probability of error (A) and average quantitative error (B) binned by precursor m/z value for IRMPD experiments. For each experiment, the RF amplitude was held constant, resulting in a fixed low-mass cutoff (LMCO) and dynamic precursor q- value. IRMPD activation times were set in a data-dependent manner by multiplying the precursor m/z by a coefficient. Using this strategy, we are able to normalize IRMPD PSM production and quantitative accuracy across a wide range of precursor m/z values. Coefficients 1-5 correspond to increased IRMPD irradiation time. Increasing irradiation time increases secondary dissociation, resulting in better quantitative accuracy, but confounding spectral interpretation.

subjected to shorter IRMPD activation times. To examine the difference in identification rate for each coefficient, we binned each individual PSM by precursor m/z and divided by the total number of spectral features sampled over the course of the analysis. resulting data provide a 'batting average' for each coefficient as a function of precursor m/z (**Fig. 9A**). There is a slight falloff in PSM probability for peptides having either low or high m/z values; we attribute this to the sampling of non-peptidic features (low m/z) and decreased QLT trapping efficiency at very low q-values (high precursor m/z). For peptides having intermediate m/z values (comprising the vast majority of PSMs), the identification rate is consistent over a wide m/z range, with coefficient 1 representing the optimal setting for PSM production. TMT reporter tag intensity (Fig. 10) is likewise more uniform for all precursor peptides. Using coefficient 1 (shortest activation times) to set the irradiation time results in the most PSMs (10,974), but the worst quantitative accuracy (average error ~ 46%). Conversely, using coefficient 5 (longest irradiation times), we obtain the best quantitative accuracy (average error ~ 16%), but the lowest number of PSMs (2,146). Coefficients 2-4 represent intermediate irradiation times, offering a compromise between PSM production and quantitative accuracy (**Table 1**).

The most common means of interrogating isobaric-tagged peptides, beam-type collisional dissociation, HCD, has similar tradeoffs.²⁵ A series of shotgun experiments using HCD to interrogate isobaric-tagged peptides reveals HCD activation conditions can be tailored to either optimize PSMs or reporter tag intensity, but not both (**Fig. 11**).⁴³ If we plot the IRMPD data displayed in figures 4 and 5

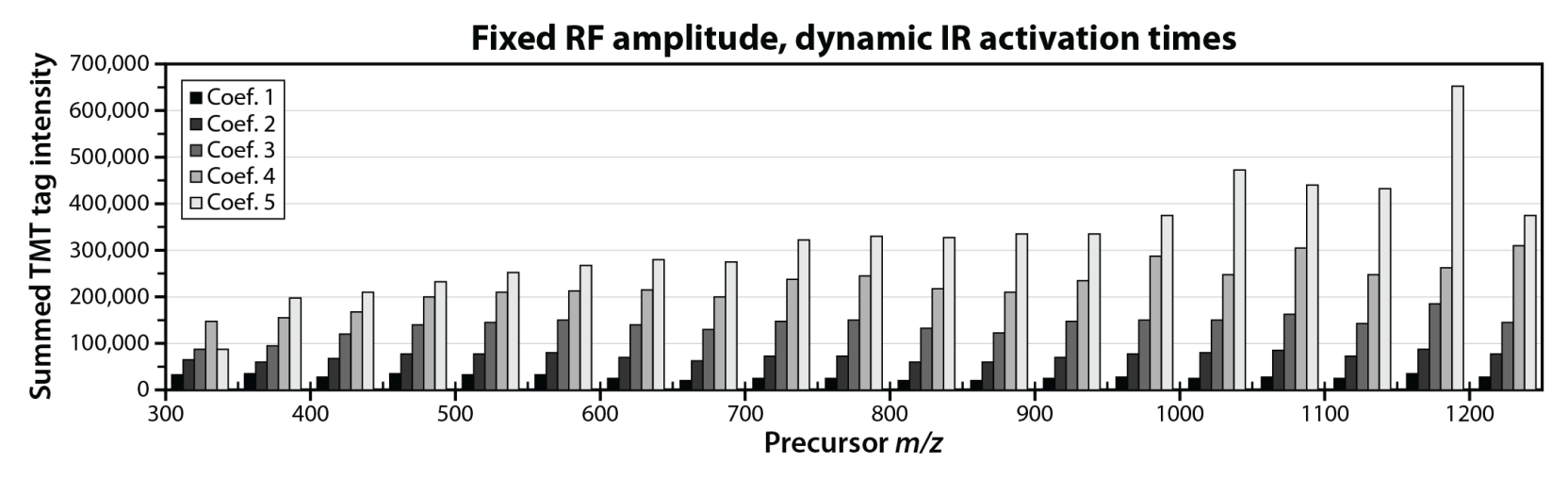


Figure 10: Average summed TMT reporter tag intensity grouped by precursor m/z value. Using fixed RF amplitude and setting IRMPD activation time dynamically results in mostly even TMT reporter tag intensity over a wide range of precursor m/z values.

Table 1. PSMs and approximate quantitative error for IRMPD using different irradiation times. Using a straightforward data-dependent IRMPD irradiation time to normalize performance vs. precursor m/z, we see that the highest numbers of PSMs occur using shorter irradiation times, with best quantitative accuracy at longer irradiation times. We attribute this to more secondary dissociation at longer times producing greater reporter tag intensity at the expense of *b*- and *y*- type fragment ions.

| | PSMs | Avg. Error |
|---------------|--------|------------|
| Coefficient 1 | 10,974 | 46% |
| Coefficient 2 | 9,877 | 28% |
| Coefficient 3 | 7,277 | 21% |
| Coefficient 4 | 4,450 | 17% |
| Coefficient 5 | 2,146 | 16% |

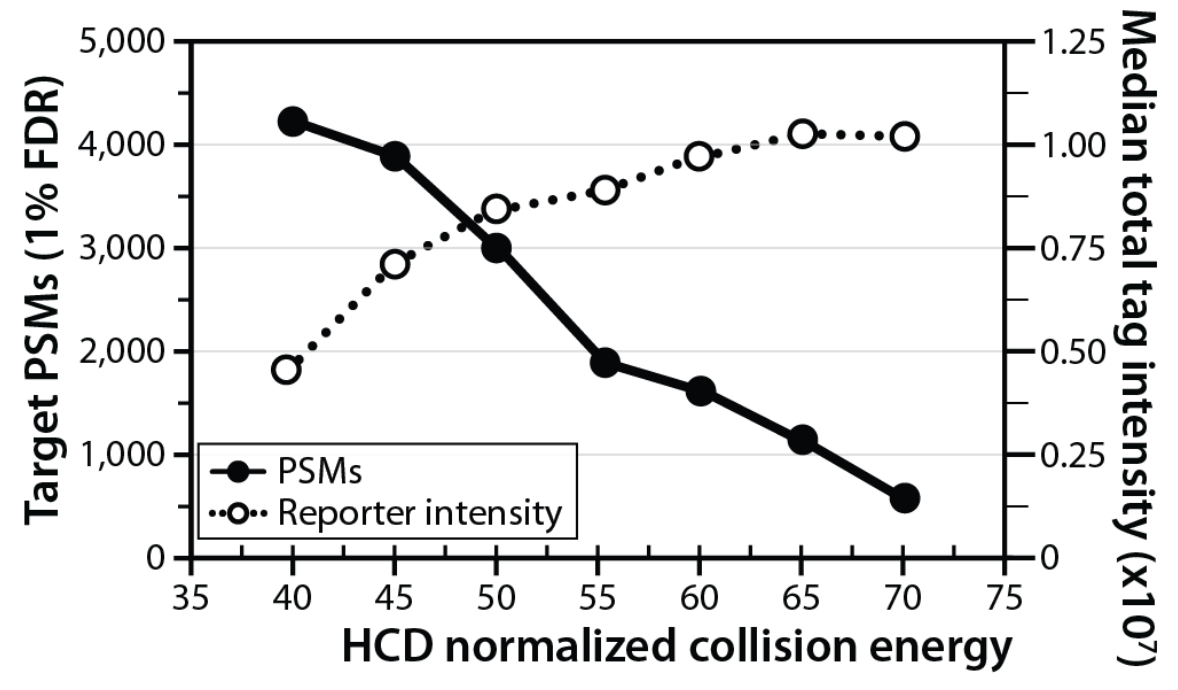


Figure 11: Peptide spectral matches (PSMs) and median reporter tag intensity as a function of HCD Collision energy. Optimal conditions for reporter tag generation are substantially higher than optimal conditions for PSM production.

similarly, treating the coefficient as an analogue to HCD collision energy, the two plots are remarkably similar (**Fig. 12**). This is presumably because HCD dissociation of *b*- and *y*- type product ions results in the formation of reporter tag, increasing the overall reporter tag intensity and quantitative accuracy. The optimal activation conditions of both IRMPD and HCD require careful consideration of the overall goals of the experiment.

Ultimately, we conclude that the use of static QLT RF amplitude and dynamic IRMPD irradiation time represents an effective strategy to both identify and quantify complex mixtures of isobaric-tagged peptides. Ideal IRMPD activation conditions for the generation of reporter tag result in a high degree of secondary activation, depleting b- and y- type product ions and complicating spectral interpretation. Fragmentation, whether in an ion trap or collision cell, can produce reporter signal; however, neither is optimized for exclusive tag production. IRMPD for as little as 30 ms results in near-exclusive conversion of precursor peptides into TMT reporter ions. To determine how this compares to iHCD, we interrogated MAAAKAAK under conditions which maximize precursor-to-reporter tag conversion efficiency. We find that IRMPD converts precursor signal to TMT reporter ions with over two-fold greater efficiency than iHCD (Figure 13). An enticing future application of the present work is the divorcing of the MS/MS event used for peptide sequencing from that used to generate reporter tag. IRMPD performed under conditions optimized for exclusive TMT reporter tag generation followed by either IRMPD under different activation conditions or other

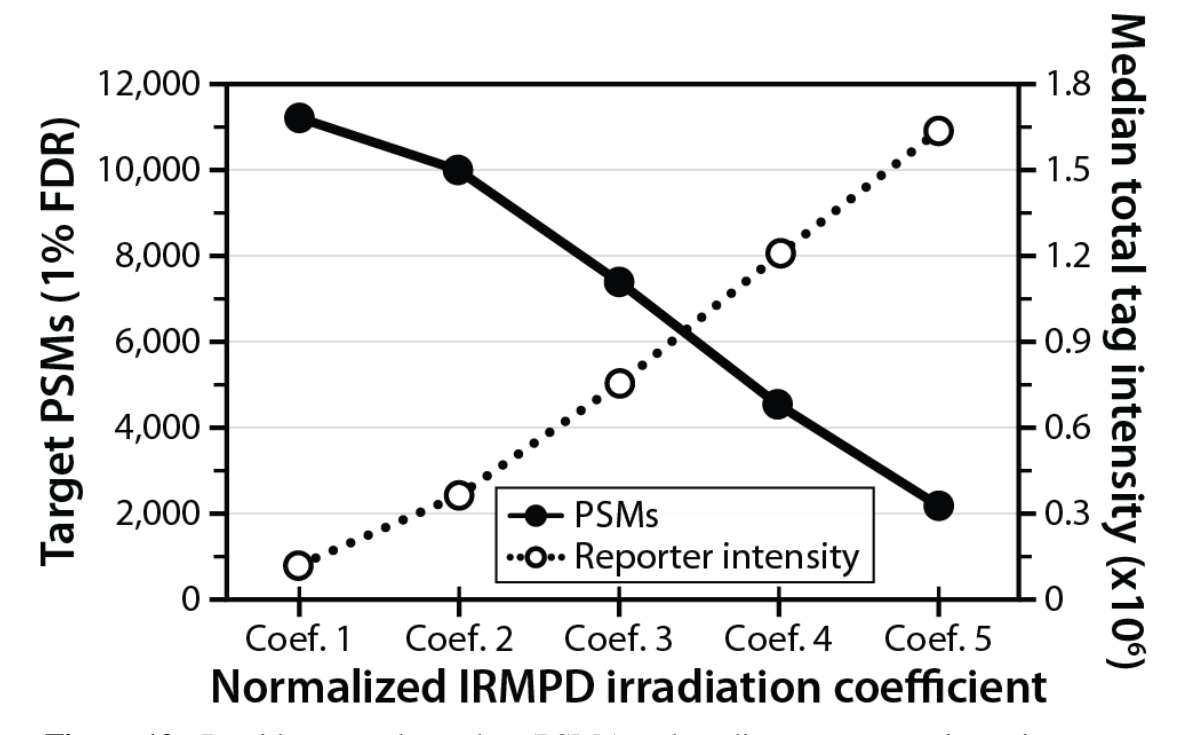


Figure 12: Peptide spectral matches (PSMs) and median reporter tag intensity as a function of Normalized IRMPD irradiation coefficient. Optimal irradiation times for reporter tag generation are substantially longer than optimal conditions for PSM production.

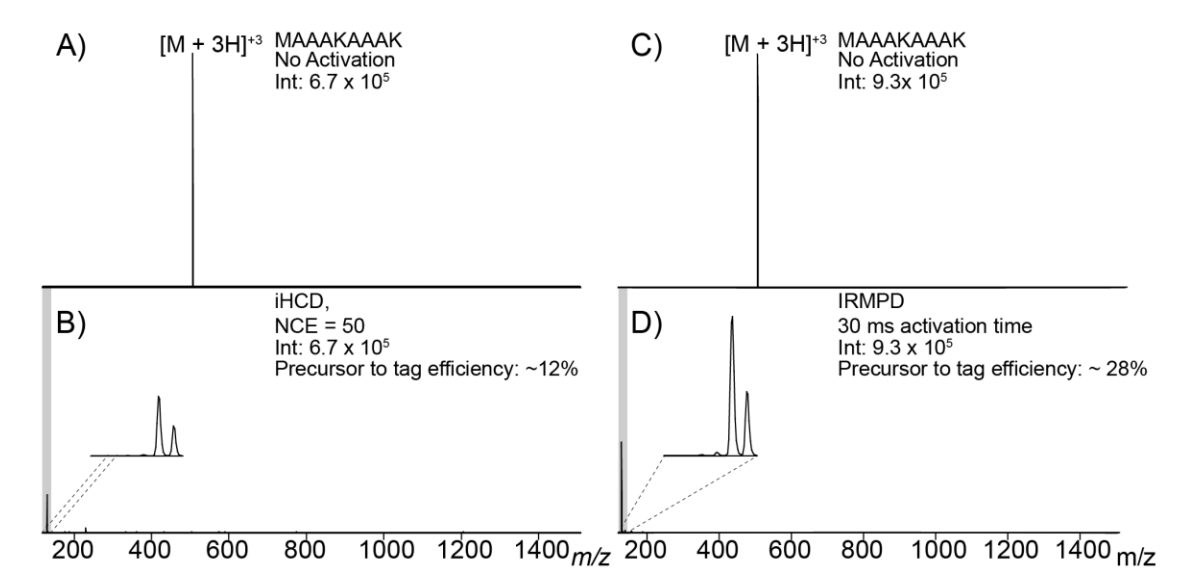


Figure 13: IRMPD (D) and iHCD (beam-type activation of precursor peptides using ESI injection optics as the collision cell, B) activation of peptide precursor MAAAKAAK. For both iHCD and IRMPD, fragmentation conditions were optimized for the production of TMT reporter ions. We find that the use of IRMPD results in a greater proportion of precursor charges being converted into TMT reporter tags as compared to iHCD.

MS/MS techniques to provide peptide sequence information would result in both peptide sequence information and highly accurate quantitative information.

Discussion

We modified a standalone dual-cell quadrupole linear ion trap (QLT) mass spectrometer to perform IRMPD in the low-pressure cell. We demonstrated that IRMPD performs at least as well as resonant-excitation CAD for shotgun peptide sequencing. The proper combinations of IRMPD activation parameters result in marginally more PSMs generated than CAD for a complex peptide mixture generated using trypsin (paired student's t-test, p=0.019) while maintaining roughly the same overall activation time (~10 ms for both CAD and IRMPD). We also evaluated IRMPD performed on a dual-cell QLT in the context of isobaric-tagged peptides. We demonstrate that IRMPD produces reporter tags with fidelity to the theoretical ratios and that the partitioning between *b*- and *y*- type ions and reporter tags is heavily dependent upon irradiation time as secondary activation of *b*- and *y*- type ions produces isobaric report tag.

We performed a series of nLC-MS/MS analyses of complex mixtures of isobaric-tagged peptides. Using fixed QLT RF amplitude results in consistent retention of TMT reporter ions, but also strong dependence between precursor m/z and the ability to both identify peptides and provide accurate quantitation. We reason that such uneven performance is a result of precursor q-value (dependent upon precursor m/z at fixed RF amplitudes) exerting influence in the degree of IRMPD secondary dissociation for a given irradiation time. To counter this, we developed an algorithm to set the IRMPD

irradiation time in a data-dependent manner, based on precursor m/z value, the ability to sequence precursor peptides and gain quantitative information are normalized across a wide precursor m/z range. While optimal settings for peptide identification are somewhat different than optimal activation settings for quantitation that an effective compromise can be reached and that IRMPD represents a viable option for the interrogation of isobaric-tagged peptides. This tradeoff is highly similar to what is encountered when using beam-type collisional activation for interrogation of isobaric-tagged peptides. Future work will focus on the use of IRMPD for isobaric tagging on high-resolution mass spectrometers, as well as a more comprehensive comparison of IRMPD to beam-type collisional activation for the interrogation of isobaric-tagged peptides.

Methods

Sample Preparation, Mass Spectrometry, LC separation

Wild-type yeast was grown and lysed, digested using trypsin, and labeled using six channel TMT tags as previously described. All experiments were performed on a modified LTQ-Velos (Thermo Fisher Scientific, San Jose, CA) dual pressure linear ion trap mass spectrometer. Briefly, the back flange of the mass spectrometer was modified to hold a ZnSe window and a stainless steel blocking disk with an aperture of 0.65" concentric with the trapping volume of the QLT (Fig. 14). All IRMPD experiments were performed using a Firestar T-100 Synrad 100-W CO₂ continuous wave laser (Mukilteo, WA). LC separations were carried out using a NanoAcquity UPLC system and auto-sampler to load samples onto a

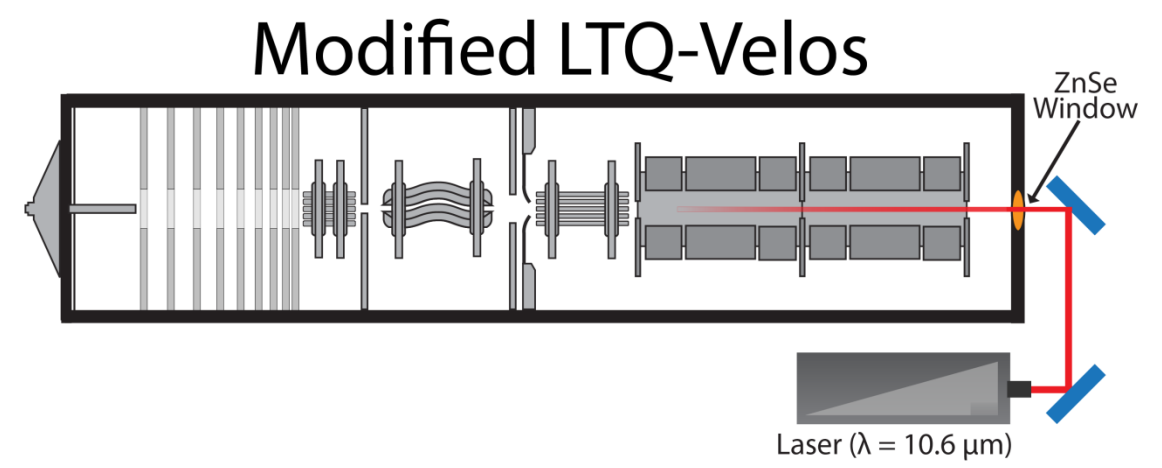


Figure 14: Modified dual-cell QLT ion trap. The addition of a ZnSe window enables IRMPD to be readily performed in the low pressure ion trap.

75 μm i.d. 5 μm particle 8 cm pre-column, and separated on a 50 μm i.d. 5 μm 25 cm analytical column (Waters, Milford, MA) as previously described.⁴⁴

During the nLC-MS/MS analysis of the unmodified complex peptide mixture, the mass spectrometry method consisted of an MS^1 analysis followed by consecutive CAD and IRMPD data dependent MS^2 scans of the 3 most intense precursors. For nLC-MS/MS analysis of TMT-tagged complex peptide mixtures, the mass spectrometry scan sequence consisted of an MS^1 survey scan followed by ten IRMPD MS/MS events interrogating the top ten most intense precursors. Activation using CAD was performed in the high pressure cell at normalized collision energy (NCE) of 35 for 10 ms; IRMPD was carried out in the low pressure cell. IRMPD conditions for each LC analysis were varied (*vida supra*). Precursors were dynamically excluded for 90 s using an isolation window of \pm 1.5 Th. AGC target values were 40,000 for MS^1 and 10,000 for MS^2 analysis.

Database Searching and Data Analysis

For unmodified and TMT-labeled peptide LC- MS/MS analyses, data reduction was performed with COMPASS, ⁴⁶ a program which converts output files to searchable text files, as described previously. ⁴⁶ OMSSA (version 2.1.8, www.yeastgenome.org) was used to search spectra against the concatenated target-decoy SGD yeast database (downloaded 01-05-2010). Average mass tolerances of +/- 5 Th and +/- 0.5 Th were used for precursor and product m/z respectively, with carbaminomethylation of cysteine set as a fixed modification and oxidation of methionine set as a variable modification. For TMT tagged samples, TMT 6-plex on the N-terminus and TMT 6-plex on lysine

residues were set as fixed modifications, with TMT 6-plex on tyrosine residues set as a fixed modification. All peptide spectrum matches (PSMs) were filtered to a false discovery rate (FDR) of 1% using expectation value (*e*-value) and the concatenated forward-reverse database method. Proteins were also reduced for parsimony and filtered to 1% FDR. Protein quantitation was evaluated with COMPASS, which corrects for isotopic impurities, normalizes reporter ion intensities, and coalesces peptide quantitation into protein quantitation. And y- type fragment ions were searched for both CAD and IRMPD spectra.

References

- Aebersold, R. & Mann, M. Mass spectrometry-based proteomics. *Nature* **422**, 198-207, doi:10.1038/nature01511 (2003).
- Hunt, D. F., Yates, J. R., Shabanowitz, J., Winston, S. & Hauer, C. R. PROTEIN SEQUENCING BY TANDEM MASS-SPECTROMETRY. *Proc. Natl. Acad. Sci. U. S. A.* **83**, 6233-6237, doi:10.1073/pnas.83.17.6233 (1986).
- Washburn, M. P., Wolters, D. & Yates, J. R. Large-scale analysis of the yeast proteome by multidimensional protein identification technology. *Nat. Biotechnol.* **19**, 242-247, doi:10.1038/85686 (2001).
- de Godoy, L. M. F. *et al.* Comprehensive mass-spectrometry-based proteome quantification of haploid versus diploid yeast. *Nature* **455**, 1251-U1260, doi:10.1038/nature07341 (2008).
- Liu, H. B., Sadygov, R. G. & Yates, J. R. A model for random sampling and estimation of relative protein abundance in shotgun proteomics. *Anal. Chem.* **76**, 4193-4201, doi:10.1021/ac0498563 (2004).
- Ong, S. E. *et al.* Stable isotope labeling by amino acids in cell culture, SILAC, as a simple and accurate approach to expression proteomics. *Mol. Cell. Proteomics* **1**, 376-386, doi:10.1074/mcp.M200025-MCP200 (2002).
- Jiang, H. & English, A. M. Quantitative analysis of the yeast proteome by incorporation of isotopically labeled leucine. *J. Proteome Res.* **1**, 345-350, doi:10.1021/pr025523f (2002).
- Du, Y., Parks, B. A., Sohn, S., Kwast, K. E. & Kelleher, N. L. Top-down approaches for measuring expression ratios of intact yeast proteins using Fourier transform mass spectrometry. *Anal. Chem.* **78**, 686-694, doi:10.1021/ac050993p (2006).

- Washburn, M. P., Ulaszek, R., Deciu, C., Schieltz, D. M. & Yates, J. R. Analysis of quantitative proteomic data generated via multidimensional protein identification technology. *Anal. Chem.* **74**, 1650-1657, doi:10.1021/ac0157041 (2002).
- MacCoss, M. J., Wu, C. C., Liu, H. B., Sadygov, R. & Yates, J. R. A correlation algorithm for the automated quantitative analysis of shotgun proteomics data. *Anal. Chem.* **75**, 6912-6921, doi:10.1021/ac034790h (2003).
- Ross, P. L. *et al.* Multiplexed protein quantitation in Saccharomyces cerevisiae using amine-reactive isobaric tagging reagents. *Mol. Cell. Proteomics* **3**, 1154-1169, doi:10.1074/mcp.M400129-MCP200 (2004).
- Thompson, A. *et al.* Tandem mass tags: A novel quantification strategy for comparative analysis of complex protein mixtures by MS/MS. *Anal. Chem.* **75**, 1895-1904, doi:10.1021/ac0262560 (2003).
- Gygi, S. P. *et al.* Quantitative analysis of complex protein mixtures using isotope-coded affinity tags. *Nat. Biotechnol.* **17**, 994-999, doi:10.1038/13690 (1999).
- Hsu, J. L., Huang, S. Y., Chow, N. H. & Chen, S. H. Stable-isotope dimethyl labeling for quantitative proteomics. *Anal. Chem.* **75**, 6843-6852, doi:10.1021/ac0348625 (2003).
- 15 Choe, L. *et al.* 8-Plex quantitation of changes in cerebrospinal fluid protein expression in subjects undergoing intravenous immunoglobulin treatment for Alzheimer's disease. *Proteomics* **7**, 3651-3660, doi:10.1002/pmic.200700316 (2007).
- Dayon, L. *et al.* Relative quantification of proteins in human cerebrospinal fluids by MS/MS using 6-plex isobaric tags. *Anal. Chem.* **80**, 2921-2931, doi:10.1021/ac702422x (2008).
- Hunt, D. F., Buko, A. M., Ballard, J. M., Shabanowitz, J. & Giordani, A. B. SEQUENCE-ANALYSIS OF POLYPEPTIDES BY COLLISION ACTIVATED DISSOCIATION ON A TRIPLE QUADRUPOLE MASS-SPECTROMETER. *Biomedical Mass Spectrometry* **8**, 397-408, doi:10.1002/bms.1200080909 (1981).
- Louris, J. N. *et al.* INSTRUMENTATION, APPLICATIONS, AND ENERGY DEPOSITION IN QUADRUPOLE ION-TRAP TANDEM MASS-SPECTROMETRY. *Anal. Chem.* **59**, 1677-1685, doi:10.1021/ac00140a021 (1987).
- 19 McLuckey, S. A. PRINCIPLES OF COLLISIONAL ACTIVATION IN ANALYTICAL MASS-SPECTROMETRY. *J. Am. Soc. Mass Spectrom.* **3**, 599-614, doi:10.1016/1044-0305(92)85001-z (1992).
- Schwartz, J. C. S., J. E. P.; Quarmby, S. T. in *53rd ASMS Conference on Mass Spectrometry and Allied Topics*.
- Cunningham, C., Glish, G. L. & Burinsky, D. J. High amplitude short time excitation: A method to form and detect low mass product ions in a quadrupole ion trap mass spectrometer. *J. Am. Soc. Mass Spectrom.* **17**, 81-84, doi:10.1016/j.jasms.2005.09.007 (2006).

- Morris, H. R. *et al.* High sensitivity collisionally-activated decomposition tandem mass spectrometry on a novel quadrupole/orthogonal-acceleration time-of-flight mass spectrometer. *Rapid Commun. Mass Spectrom.* **10**, 889-896, doi:10.1002/(sici)1097-0231(19960610)10:8<889::aid-rcm615>3.3.co;2-6 (1996).
- Tang, X. J., Ens, W., Standing, K. G. & Westmore, J. B. DAUGHTER ION MASS-SPECTRA FROM CATIONIZED MOLECULES OF SMALL OLIGOPEPTIDES IN A REFLECTING TIME-OF-FLIGHT MASS-SPECTROMETER. *Anal. Chem.* **60**, 1791-1799, doi:10.1021/ac00168a029 (1988).
- Verentchikov, A. N., Ens, W. & Standing, K. G. REFLECTING TIME-OF-FLIGHT MASS-SPECTROMETER WITH AN ELECTROSPRAY ION-SOURCE AND ORTHOGONAL EXTRACTION. *Anal. Chem.* **66**, 126-133, doi:10.1021/ac00073a022 (1994).
- Olsen, J. V. *et al.* Higher-energy C-trap dissociation for peptide modification analysis. *Nat. Methods* **4**, 709-712, doi:10.1038/nmeth1060 (2007).
- McAlister, G. C., Phanstiel, D. H., Brumbaugh, J., Westphall, M. S. & Coon, J. J. Higher-energy Collision-activated Dissociation Without a Dedicated Collision Cell. *Mol. Cell. Proteomics* **10**, doi:10.1074/mcp.O111.009456 (2011).
- 27 Madsen, J. A., Boutz, D. R. & Brodbelt, J. S. Ultrafast Ultraviolet Photodissociation at 193 nm and its Applicability to Proteomic Workflows. *J. Proteome Res.* **9**, 4205-4214, doi:10.1021/pr100515x (2010).
- Brodbelt, J. S. & Wilson, J. J. INFRARED MULTIPHOTON DISSOCIATION IN QUADRUPOLE ION TRAPS. *Mass Spectrom. Rev.* **28**, 390-424, doi:10.1002/mas.20216 (2009).
- 29 Reilly, J. P. ULTRAVIOLET PHOTOFRAGMENTATION OF BIOMOLECULAR IONS. *Mass Spectrom. Rev.* **28**, 425-447, doi:10.1002/mas.20214 (2009).
- Black, D. M., Payne, A. H. & Glish, G. L. Determination of cooling rates in a quadrupole ion trap. *J. Am. Soc. Mass Spectrom.* **17**, 932-938, doi:10.1016/j.jasms.2006.01.001 (2006).
- Boue, S. M., Stephenson, J. L. & Yost, R. A. Pulsed helium introduction into a quadrupole ion trap for reduced collisional quenching during infrared multiphoton dissociation of electrosprayed ions. *Rapid Commun. Mass Spectrom.* **14**, 1391-1397, doi:10.1002/1097-0231(20000815)14:15<1391::aid-rcm36>3.0.co;2-o (2000).
- Hashimoto, Y., Hasegawa, H. & Waki, L. High sensitivity and broad dynamic range infrared multiphoton dissociation for a quadrupole ion trap. *Rapid Commun. Mass Spectrom.* **18**, 2255-2259, doi:10.1002/rcm.1619 (2004).
- Newsome, G. A. & Glish, G. L. Improving IRMPD in a Quadrupole Ion Trap. *J. Am. Soc. Mass Spectrom.* **20**, 1127-1131, doi:10.1016/j.jasms.2009.02.003 (2009).
- Hashimoto, Y., Hasegawa, H., Yoshinari, K. & Waki, I. Collision-activated infrared multiphoton dissociation in a quadrupole ion trap mass spectrometer. *Anal. Chem.* **75**, 420-425, doi:10.1021/ac025866x (2003).

- Payne, A. H. & Glish, G. L. Thermally assisted infrared multiphoton photodissociation in a quadrupole ion trap. *Anal. Chem.* **73**, 3542-3548, doi:10.1021/ac010245+ (2001).
- Kjeldsen, F., Giessing, A. M. B., Ingrell, C. R. & Jensen, O. N. Peptide sequencing and characterization of post-translational modifications by enhanced ion-charging and liquid chromatography electron-transfer dissociation tandem mass spectrometry. *Anal. Chem.* **79**, 9243-9252, doi:10.1021/ac701700g (2007).
- Pikulski, M., Wilson, J. J., Aguilar, A. & Brodbelt, J. S. Amplification of infrared multiphoton dissociation efficiency in a quadruple ion trap using IR-active ligands. *Anal. Chem.* **78**, 8512-8517, doi:10.1021/ac061472k (2006).
- Madsen, J. A. & Brodbelt, J. S. Comparison of Infrared Multiphoton Dissociation and Collision-Induced Dissociation of Supercharged Peptides in Ion Traps. *J. Am. Soc. Mass Spectrom.* **20**, 349-358, doi:10.1016/j.jasms.2008.10.018 (2009).
- Gardner, M. W., Vasicek, L. A., Shabbir, S., Anslyn, E. V. & Brodbelt, J. S. Chromogenic cross-linker for the characterization of protein structure by infrared multiphoton dissociation mass spectrometry. *Anal. Chem.* **80**, 4807-4819, doi:10.1021/ac800625x (2008).
- Second, T. P. *et al.* Dual-Pressure Linear Ion Trap Mass Spectrometer Improving the Analysis of Complex Protein Mixtures. *Analytical Chemistry* **81**, 7757-7765, doi:10.1021/ac901278y (2009).
- Gardner, M. W. *et al.* Infrared Multiphoton Dissociation of Peptide Cations in a Dual Pressure Linear Ion Trap Mass Spectrometer. *Anal. Chem.* **81**, 8109-8118, doi:10.1021/ac901313m (2009).
- Sleno, L. & Volmer, D. A. Ion activation methods for tandem mass spectrometry. *J. Mass Spectrom.* **39**, 1091-1112, doi:10.1002/jms.703 (2004).
- Wenger, C. D. *et al.* Gas-phase purification enables accurate, multiplexed proteome quantification with isobaric tagging. *Nat. Methods* **8**, 933-935, doi:10.1038/nmeth.1716 (2011).
- McAlister, G. C., Phanstiel, D., Wenger, C. D., Lee, M. V. & Coon, J. J. Analysis of Tandem Mass Spectra by FTMS for Improved Large-Scale Proteomics with Superior Protein Quantification. *Anal. Chem.* **82**, 316-322, doi:10.1021/ac902005s (2010).
- Madsen, J. A. *et al.* Top-Down Protein Fragmentation by Infrared Multiphoton Dissociation in a Dual Pressure Linear Ion Trap. *Anal. Chem.* **81**, 8677-8686, doi:10.1021/ac901554z (2009).
- Wenger, C. D., Phanstiel, D. H., Lee, M. V., Bailey, D. J. & Coon, J. J. COMPASS: A suite of pre- and post-search proteomics software tools for OMSSA. *Proteomics* 11, 1064-1074, doi:10.1002/pmic.201000616 (2011).
- 47 Moore, R. E., Young, M. K. & Lee, T. D. Qscore: An algorithm for evaluating SEQUEST database search results. *J. Am. Soc. Mass Spectrom.* **13**, 378-386, doi:10.1016/s1044-0305(02)00352-5 (2002).

Elias, J. E. & Gygi, S. P. Target-decoy search strategy for increased confidence in large-scale protein identifications by mass spectrometry. *Nat. Methods* **4**, 207-214, doi:10.1038/nmeth1019 (2007).

Chapter 7

Increased Throughput of Proteomics Analysis by Multiplexing High-Resolution Tandem Mass Spectra

Summary

High-resolution and high-accuracy Fourier transform mass spectrometry (FTMS) is becoming increasingly attractive due to its specificity. However, the speed of tandem FTMS analysis severely limits the competitive advantage of this approach relative to faster low-resolution quadrupole ion trap MS/MS instruments. Here we demonstrate an entirely FTMS-based analysis method with a 2.5 – 3.0-fold greater throughput than a conventional FT MS/MS approach. The method consists of accumulating together the MS/MS fragment ions from multiple precursors, with subsequent high-resolution analysis of the mixture. Following acquisition, the multiplexed spectrum is de-convoluted into individual MS/MS spectra which are then combined into a single concatenated file and submitted for peptide identification to a search engine. The method is tested both in silico using a database of MS/MS spectra as well as in situ using a modified hybrid QLT-orbitrap mass spectrometer. The performance of the method in the experiment was consistent with theoretical expectations.

Introduction

Mass spectrometry (MS)-based proteomics experiments typically begin with proteolytic digestion of a protein containing sample. This complex mixture is then chromatographically separated and interrogated by MS and tandem MS (MS/MS). Mass accuracy in both the MS and MS/MS mode is closely tied to the confidence of the resulting peptide identifications.¹⁻⁴

This relationship implies that the use of high-resolution and high-accuracy mass analyzers (i.e., FTICR and FT Orbitrap) should result in higher confidence peptide identification than lower resolution and accuracy mass analyzers. Another important requirement, however, is data acquisition speed, and here the Fourier transform (FT) analyzers face a fundamental limitation manifested by the strong link between their resolving power, (R), and the length of the acquisition period (T):

$$T \sim 2f/R \tag{Eqn 1}$$

where f is the resonance frequency of the ion of interest.⁵ At a resolving power of 100 000 and f = 50 kHz, the acquisition period (T) is 1 s, or the maximum rate of acquisition of one scan/s. Other analyzers, such as quadrupole ion traps (QIT), possess higher acquisition rates. Thus, many researchers operating hybrid QIT FT MS instruments utilize the FT analyzer only for MS¹ scans. However, the analytical advantages of high resolution and mass accuracy MS/MS spectra are compelling, especially for reliable peptide identification,⁴ blind PTM determination,⁶ and de novo sequencing.⁷

One way to improve the acquisition rate during FTMS analysis of MS/MS spectra is to employ spectral multiplexing. Several methods of multiplexing MS/MS spectra have been described in the literature, with most methods utilizing physical multiplexing,

i.e., several precursors are fragmented simultaneously. One approach developed by Williams *et al.*⁸ aimed to increase signal-to-noise ratio by repeating MS/MS experiments *n* times on appropriate subsets of *n* precursor ions with subsequent assignment of product ions to the corresponding precursor ions. Each time an acquisition was made, *n*-1 precursor ions were fragmented simultaneously, and each time a new *n*th precursor was left intact. A Hadamard transform (HT) was then used to de-convolute the resulting data and thus determine MS/MS spectra for each of the precursor ions.

Another multiplexed MS/MS approach which aimed at increasing signal-to-noise relied on FT techniques similar to those used in two-dimensional (2D) NMR experiments. In this method, precursor ions were excited into their cyclotron orbits by an RF excitation pulse, which was then followed by an RF de-excitation pulse after a specific delay time (td). This de-excitation pulse changed the abundance of specific precursor ions according to the phase difference, which is dependent on the precursor ion m/z ratio. The product ion spectra were then recorded as a function of td, and the FT of this function allowed the product ions to be related to their corresponding precursor ions by their abundance changes. Two variations to this approach have been described, one by Pfandler *et al.*⁹ and another by Ross *et al.*¹⁰

Both the HT and 2D approaches to multiplexing on Fourier transform ion cyclotron resonance (FTICR) require acquisition of n MS/MS spectra to obtain the product ion spectra of n precursor ions. Thus, these methods provide signal-to-noise ratio enhancements but no increase in the analysis speed. A third approach developed by Masselon $et\ al.^{11}$ allowed multiplexed MS/MS to be performed in a single spectral

acquisition. This approach relies on database searching and the high mass accuracy and resolution capabilities of FTICR. Fragmentation products of n precursor ions were detected in one mass spectrum. The precursor and fragment m/z values were then compared to hypothetical MS/MS spectra of peptides from a protein database. The high mass accuracy of the FTICR mass spectrometer limited the number of potential candidate peptides. Ultimately, assignment of the product ions to their respective precursor ions was accomplished by matching the peptide mass tag derived from experimental data to candidate peptide sequence. The efficiency of this approach with a mainstream search engine has not been reported, and therefore the efficacy of this technique remains somewhat ambiguous. Our experiments with physical multiplexing of high-resolution mass spectra and matching the resultant spectrum against the database showed a dramatic drop in matching efficiency as the multiplexing factor n grows.

A multiplexing method for performing MS/MS on n peptide ions simultaneously in a quadrupole ion trap mass spectrometer (QIT) was developed by Wilson and Vachet. This method takes advantage of the inherent mass bias associated with ion accumulation in the QIT to encode the intensity of precursor ions in a way that allows the corresponding product ions to be identified. The intensity encoding scheme utilizes the Gaussian distributions that characterize the relationship between ion intensities and rf trapping voltages during ion accumulation. This approach uses two arbitrary waveforms, one for isolation and one for dissociation, to gather product ion spectra from n precursor ions with as few as two product ion spectra. This approach is not suitable for high-resolution mass spectra that are not acquired using a QIT.

Another approach to multiplexing was devised by Waters and termed MS^E. ¹³ All ions eluting to the instrument were fragmented, with the resulting fragments grouped together according to shared elution profiles. The utility of this method is limited when there are many co-eluting molecular species, a common occurrence in the analysis of complex protein mixtures, e.g., full or partially separated proteome digests.

Finally, direct database submission of multiplexed mass spectra has also been discussed in literature. 14,15 Such methods usually rely strongly on the mass accuracy of fragment ions and generally suffer from interference between true MS/MS fragments of a given precursor and fragments of other molecules present in the same precursor selection window. Aebersold's group subsequently provided novel software approaches for analysis of spectra acquired on low-resolution ion trap instrumentation. The ProbID tree software relies on an iterative search approach, where fragment ions resulting from identified peptides are removed prior to researching the data. 16 Though this approach does provide an improvement over direct submission of multiplexed spectra, it carries with it the disadvantages of performing multiple, iterative database searches. Such iterative searching represents an inherent gain in the necessary analysis time, a drawback which our method does not suffer from, as our multiplexing software was developed to enhance throughput. Bern et al. have recently revisited this topic, working to provide elegant software solutions to de-convolve low-resolution spectra resulting from dataindependent-acquisition (DIA) approaches using ion trap instrumentation.¹⁷ However, though ultimately improving peptide identification rates by $\sim 25\%$, this approach not only requires iterative searching due to processing speed concerns but also the use of a specialized database search algorithm, ByOnic, which employs de novo processing. This requisite de novo capability is due to the large precursor windows and precursor mass uncertainty with both the DIA approach as well as low-resolution tandem mass spectra, in general. This example again demonstrates the advantage of performing multiplexing techniques on an instrument having a high resolution mass analyzer.

Here we report on a novel multiplexing approach that is free from the above shortcomings. The method utilizes physical multiplexing of n spectra, followed by software-based de-convolution, resulting in n individual, database searchable MS/MS data sets. The de-convolution procedure, the key element of the approach, relies on accurate measurement of fragment ions and the fact that the charge separation reaction, which produces complementary ionic products, is the most frequent outcome of low-energy collisional dissociation of multiply protonated tryptic peptides.

We demonstrate, using the SwedCAD database of 15,000 high-resolution collision-dissociation mass spectra of doubly-protonated precursor, that this approach has solid theoretical basis and that the efficiency of database search using the extracted individual MS/MS spectra exceeds 90%. Furthermore, practical implementation of the method on an LTQ Orbitrap (Thermo Fisher Scientific, Bremen, Germany) improves the number of identified peptides and proteins by more than a factor of two compared to conventional FTMS MS/MS methodology.

Results

Multiplexing

The method is intended for hybrid FTMS instruments, in which the possibility exists to accumulate fragment ions from several independent MS/MS events in a separate RF device, (e.g., the C-trap of the LTQ Orbitrap). The analysis cycle (Fig.1) consists of (1) acquisition of a high-resolution "survey" MS spectrum followed by identification of m/z and z values of n multiply protonated precursors. Such identification is usually performed based on a short (64 ms or shorter) fraction of the total transient, and therefore subsequent MS/MS events can proceed while the rest of the transient (lasting 0.5 - 2.0 s) is being acquired. (2) The identified precursors are isolated and fragmented individually in the ion trap, with the product ions of different precursors being mixed together and stored in another ion trap (i.e., C-trap). (3) After completing the last MS/MS event, the fragment mix is injected into the FT analyzer and detected with high resolution. Therefore, the shortest cycle duration (disregarding the "overhead" instrumental time between different cycle stages) is equal to the duration of two high-resolution mass spectra, whereas the acquired information is equivalent to one MS and n MS/MS highresolution spectra. This should provide an improvement in the acquisition speed by a factor of k(n + 1)/2 (where is k is the efficiency of de-convolution) compared to a cycle with one survey and n individually acquired high-resolution MS/MS spectra. With n = 4and k = 0.9 (realistic values, vide infra), an improvement in speed of (0.9)*(5/2) = 2.3 is achieved.

De-convolution of the multiplexed MS/MS spectra into n virtual individual MS/MS spectral files is performed by software developed in house which creates a text input file for Mascot in the .mgf format from the raw spectral data. First, all the ions in

1. Survey MS

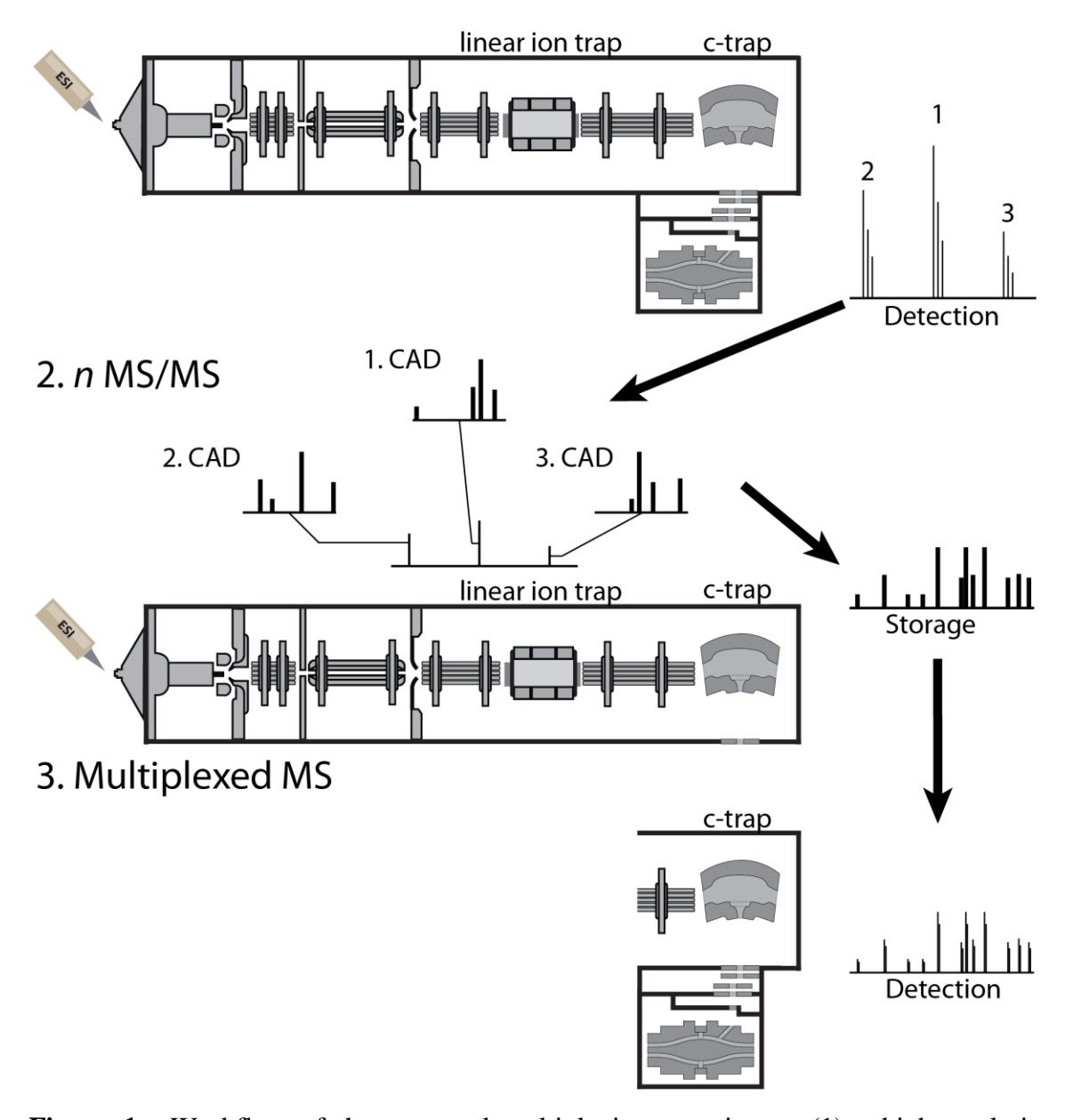


Figure 1. Workflow of the proposed multiplexing experiment: (1) a high-resolution survey spectrum is acquired, and n multiply charged precursors are identified; (2) n CAD MS/MS experiments are performed in the linear ion trap with the fragment ions stored in the c-trap; (3) a single high-resolution MS detection is performed of the multiplexed MS/MS experiments. This experiment is then followed by deconvolution of n individual MS/MS data sets.

the multiplexed MS/MS spectra are de-charged and de-isotoped.² This yields a list of neutral masses and abundances. In cases when the charge state cannot be established because of the lack of isotopic peaks, all possible charge states, from 1 to z (z being the charge state of the precursor) are assigned to the single peak present. After de-charging and de-isotoping, complementary fragment pairs are derived for each precursor molecular mass. To this end, the mass-sorted list of neutral fragments is checked for masses which when summed with a larger mass from the same list yield a value equal to the precursor mass within given mass accuracy, typically +/- 20 mDa.

Simulation of Multiplexing and Deconvolutions

Figure 2 shows the workflow for an *in silico* experiment in which 1000 high-resolution MS/MS spectra of doubly charged tryptic peptides were randomly selected from the online SwedCAD¹² database. These data sets were submitted to Mascot search engine, where they received identifications. The Mowse score (M-score)¹⁸ distribution for these identifications is shown in Figure 3, bottom panel. In total, 980 peptide identifications were above the threshold for a confident identification. The remaining 20 mass spectra (2%) were not identified mainly because the protein database has changed after the identified spectra were put in the MS/MS database, but also because the original identification was performed using both collisional-activated dissociation (CAD) and electron capture dissociation (ECD) data for the same peptide.⁴ In parallel, groups of

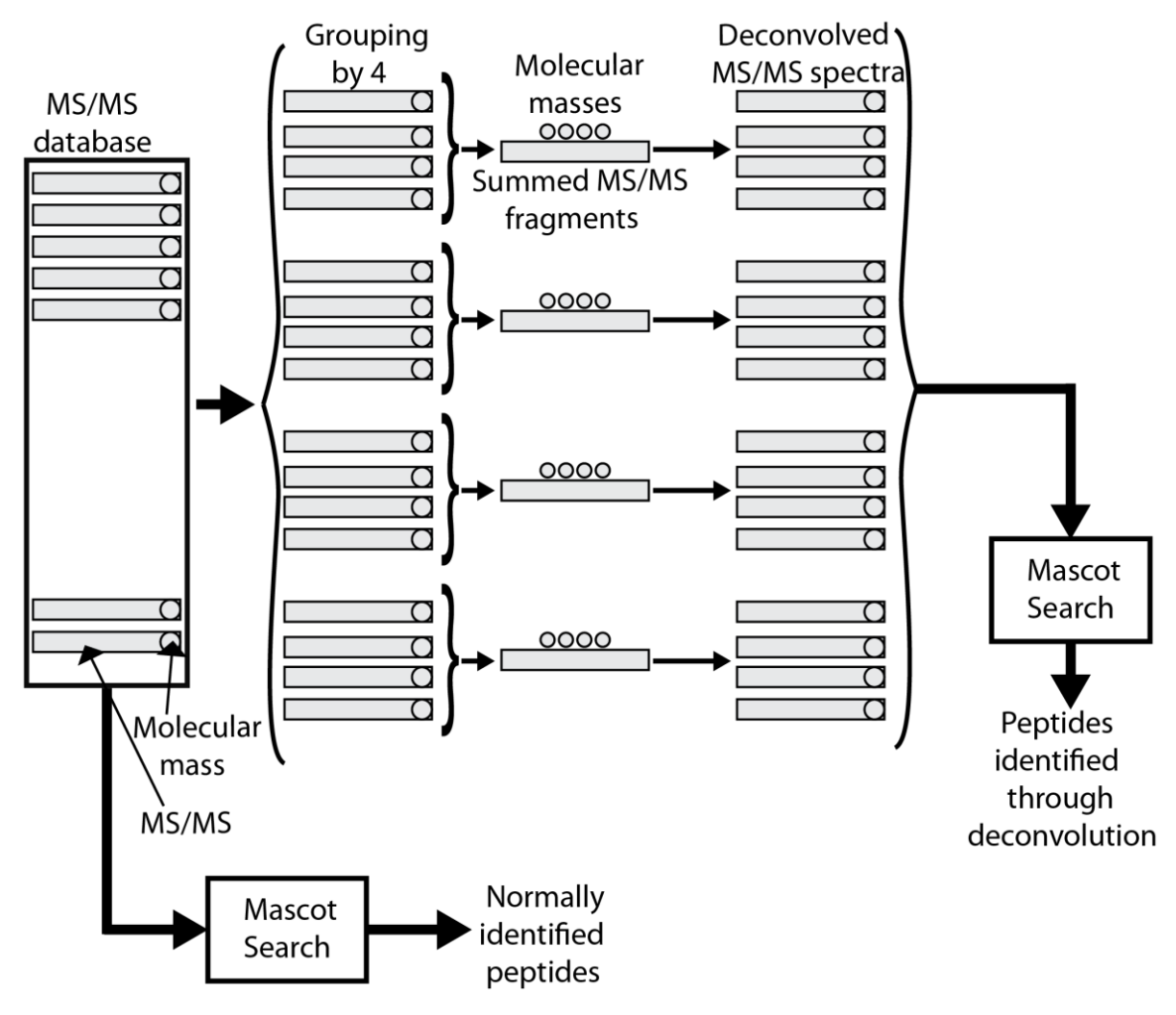


Figure 2. Workflow for an *in silico* four-plexing experiment in which 1000 high-resolution MS/MS spectra of doubly-protonated tryptic peptides were randomly selected from the SwedCAD database.

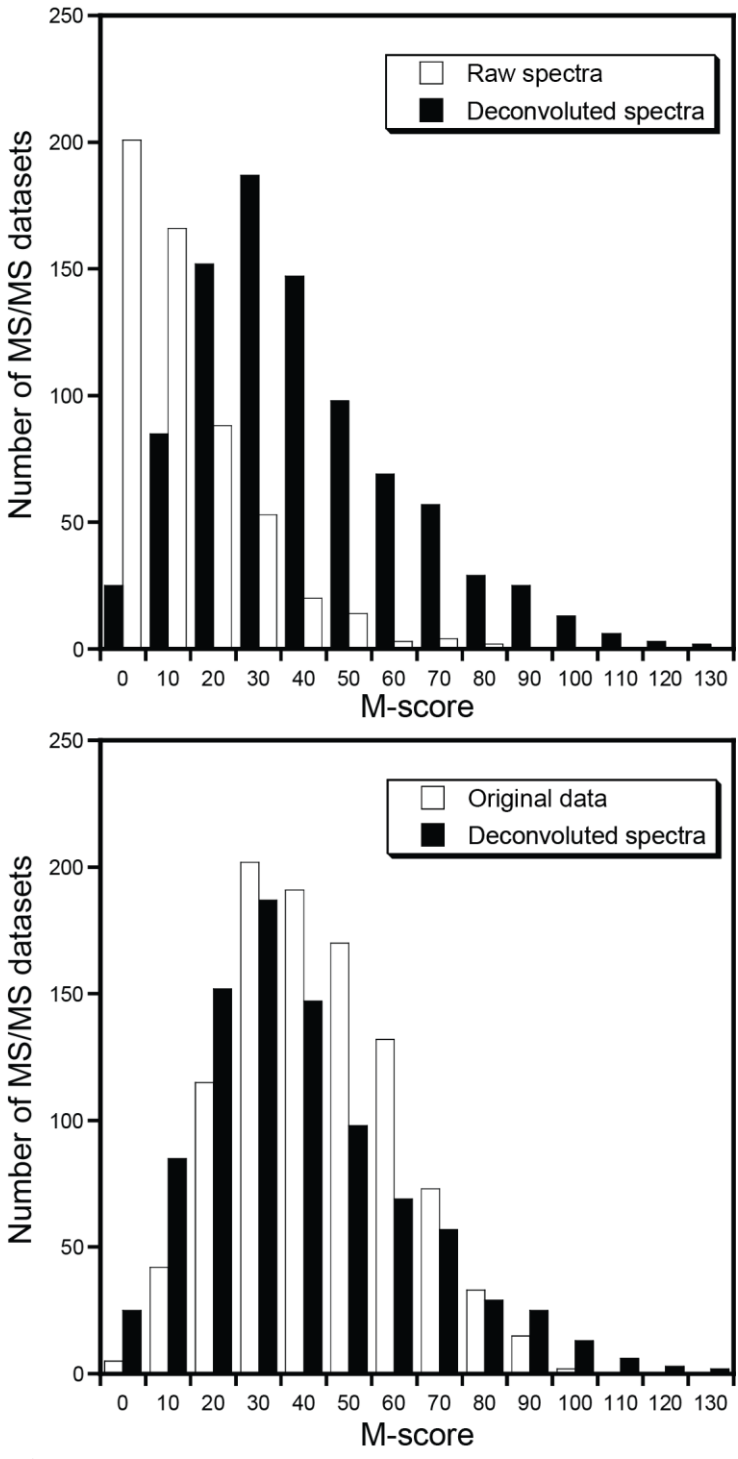


Figure 3. Mowse score (M-score) distributions for the identifications obtained in the in silico four-plexing experiment outlined in Figure 2. Black columns: upon deconvolution. White columns: top panel – without deconvolution; bottom panel – the original MS/MS data sets.

four spectra were mixed together to produce 250 convolved spectral files that were supplemented by 250 spectra each comprising four precursor masses. These convolved spectral files were submitted to Mascot using 1000 precursor masses (each convolved data set was submitted four times, each time with a new precursor mass). The distribution of the obtained M-scores is shown in the top panel of **Figure 3** (average M-score 17.5). Overall, 551 above threshold identifications were obtained, or 61% of the original number.

Using the de-convolution procedure described above, the 250 convolved spectra were de-convolved back into 1000 individual spectral files which were then concatenated into a single file and also submitted to Mascot. The M-score distribution of the deconvolved data set, shown in the top panel of Figure 2, gave the average M-score 43.7, which is not significantly different from the value 44.5 (the value obtained from the original data and displayed on the bottom panel). In total, 899 peptides were identified after de-convolution, giving the efficiency $k \approx 90\%$. Sequences of only two identified peptides after de-convolution did not coincide with the sequence identified before deconvolution, corresponding to <0.22% disagreement rate with the original Mascot identifications. This compared favorably with a value typical for many proteomics studies (1% false discovery rate).

Therefore, utilization of the de-convolution procedure produced superior results as compared to a direct search of convoluted data. Removal of the fragments of the best Mascot assigned peptide from the four-convoluted data set and subsequent resubmission of the remaining data set 15 is still inferior to the de-convolution procedure, since the

average M-score of the best assignment out of four for each of the 250 convoluted data sets was ≈35, far below the average value obtained with the de-convolution procedure.

Figure 4 shows the comparison of the average Mascot scores in the deconvolution procedure and direct submission of convolved spectra as a function of the number n of multiplexed spectra. The slight increase in value for the de-convolved spectra, as compared to direct submission at n = 1, is due to the improved data set quality due to the removal of many unrelated peaks. Overall, the results of direct submission of the convolved spectra rapidly degrade with n, whereas the falloff for de-convoluted spectra is much less steep.

Role of Mass Accuracy

Figure 5 shows the true number of the complementary pairs present in all 1000 mass spectra versus the number of de-convolved complementary pairs. At (20 mDa mass window, ca. 6300 complementary pairs are found, of which ca. 4500 are true pairs. Obviously, the fact that 25% of all found complementary pairs were spurious matches did not affect the Mascot search too badly, but it follows from the trends in Figure 5 that an improvement in mass accuracy in the MS/MS data sets would further increase the efficiency of the de-convolution method.

Experimental Verification

We modified the firmware of a hybrid mass spectrometer comprising both ion trap and orbitrap mass analyzers (Thermo Fisher Scientific, Bremen, Germany) to allow implementation of the n-multiplexing experiment. The scan cycle consisted of an MS¹ scan (R = 100K) followed by n MS/MS events in the quadrupole linear ion trap (QLT)

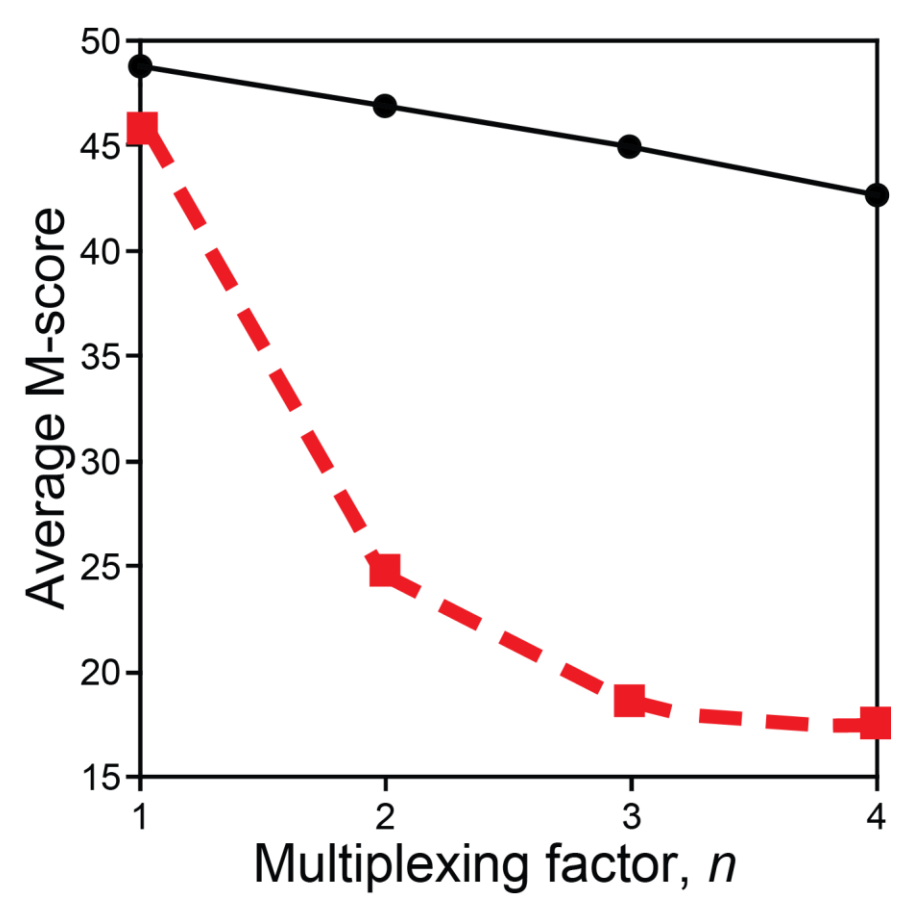


Figure 4. Comparison of the average M-scores obtained after complementary-pair deconvolution (circles) and direct Mascot search without deconvolution (squares) for in silico n-plexing experiments with different n.

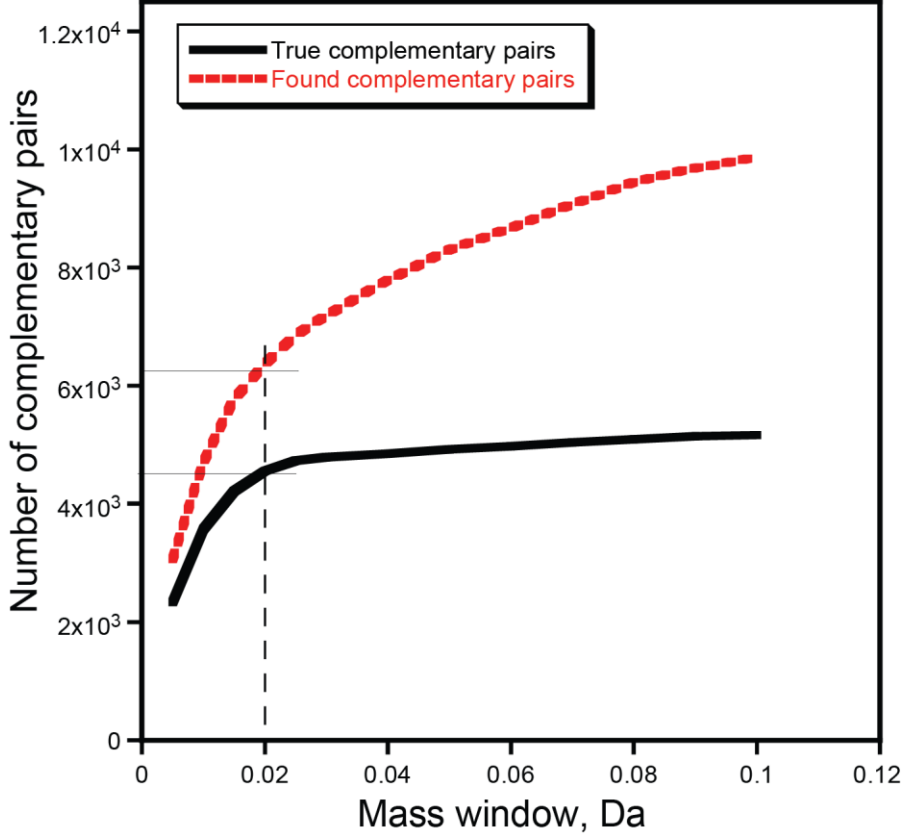


Figure 5. Number of complementary mass pairs extracted by deconvolution procedure in the *in silico* four-plexing experiment as a function of the mass window for fragment masses.

for the most abundant precursor ions with an assigned charge of at least 2. Following each MS/MS event, the product ion population was sent to the c-trap for storage. After all n fragment populations were accumulated in the c-trap, the summed ion population was injected into the orbitrap analyzer for detection (R = 60K). The firmware recorded accurate monoisotopic m/z values for all n precursors in the scan header of each multiplexed MS/MS event.

As a control, an LC-MS/MS experiment was performed on the same sample using a standard data-dependent FTMS method. In this case, following the MS¹ event, the n most intense precursors were interrogated. Precursors were subjected to the same charge state screening as the multiplexing experiment, and each MS/MS event consisted of precursor activation followed by independent m/z analysis in the orbitrap.

In a series of experiments (data not shown), the efficiency of multiplexing, defined as the percent retention of ions from the first activation retained in the c-trap through the nth activation, was found to have a dependence upon both the number of multiplexed events (n) and the number of ions activated in each MS/MS event (automatic gain control, AGC). To investigate these variables, a series of experiments comparing multiplexed and control analyses for different AGC target values and number of multiplexed MS/MS spectra was performed (**Table 1**). For each comparison, multiplexing yielded 2-3 times more identified peptides (M-score > 20) and proteins compared to the control experiment. At the same time, the size of the .mgf file (Mascot search file) was reduced by 67-75%, with the required search time reduced by $\sim 25\%$. These results confirm the theoretical expectations of the efficiency of de-convolution

Table 1. Comparison of the result of multiplexing experiment with n merged MS/MS events and control experiments with n=1

| N | AGC Target | Analysis | Total | IDs; 1% | Exp./Control | Exp./Control |
|---|---------------------|------------|-------|---------|--------------|--------------|
| | Value | | IDs | FDR | (Total IDs) | (1% FDR) |
| 1 | 1 x 10 ⁴ | Control | 562 | 536 | 1 | 1 |
| 3 | 1×10^4 | Experiment | 1404 | 1057 | 2.50 | 1.97 |
| 1 | 5×10^4 | Control | 723 | 563 | 1 | 1 |
| 3 | 5×10^4 | Experiment | 1572 | 1166 | 2.17 | 2.07 |
| 1 | 1×10^4 | Control | 612 | 487 | 1 | 1 |
| 4 | 1×10^4 | Experiment | 1730 | 1127 | 2.83 | 2.31 |

procedure and provides basis for implementation of the de-convolution procedure in routine proteomics applications.

Discussion

Here we demonstrated that an entirely FTMS-based method of MS/MS spectra multiplexing provides a 2.5 – 3.0-fold greater overall throughput than a typical FTMS method, with a negligible loss of information. The method is tested both in silico as well as experimentally, and it showed the expected performance. We hope that this convolution-deconvolution scheme will be widely used in practice for increasing the throughput of proteomics experiments.

Methods

Cell Culture and Protein Harvesting

Wild-type Saccharomyces cerevisiae were grown and proteins harvested as previously described.¹⁹ Briefly, yeast was grown in rich media to an OD600 of 0.97, spun down, washed with sterile water, and pelleted via centrifugation at 10 000g for 5 min. The cell pellet was added to a volume of lysis buffer containing protease inhibitors. The sample was French-pressed three times and centrifuged for 15 min at 30 000g at 4° C.

Digestion

To reduce and alkylate cysteine residues, protein was incubated in 2.5 mM DTT for 25 min at 60 $^{\circ}$ C followed by incubation in 7 mM iodoacetamide in the dark at room

temperature for 30 min. Alkylation was capped by incubation in 2.5 mM DTT for 15 min at room temperature. The samples were digested with trypsin (Promega, Madison, WI), desalted, and the eluent lyophilized following established protocol.

Spectral File Generation and Database Searching

All .raw files resulting from MS/MS analysis were transformed to .mgf files using inhouse software as described above. Mascot Generic Format files corresponding to control runs were created using a multiplexed *n* of 1, whereas those created from experimental analyses used *n* corresponding to the level of multiplexing (3 or 4). The m/z tolerance for fragment ions was set to 0.01 Da, and no intensity cutoff was implemented. Database search was performed against a concatenated forward and reversed *S. cerevisae* (*Saccharomyces* Genome Database; version modified Feb 3, 2011; concatenated version generated in-house) using MASCOT version 2.3 (Matrix Science, London, U.K.). The search was set for tryptic peptides, using a peptide tolerance of 5 ppm with an MS/MS tolerance of 0.005 Da. A fixed modification of carbaminomethylation and a variable modification of methionine oxidation were used, with a maximum of two missed cleavages.

References

- Zubarev, R. & Mann, M. On the proper use of mass accuracy in proteomics. *Mol. Cell. Proteomics* **6**, 377-381, doi:10.1074/mcp.M600380-MCP200 (2007).
- Bruce, J. E., Anderson, G. A., Wen, J., Harkewicz, R. & Smith, R. D. High mass-measurement accuracy and 100% sequence coverage of enzymatically digested bovine serum albumin from an ESI-FTICR mass spectrum. *Anal. Chem.* **71**, 2595-2599, doi:10.1021/ac990231s (1999).
- Palmblad, M., Wetterhall, M., Markides, K., Hakansson, P. & Bergquist, J. Analysis of enzymatically digested proteins and protein mixtures using a 9.4

- Tesla Fourier transform ion cyclotron mass spectrometer. *Rapid Commun. Mass Spectrom.* **14**, 1029-1034, doi:10.1002/1097-0231(20000630)14:12<1029::aid-rcm984>3.0.co;2-# (2000).
- Nielsen, M. L., Savitski, M. M. & Zubarev, R. A. Improving protein identification using complementary fragmentation techniques in Fourier transform mass spectrometry. *Mol. Cell. Proteomics* **4**, 835-845, doi:10.1074/mcp.T400022-MCP200 (2005).
- 5 Marshall, A. G., Hendrickson, C. L. & Jackson, G. S. Fourier transform ion cyclotron resonance mass spectrometry: A primer. *Mass Spectrom. Rev.* **17**, 1-35, doi:10.1002/(sici)1098-2787(1998)17:1<1::aid-mas1>3.0.co;2-k (1998).
- Savitski, M. M., Nielsen, M. L. & Zubarev, R. A. ModifiComb, a new proteomic tool for mapping substoichiometric post-translational modifications, finding novel types of modifications, and fingerprinting complex protein mixtures. *Mol. Cell. Proteomics* **5**, 935-948, doi:10.1074/mcp.T500034-MCP200 (2006).
- Savitski, M. M., Nielsen, M. L., Kjeldsen, F. & Zubarev, R. A. Proteomics-grade de novo sequencing approach. *J. Proteome Res.* **4**, 2348-2354, doi:10.1021/pr050288x (2005).
- Williams, E. R., Loh, S. Y., McLafferty, F. W. & Cody, R. B. HADAMARD-TRANSFORM MEASUREMENT OF TANDEM FOURIER-TRANSFORM MASS-SPECTRA. *Anal. Chem.* **62**, 698-703, doi:10.1021/ac00206a010 (1990).
- 9 Pfandler, P., Bodenhausen, G., Rapin, J., Walser, M. E. & Gaumann, T. BROAD-BAND TWO-DIMENSIONAL FOURIER-TRANSFORM ION-CYCLOTRON RESONANCE. *J. Am. Chem. Soc.* **110**, 5625-5628 (1988).
- Ross, C. W., Guan, S. H., Grosshans, P. B., Ricca, T. L. & Marshall, A. G. 2-DIMENSIONAL FOURIER-TRANSFORM ION-CYCLOTRON RESONANCE MASS-SPECTROMETRY MASS-SPECTROMETRY WITH STORED-WAVE-FORM ION RADIUS MODULATION. *J. Am. Chem. Soc.* **115**, 7854-7861, doi:10.1021/ja00070a035 (1993).
- Masselon, C. *et al.* Accurate mass multiplexed tandem mass spectrometry for high-throughput polypeptide identification from mixtures. *Anal. Chem.* **72**, 1918-1924, doi:10.1021/ac991133+ (2000).
- Wilson, J. & Vachet, R. W. Multiplexed MS/MS in a quadrupole ion trap mass spectrometer. *Anal. Chem.* **76**, 7346-7353, doi:10.1021/ac048955d (2004).
- Geromanos, S. J. *et al.* The detection, correlation, and comparison of peptide precursor and product ions from data independent LC-MS with data dependant LC-MS/MS. *Proteomics* **9**, 1683-1695, doi:10.1002/pmic.200800562 (2009).
- Meng, F. Y. *et al.* Informatics and multiplexing of intact protein identification in bacteria and the archaea. *Nat. Biotechnol.* **19**, 952-957, doi:10.1038/nbt1001-952 (2001).
- Venable, J. D., Xu, T., Cociorva, D. & Yates, J. R. Cross-correlation algorithm for calculation of peptide molecular weight from tandem mass spectra. *Anal. Chem.* **78**, 1921-1929, doi:10.1021/ac051636h (2006).

- Zhang, N. *et al.* ProblDtree: An automated software program capable of identifying multiple peptides from a single collision-induced dissociation spectrum collected by a tandem mass spectrometer. *Proteomics* **5**, 4096-4106, doi:10.1002/pmic.200401260 (2005).
- Bern, M. *et al.* Deconvolution of Mixture Spectra from Ion-Trap Data-Independent-Acquisition Tandem Mass Spectrometry. *Anal. Chem.* **82**, 833-841, doi:10.1021/ac901801b (2010).
- Perkins, D. N., Pappin, D. J. C., Creasy, D. M. & Cottrell, J. S. Probability-based protein identification by searching sequence databases using mass spectrometry data. *Electrophoresis* **20**, 3551-3567, doi:10.1002/(sici)1522-2683(19991201)20:18<3551::aid-elps3551>3.0.co;2-2 (1999).
- Swaney, D. L., McAlister, G. C. & Coon, J. J. Decision tree-driven tandem mass spectrometry for shotgun proteomics. *Nat. Methods* **5**, 959-964, doi:10.1038/nmeth.1260 (2008).